UNDERSTANDING POLYMER FLOCCULANTS IN THE TREATMENT OF OIL SANDS TAILINGS

by

Daniel Victor Dixon

A thesis submitted in partial fulfillment of the requirements for the degree of

Doctor of Philosophy

in

Chemical Engineering

Department of Chemical and Materials Engineering

University of Alberta

ABSTRACT

The extraction of bitumen from oil sands is an energy and water-intensive process that produces a tailings byproduct containing sands, clays, water, and residual bitumen. Larger particles eventually settle out of the tailings, but fine particles – stabilized by the residual bitumen – remain suspended, forming a thick slurry called mature fine tailings (MFT). The stability of MFT makes it resistant to conventional treatment methods used for other types of mineral tailings. As a result, large quantities of MFT have accumulated in tailings ponds that must be remediated. Polymer flocculants are widely used to aggregate the fine particles and recover some water from tailings, but commercial anionic polyacrylamide-based flocculants do not perform well when treating MFTs. Research into modifications of polyacrylamides and novel polymers has found promising results for improved dewatering of MFT, but these polymers are often limited by high dose requirements or generate sediments with insufficient solids contents.

Polymer flocculants, like any other polymer, have a statistical distribution of chain lengths. The study of how this and other polymer microstructural details affect flocculation performance has been underexplored in the field of oil sands and other mineral tailings treatment. In this thesis, three studies were done to investigate how polymer properties impact their flocculation performance in clays and MFT.

First, the effect of polymer molecular weight distribution (MWD) on flocculation was investigated. A series of high molecular weight polyacrylamide polymers with a narrow MWD were synthesized using a controlled radical polymerization technique. These polymers were then used alone or in blends to emulate broad MWD flocculants. These polymers flocculated kaolinite and the size of the aggregates formed was monitored.

Polyacrylamide flocculants with narrow MWDs made larger clay aggregates than those with broad MWDs at equal doses. In the polymer blends, the fraction of the high molecular weight component was the best indicator of aggregate size formation; the low molecular weight fraction had less influence on final aggregate size. These findings suggest that polymers with narrow MWDs can be used in lower dosages than standard flocculants that have broad MWDs with a similar concentration of high molecular weight polymer chains.

Second, a two-step flocculation process using anionic hydrolyzed polyacrylamide (HPAM) and cationic poly(vinylbenzyl trimethylammonium chloride) (PVBTMAC) was studied for the treatment of MFT. The charge density of the HPAM and the dose of HPAM and PVBTMAC were investigated for their influence on several flocculation performance metrics, including settling rate, capillary suction time (a measure of sediment dewaterability), supernatant turbidity, and zeta potential. The charge density of HPAM had a different optimum value depending on which metric you wish to optimize for – settling rate or dewaterability. PVBTMAC played a role in charge neutralization after the addition of HPAM to further consolidate the flocs formed and produce a clear supernatant. Additionally, the two-step flocculation process could treat undiluted MFT slurries, resulting in high solids content after low pressure filtration.

Third, a population balance model describing the change in aggregate size during MFT flocculation was developed. Experimental data of PVBTMAC adsorption and flocculation of MFT was used for model development. The knowledge of the polymer adsorption behaviour was used in the model to determine how polymer dose impacts aggregate size. The developed model is another step toward a more quantitative understanding of how polymer properties affect the flocculation of MFT.

PREFACE

Chapter 3 of this thesis has been published published as D.V. Dixon, J.B.P. Soares, Molecular weight distribution effects of polyacrylamide flocculants on clay aggregate formation. *Colloids and Surfaces A: Physicochemical and Engineering Aspects*, **2022**, *129487*. I was responsible for the design of experiments, data collection, data analysis, and manuscript composition. Dr. J. Soares contributed to manuscript composition, editing, and supervision.

Chapter 4 of this thesis has been submitted for publication as D.V. Dixon, J.B.P. Soares, Dual anionic and cationic polymer flocculants for the treatment of oil sands tailings: a study of dose and charge density, **2022**. I was responsible for the design of experiments, data collection, data analysis, and manuscript composition. Dr. J. Soares contributed to manuscript composition, editing, and supervision.

Chapter 5 of this thesis has been submitted for publication as D.V. Dixon, J.B.P. Soares, Using polymer adsorption data and a population balance model to estimate how polymer dosage affects the flocculation of mineral tailings, **2022**. I was responsible for the design of experiments, data collection, data analysis, model development, and manuscript composition. Dr. J. Soares contributed to manuscript composition, editing, and supervision.

The paper in Appendix A has been published as D.V. Dixon, S.R. Stoyanov, Y. Xu, H. Zeng, J.B.P. Soares, Challenges in developing polymer flocculants to improve bitumen quality in non-aqueous extraction processes: an experimental study, *Petroleum Science* **2020**, *17*, 811–821. I was responsible for the design of experiments, data collection, data analysis, and manuscript composition. Dr. Y. Xu provided edits. Dr. S.R. Stoyanov, Dr. H. Zeng, and Dr. J. Soares contributed to editing and supervision.

Part of the work in Appendix B has been presented in an appendix of the PhD thesis of Dr. Vahid Vajihinejad as supporting information. I was responsible for the data collection, analysis, and writing everything in Appendix B.

ACKNOWLEDGEMENTS

There are a number of people I would like to thank that made completion of this thesis possible. First, I'd like to thank Prof. João Soares for his constant support, patience, and guidance throughout my time at the University of Alberta. I would also like to thank Prof. Hongbo Zeng and Dr. Stanislav Stoyanov for their expert advice and support. I am thankful of the IOSI labs and Dr. Neda Nazemifard for use of their research facilities. I would also like to express my gratitude to all of my colleagues for their enriching discussions, support, and friendly atmosphere in the labs.

I am truly thankful to all my friends and family. The community of friends I have met in Edmonton has been immensely welcoming and supportive of me since I moved here. Finally, of course, I would like to thank Holly and Emily for their unwavering support.

TABLE OF CONTENTS

LIST OF TABLES

LIST OF FIGURES

LIST OF ACRONYMS AND SYMBOLS

ACRONYM

APAM	anionic polyacrylamide
APS	ammonium persulfate
ATR	attenuated total reflectance
ATRP	atom transfer radical polymerization
CFD	computational fluid dynamics
CRP	controlled radical polymerization
CST	capillary suction time
DADMAC	diallyldimethylammonium chloride
DLVO theory	Derjaguin, Landau, Verwey, and Overbeek theory
EDL	electric double layer
EPDM	ethylene propylene diene monomer polymer
FBRM	focused beam reflectance measurement
FTIR	Fourier transform infrared spectroscopy
GPC	gel permeation chromatography
HPAM	hydrolyzed polyacrylamide
ICP-OES	inductively coupled plasma optical emission spectroscopy
ISR	initial settling rate
LCST	lower critical solution temperature
MFT	mature fine tailings
MWD	molecular weight distribution
NaFS	sodium formaldehyde sulfoxylate
NMR	nuclear magnetic resonance
NTU	nephelometric turbidity unit
PAA	poly(acrylic acid)
PAM	polyacrylamide
PDI	polydispersity index
PEO	poly(ethylene oxide)
PEI	polyethylenimine

PVBTMAC	poly(vinylbenzyl trimethylammonium chloride)
RAFT	reversible addition fragmentation chain transfer
RCF	relative centrifugal force
RDRP	reversible deactivation radical polymerization
SEC	size exclusion chromatography
SLS	sodium lauryl sulfate
SRF	specific resistance to filtration
V-50	2,2'-Azobis(2-methylpropionamidine)dihydrochloride
XRD	X-ray diffraction

SYMBOL

a	fitted parameter
b	fitted parameter
D	impeller diameter
D_f	mass fractal dimension
d_i	diameter of aggregate i
Da	daltons
e	electron charge
G	average shear rate
h	fitted parameter
k_{ad}	adsorption rate constant
k_B	Boltzmann constant
k_d	aggregate size decay constant
M_n	number average molecular mass
M_w	weight average molecular mass
M_z	z-average molecular mass
n_{part}	number concentration of particles
$n(v,t)$	number of aggregates of volume v per unit volume at time t
N	rotational speed of impeller

N_i	number concentration of particle *i*
N_p	impeller power number
ppm	parts per million (mass)
$Q(v, v')$	aggregation kernel for aggregates of size v and v'
$S(v)$	breakage kernel for aggregates of size v
t	time
T	temperature
v_i	volume of particle *i*
V	volume of suspension
X_i	coded variable of factor *i* for regression model
Y_i	predicted response from regression model
z_i	valence number of ion *i*
$\alpha_{i,j}$	capture efficiency between particles *i* and *j*
$\beta_{i,j}$	Collision frequency between particles *i* and *j*
β_i	coefficient in regression model for factor *i*
$\Gamma(v, v')$	breakage distribution function
ε	relative permittivity
ε_0	permittivity of free space
ϵ	average energy dissipation rate
θ	effective surface coverage
θ_{max}	effective surface coverage at peak aggregate size
κ^{-1}	Debye length
ν	kinematic viscosity
$\rho_{\infty i}$	bulk number concentration of ion *i*
τ_{ad}	characteristic adsorption time

Chapter 1 INTRODUCTION

1.1 MOTIVATION

Mining and extraction of bitumen from oil sands using variants of the Clark hot water extraction process has been in operation in Alberta for several decades [1]. This process is water and energy intensive: *in-situ* extraction processes require about 0.2 barrels of non-saline water per barrel of oil produced and surface mining operations may need up to 2.5 barrels of water per barrel of oil produced [2,3]. A by-product of this process are mineral tailings which are deposited in constructed ponds to store the spent process water and minerals after bitumen froth flotation. These tailings are composed of water, sand, clays, residual bitumen, and inorganic salts [4]. Water recycling is extensively used in the industry, but challenges unique to the treatment of the oil sands tailings ponds limit the amount of water that can be recovered and hinder progress in tailings pond remediation [4,5]. Large particles in the tailings ponds will settle out, but fine particles stabilized by the residual bitumen can remain suspended indefinitely, forming a thick slurry consisting of about 30 – 40% solids, 1 – 5% bitumen, and the remaining mass water. This slurry is called mature fine tailings (MFT). With the continued production of bitumen from oil sands, the accumulation of MFT remains an environmental concern that calls for improved treatment and remediation methods.

Polymer flocculants are used to treat mineral tailings; in the case of MFT, they are usually high molecular weight anionic copolymers of acrylamide. The effectiveness of these conventional flocculants is limited by a few factors. First, the sediments formed from the flocculants tend to have a gel-like structure that retains water and degrades under shear stress. Second, the quality of the supernatant water is poor without the addition of inorganic coagulants. This poses problems for the rest of the bitumen extraction process because di- and trivalent cations will accumulate in the water that is recycled and inhibit the bitumen extraction efficiency from the oil sands. Finally, the high molecular weight of the polyacrylamides results in very viscous polymer solutions that are difficult to disperse into the also viscous MFT slurry, creating a spatially heterogeneous distribution of polymer.

These limitations highlight the need for flocculants that are designed specifically for the treatment of oil sands tailings. Novel polymeric materials and a better understanding of how polymers behave in tailings are needed to make progress in this area.

1.2 Research Objectives

The purpose of this thesis was to improve our understanding of flocculant behaviour as applied toward the treatment of MFT. This was done by pursuing the following objectives:

i) Synthesis of well-defined polymer flocculants with controlled molecular weight distributions and chemical composition.
ii) Investigation of how the molecular weight distribution of flocculants affect the formation of particle aggregates.
iii) Study on how anionic and cationic flocculants can synergistically improve flocculation performance of MFT.
iv) Development of a model relating polymer adsorption on flocculation kinetics of MFT.

1.3 Thesis Outline

This thesis is organized into six chapters.

Chapter 1 introduces the challenges associated with MFT treatment and outlines the objectives of this thesis.

Chapter 2 discusses the fundamentals related to MFT, flocculation, and tailings treatment, and controlled radical polymerization. It also reviews the literature of polymer flocculants for the treatment of MFT.

Chapter 3 presents a study on how the molecular weight distribution of polyacrylamide can affect the size of clay aggregates formed during flocculation. This chapter was published

as D.V. Dixon, J.B.P. Soares, Molecular weight distribution effects of polyacrylamide flocculants on clay aggregate formation, *Colloids and Surfaces A: Physicochemical and Engineering Aspects* **2022**, *129487*.

Chapter 4 is a study of a two-step flocculant treatment of MFT using anionic polyacrylamide and cationic poly(vinylbenzyl trimethylammonium chloride). This chapter was submitted for publication as D.V. Dixon, J.B.P. Soares, Dual anionic and cationic polymer flocculants for the treatment of oil sands tailings: a study of dose and charge density, *Journal of Water Process Engineering,* **2022**.

Chapter 5 is a population balance model study of the flocculation of MFT that incorporates polymer adsorption data to predict dose response. This chapter was submitted for publication as D.V. Dixon, J.B.P. Soares, Using polymer adsorption data and a population balance model to estimate how polymer dosage affects the flocculation of mineral tailings, *Industrial and Engineering Chemistry Research* **2022**.

Chapter 6 summarizes the results of the thesis and contains recommendations for future work.

Appendix A contains work on finding oil soluble polymer flocculants for the removal of fine solids in diluted bitumen. This was published as D.V. Dixon, S.R. Stoyanov, Y. Xu, H. Zeng, J.B.P. Soares, Challenges in developing polymer flocculants to improve bitumen quality in non-aqueous extraction processes: an experimental study, *Petroleum Science* **2022**, *17,* 811–821.

Appendix B contains work on using *in-situ* NMR reactions to get polymer reactivity data for PVBTMAC and to calculate reactivity ratios for copolymers of PAM and VBTMAC.

Chapter 2 BACKGROUND AND LITERATURE REVIEW

2.1 MFT COMPOSITION AND STABILITY

Mature fine tailings, the final state of oil sands tailings after coarse particles have settled out, is a thick slurry containing over 30 wt.% solids and 1 – 5 wt.% bitumen, forming a stable gel-like colloidal suspension in water with a pH of about 8. The solid mineral content of MFT consists largely of fine particles (defined in the oil sands industry as particles below 44 μm), with a significant fraction of particles being clays below 2 μm in size [6]. The clay minerals in MFT mostly consist of kaolinite and illite, the mixed-layer clays kaolinite-smectite and illite-smectite, and a small fraction montmorillonite and chlorite clays [7,8]. Table 2-1 list the characteristics of clays commonly found in oil sands ore.

Table 2-1: Characteristics of clays commonly found in oil sands [4].

Mineral	Kaolinite	Illite	Montmorillonite	Chlorite
Abundance (wt. %)	69	28	0.3	1
Structure type	Two-Layer (TO)		Three-Layer (TOT)	
Isomorphic substitution	Low in T	High in T	Both in T and O	
Compensating ions	K^+	K^+	Na^+, Ca^{2+}	$Mg(OH)_2(O)$
Specific surface area (m^2/g)	10-20	65-100	700-840	42
Cation exchange capacity (meq/100 g)	3-5	10-40	80-150	10-40

The two major clay components in MFT – kaolinite and illite – are non-swelling clays. Their structures are depicted in Figure 2-1. Kaolinite is a two-layer clay consisting of a tetrahedral silcon-oxygen sheet bonded to an octahedral aluminum-oxygen-hydroxyl sheet. The tetrahedral-octahedral unit layers are stacked upon each other via hydrogen bonds between the hydroxyl groups of the octahedral sheet and the oxygens on the surface of the tetrahedral sheets. The isomorphic substitution of Al^{3+} and Si^{4+} in the silica tetrahedral sheet creates a permanent negative charge that is stable over a wide pH range [9]. The face of the octahedral sheet and the edges of the clay layer are more sensitive to pH. At the pH

range typical of oil sands tailings (~ 8) the surfaces and edges of kaolinite will have a net negative charge [4]. Illite, the other clay abundant in MFT, is a three-layer clay that has an additional tetrahedral silica layer with the octahedral layer in between. A high degree of isomorphic substitution in the tetrahedral layers of illite results in a net negative charge that attracts counterions, such as K^+, to the interlayer, binding the unit layers strongly. This limits the ion exchange capacity of the clay and also prevents interlayer swelling [4,9]. Illite also carries a net negative charge in pH ranges relevant to oil sands tailings.

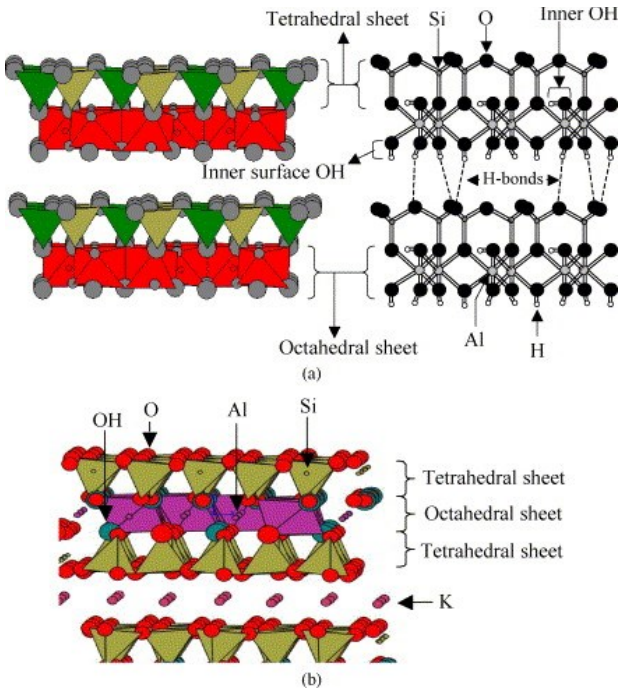

Figure 2-1: Structure of clay minerals: (a) kaolinite (b) illite [9].

Swelling clays present in MFT may include montmorillonite and chlorite. Montmorillonite is a three-layer clay that exhibits isomorphic substitution in the tetrahedral and octahedral layers. Since counterions cannot sit close to the octahedral sheet, the negative charge becomes delocalized and the ions are not bound as tightly to the tetrahedral layer. This allows cation exchange and interlayer swelling from water. Chlorite is another three-layer clay with isomorphic substitution throughout, with a magnesium hydoxyl layer in between

the three-layer sheets [4]. These swelling clays can expand in water making the MFT more viscous.

The colloidal stability of MFT suspensions is usually explained by the presence of nanosized clays and highly negative surfaces charges [6,7]. The DLVO theory can describe why the fine particles will not aggregate considering two forces: attractive van der Waals forces and repulsive electrical double layer forces. Van der Waals forces are a collection of short-range interactions involving permanent or induced dipoles between molecules. The electric double layer (EDL) forms around a particle with a charged surface in solution, where counterions attracted to the surface form what is called the Stern layer. Beyond that first layer of counterions, a more diffuse layer of counterions and co-ions are present. Counterion concentration is at a maximum near the charged particle surface and decays to the bulk concentration further from the particle surface. Co-ion concentration is depleted close to the particle surface and increases with distance until the bulk concentration is reached. Figure 2-2 is a schematic representation of the EDL [10]. The characteristic thickness of the EDL is called the Debye length, κ^{-1}, defined as:

$$\kappa = \left(\frac{e^2}{\varepsilon_0 \varepsilon k_B T} \sum_i \rho_{\infty i} z_i^2 \right)^{\frac{1}{2}} \tag{2-1}$$

where $\rho_{\infty i}$ is the ion number density, z_i is the valence of ion i in solution, e is the elementary charge of an electron, ε_0 is the permittivity of free space, ε is the relative permittivity of the medium, k_B is Boltzmann's constant, and T is temperature. When the concentration of ions in solution increases, the Debye length decreases, which means particles will have weaker long range electrostatic repulsion.

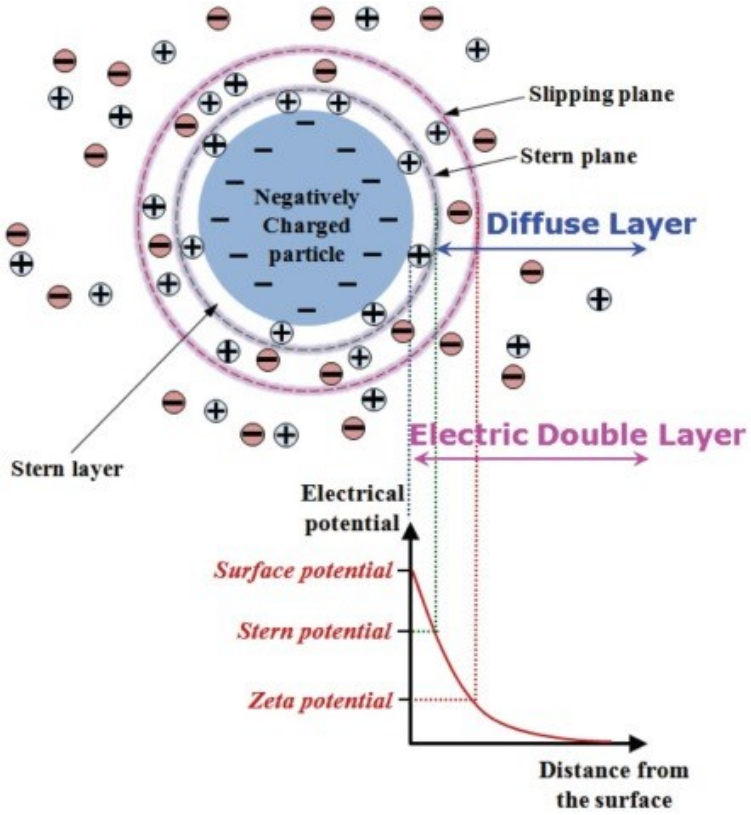

Figure 2-2: Electric double layer of a negatively charged particle [11].

Due to the structure of the EDL, the charge of a particle in solution cannot be measured directly because of the presence of counterions that move with the particle. Instead, the electric potential at the slipping plane (Figure 2-2) is more easily measured and called the zeta-potential.

Combining van der Waals forces with EDL forces leads to the classic DLVO theory, which give us an idea about the stability of a suspension. In Figure 2-3, the interaction energy over distance between two surfaces outlines a number of possible interaction potentials depending on the surface charges. At high surface charges, the repulsive energy from the double-layer acts as an energy barrier, preventing particle aggregation. At low surface charges, van der Waals attractive forces are strong enough to cause aggregation. Increasing the ion concentration in solution is one way of reducing the repulsive energy by

compressing the double layer. A stable suspension occurs when the net interaction energy is repulsive with a high energy barrier preventing aggregation.

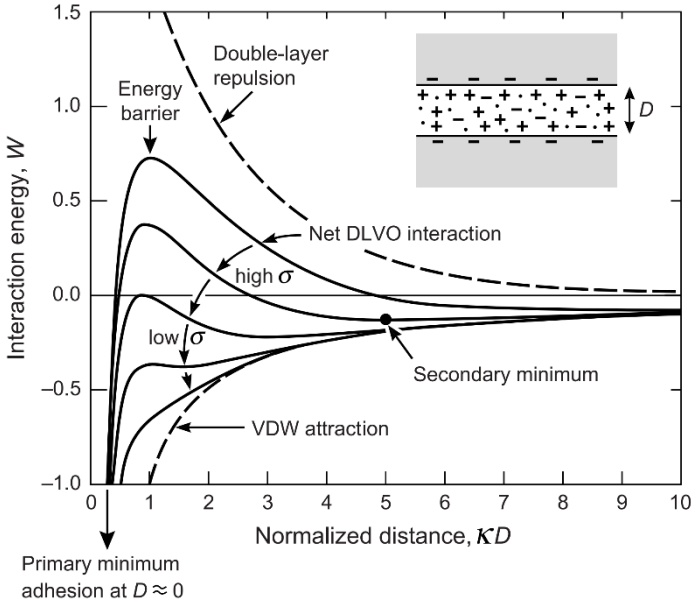

Figure 2-3: Interaction energy versus distance profiles using DLVO theory [10].

In the context of MFT treatment, the small size and highly negative surface charges of the clays mean they can exist as stable suspensions. Coagulation of MFT with the addition of a high concentration of inorganic salts is one way to suppress the double layer around the particles and promote aggregation. One example of this is the addition of gypsum (calcium sulphate dihydrate) in the composite tailings process for MFT treatment. Aggregation and sedimentation can be achieved, but the disadvantage of this method is that the excessive amount of calcium ions accumulated in the recovered water reduces bitumen recovery upstream of this process [12,13].

Concepts from DLVO theory are an excellent way to describe MFT colloidal stability, but it alone does not account for all intermolecular interactions that contribute to the stability of MFT. Bitumen, salts, and other chemical species are present in MFT and can give rise to several additional phenomena, such as hydration interactions, steric forces, and

hydrophobic interactions [14]. The role bitumen plays in MFT stability is not completely understood, but its presence has been observed to affect the rheological properties of MFT [15].

2.2 Flocculation Fundamentals

Polymer-induced flocculation – simply referred to as flocculation in this thesis – is the use of polymers to cause aggregation of particles. The primary mechanism to achieve this is the use of high molecular weight polymers to form bridges between multiple particles holding them together as aggregates. A second mechanism, through the use of polyelectrolytes to neutralize particle charge and induce aggregation, is also sometimes referred to as flocculation, but can also be classified as coagulation.

Flocculation happens when a polymer molecule adsorbs onto a particle and then a tail or loop of the adsorbed polymer adheres to one or more additional particles. If the bridging force is sufficiently strong, the particles will remain together in a floc. If the flocs formed are large enough and dense enough, they will settle out of the suspension. Flocculation by adsorbing polymers has been studied and the interaction forces have been directly measured in the early 1980s [16–18]. Figure 2-4 is a schematic diagram of a polymer chain adsorbed on a surface. For effective flocculation, the polymer tails and loops needs to extend away from the surface far enough to form bridges with other particles [19,20].

The adsorption of polymers onto mineral surfaces may happen by several mechanisms, such as hydrogen bonding – where polymers such as polyacrylamide (PAM) and polyethylene oxide (PEO) can bond with silanol groups on silica – and electrostatic attraction – where oppositely charged polyelectrolytes and minerals will attract. Hydrophobic interactions – where non-polar segments of a polymer may adsorb on a hydrophobic surface – and ion bridging – where oppositely charged ions can facilitate adsorption between polymers and surfaces of the same charge – are also relevant ways for polymers to adsorb to the surfaces of suspended solids, leading to flocculation [20].

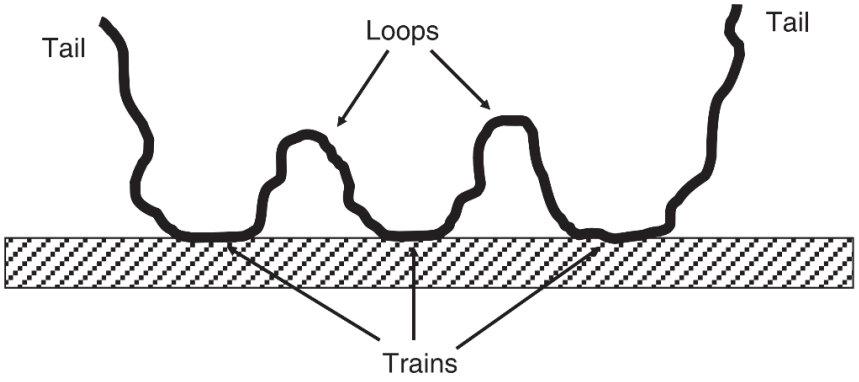

Figure 2-4: Equilibrium conformation of an adsorbed polymer chain [20].

The free energy of adsorption of a polymer segment does not need to be high: about 0.3 k_BT is enough. Because many segments will adsorb onto the surface, it does not take much for the entropy penalty from adsorption to be overcome [20,21]. In fact, if the adsorption affinity is too high, then a polymer may not extend out from the surface far enough to reach another particle for flocculation. The distance polymers need to reach for flocculation must exceed the Debye length, the length the electrostatic effects of the particles persists in solution (Equation 2-1), otherwise the electric double layer of the particle with act as a barrier to aggregation (Figure 2-5).

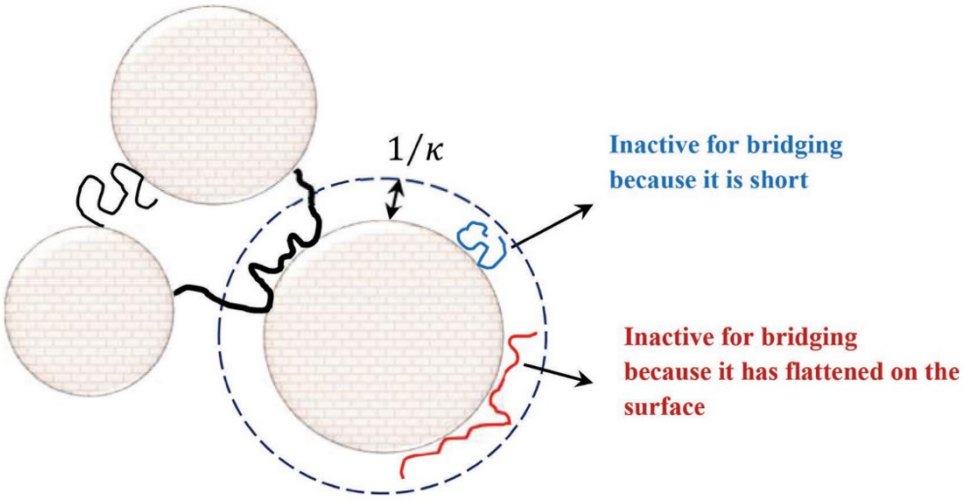

Figure 2-5: Possible polymer conformations during adsorption and flocculation [22]. κ^{-1} is the Debye length

Flocculation is a dynamic process that involves at least three major phenomena: polymer adsorption, polymer rearrangement, and particle aggregation. The adsorption of polymer onto undersaturated surfaces, as is usually the case in flocculation, is typically transport limited (adsorption is faster), resulting in an adsorption rate that relies only on the bulk concentration of polymer [21,23]. A characteristic adsorption time can be estimated from Equation (2-2):

$$\tau_{ad} = \frac{\ln(1-\phi)}{k_{ad} n_{part}} \tag{2-2}$$

where τ_{ad} is the characteristic adsorption time, ϕ is the fraction of polymer needed for the onset of flocculation, k_{ad} is the adsorption rate constant, and n_{part} is the number concentration of particles in suspension [20,24,25]. After adsorption, polymers can begin to rearrange on the particle surface (Figure 2-6), which has implications for how far the polymer chain extends into the solution, thereby affecting the flocculation efficiency. Polymers can also rearrange after flocculation, which is evident by an observed change in floc size [20,22,26].

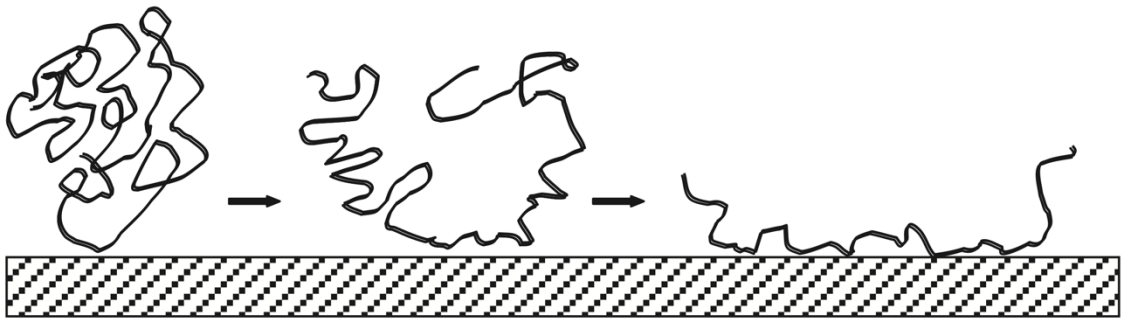

Figure 2-6: Polymer rearrangement after initial adsorption [20].

2.3 FLOCCULANTS FOR OIL SANDS TAILINGS TREATMENT

This section will review some of the recent literature on the use of flocculants for the treatment of oil sands tailings.

2.3.1 FLOCCULANTS WITH NOVEL POLYMER CHEMISTRY OR ARCHITECTURE

To find alternatives to polyacrylamides, many polymers with different chemical compositions and architectures have been made with various levels of success for MFT treatment. Hethnawi *et al*. developed a titanomagnetite nanoparticle (NTM) grafted with polyacrylamide (PAM) and sodium laurel sulfate (SLS) for the treatment of MFT [27]. The synthesized NTM were 20 – 30 nm in diameter and coated with acrylamide monomers in acidic conditions. The polymer graft layer was made via free radical polymerization of acrylamide with SLS. The study used a response surface method experimental design to optimize the amount of PAM and SLS in the grafting polymerization for better flocculation outcomes. The SLS made the nanoparticle flocculant more hydrophobic for better dewatering performance. When treating MFT with 15 wt% solids, the authors found that the NTM flocculant with the highest mass of PAM and SLS had the best performance as measured by initial settling rate (ISR), capillary suction time (CST), specific resistance to filtration (SRF), and turbidity of the supernatant water. The authors attributed the flocculation performance to the higher density of the NTM compared to pure polymer flocculants, allowing for better sedimentation and dispersion through the suspension, and the hydrophobic SLS for preventing high water retention in the sediment.

Degradable polymers were studied for their ability to allow MFT sediments to further densify over time after their initial flocculation (Figure 2-7). Polycaprolactone choline iodide ester methacrylate (PCL_2ChMA) macromonomer-based polymers were designed for the degradation of the polyester sidechains [28,29]. The degradable polymers demonstrated a reduction in CST, a measure of water retention, after accelerated degradation of the polyester linkage in the sidechain. This reduction in CST was not seen in comparable polymers without the ester bonds [28]. In a follow-up study, modifications to PCL_2ChMA were explored by changing the methacrylate monomer to an acrylate monomer and by

changing the caprolactone unit in the macromonomer with a lactic acid unit. Results were comparable between the methacrylate and the acrylate monomer backbones, but the lactic acid containing side chains led to faster compaction of the MFT sediment layer compared to the caprolactone polymers [29].

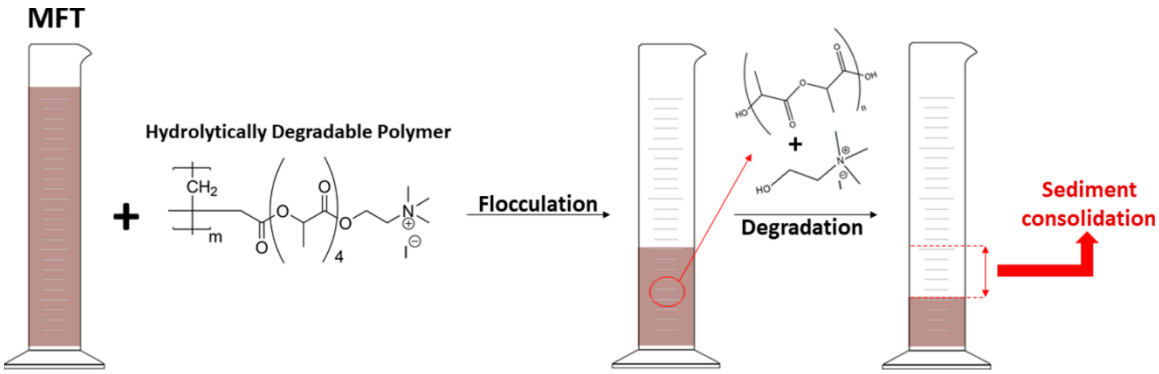

Figure 2-7: Proposed mechanism of hydrolytically degradable polymer flocculants [29].

To reduce water retention in the sediments of treated MFT compared to commercial PAM, flocculants with hydrophobic polymer backbones have been made. One example of these polymers is an ethylene, propylene, diene terpolymer (EPDM) grafted with poly(methyl acrylate) hydrolyzed for water solubility, making EPDM-*g*-HPMA [30,31]. In a detailed study of graft density along the EPDM backbone and graft length of the HPMA sidechains, it was found that highest solids content in the sediment and lowest turbidity in the water supernatant was achieved with a low graft density and long side chain length. When used in combination with filtration after flocculation, a graft density of 13% with a graft molecular weight of 179 kg/mol was able to achieve 43 wt. % solids content with 34 kPag (5 psig) of pressure over 1 hour [31].

Hydrophobically modified polyacrylamides have also been studied in high salinity environments to see how their adsorption behaviour changes on surfaces relevant to mineral tailings [32,33]. A copolymer of acrylamide, acrylic acid, and 0.3% hexadecyl dimethyl allyl ammonium chloride was synthesized. This hydrophobically modified PAM

(HMPAM) was compared with conventional anionic PAM. Using a quartz crystal microbalance with dissipation (QCM-D) adsorption on both silica and alumina surfaces was studied. HMPAM had more adsorption than PAM on both the negatively charged silica surface and the positively charged alumina surface. Increasing salt concentration also increased adsorption due to suppression of the electric double layer. Adhesion forces were also measured with atomic force microscopy and were in agreement with the adsorption experiments [32]. Even with a small fraction of hydrophobic monomers incorporated into the polymer the difference in adhesion was quite dramatic, likely due to changes in the polymer conformation because of the long, 16 carbon sidechain.

Polymer chains can range in architecture from completely linear to highly branched. This may influence the polymer size in solution and the flexibility of the polymer chains to move and rearrange on the surface. In a recent study, Lim and Adachi demonstrated that branched polyelectrolytes increase the initial flocculation rate of polystyrene latex particles over comparable linear polymers [34]. Using three cationic PAM based polyelectrolytes (0, 3, and 6 branches) with the same charge density of 40%, flocculation of anionic latex particles was studied by determining the adsorbed layer thickness and counting the change in the suspended particle population. Hydrodynamic layer thickness of particles with and without polymer was determined by recording the Brownian motion of the particles through optical microscopy. By relating the mean squared displacement of the particles to the diffusion coefficient, the Stokes-Einstein relation was then used to estimate the polymer layer thickness. The branched polymers consistently resulted in a thicker adsorbed layer compared to the linear polymer at low and high ionic strength. This also resulted in a faster initial flocculation rate. This was attributed to branched polymers unable to rearrange into flat layers along the particle surfaces, instead remaining extended out from the surface increasing the probability of collision with other particles.

The effects of polymer branching was studied in the context of MFT treatment by Nguyen and Soares [35]. A cationic polyelectrolyte, poly(vinyl benzyl trimethyl ammonium chloride) (PVBTMAC) was synthesized by a controlled radical polymerization reaction, atom transfer radical polymerization (ATRP). A linear, 3-arm star, and 4-arm star polymer (M_n = 3000 kg/mol for each) were synthesized and used to treat a 5 wt. % solids MFT

sample. In all cases the branched polymers outperformed the linear polymers in terms of initial settling rate. However, all three polymers resulted in a similar CST and final solids content in the sediment. It appears from this study that branching morphology mainly effects the initial settling rate, this could be due to lower viscosity of the branched polymers adsorbing faster onto the particles and/or a more extended conformation from the particle surfaces allowing for more successful collision events leading to flocculation.

Block copolymers are another way that polymers can be structured. Instead of different monomers being distributed throughout the polymer chain blocks of a single monomer type can be synthesized. This can potentially alter the polymer conformation in solution and its interactions with other materials. In a study by Dao *et al*. a four-arm star AB block copolymer was made with acrylamide and acrylic acid for the flocculation of kaolinite (3 wt.%) [36]. The polymers were synthesized using a controlled radical polymer reaction, reversible addition-fragmentation chain transfer (RAFT), using a 4-armed chain transfer agent to facilitate the growth of the star copolymer. PAM blocks were in the core of the polymer and the poly(acrylic acid) (PAA) blocks were at the chain ends. Settling rate of the kaolinite flocs was comparable between the block copolymers and a random copolymer control when $[Ca^{2+}]$ = 0.05 M, but at higher concentrations of Ca^{2+} (0.10 and 0.50 M) the block copolymers resulted in faster settling.

Dao *et al*. did another study with linear ABA triblock copolymers where PAM was the centre block and PAA were the end blocks [37]. The RAFT synthesis of the block copolymers allowed for controlled growth of the polymer chains resulting in low dispersity polymers. Flocculation of 3 wt. % kaolinite at three concentrations of Ca^{2+} was evaluated based on settling rate and turbidity. The results were compared to a random copolymer of PAM and PAA and the homopolymers as controls. A block copolymer containing about 40 wt. % PAA had the highest settling rate at all ionic strengths and the PAA and PAM homopolymers had the lowest settling rates. Turbidity of all the block copolymers was lower than the random copolymer and the homopolymers at all ionic strengths. The authors speculate that the random copolymers will reduce in size more in the presence of cations (due to charge screening effects) compared to the block copolymers where the anionic

groups are only at the chain ends, thereby making the block copolymers larger in solution in high salt conditions allowing for more efficient bridging flocculation.

2.3.2 FLOCCULANTS DERIVED FROM NATURAL MATERIALS

Natural polymers are often looked at as potential flocculants for better degradability, lower toxicity in the environment, or the ability to be sourced from renewable feedstocks. To make effective flocculants typically these materials need to be chemically modified or grafted with synthetic polymers.

Zhang *et al*. evaluated the flocculation performance of a hyperbranched polyethylenimine (PEI) grafted onto cellulose [38]. Cellulose (M_w = 20 kg/mol) was modified to convert some hydroxyl groups to aldehydes then a branched PEI (M_w = 0.6 kg/mol) was grafted onto the cellulose through the formation of a Schiff's base. Flocculation of a dilute kaolin suspension (0.05 wt.%) and a few industrial wastewaters was evaluated. They demonstrated that the cationic PEI/cellulose could effectively reduce the turbidity, total suspended solids, and chemical oxygen demand in wastewater without added coagulants, making the cellulose-based flocculant effective for dilute suspensions.

A recent study by Zheng and Taylor looked at a non thermo-responsive and thermo-responsive cationic starch for the treatment of MFT [39,40]. The non thermo-responsive starch contained 2-hydroxypropyltrimethylammonium groups giving the starch an overall negative charge. The thermo-responsive starch contained the same cationic functional groups along with hydroxybutyl groups giving the polymer a lower critical solution temperature (LCST). The LCST is a property of some thermo-responsive polymers where the polymers will become immiscible in solution above a critical temperature called the LCST. For the thermo-responsive cationic starch in this study the LCST ranged from 30 – 36 °C in process water, depending on polymer dose [39]. The starches were tested with 2 wt. % and 10 wt. % MFT. Both starches produced clear supernatant at high doses (10 g polymer/kg solids) and fast settling rates, and higher solids content in the MFT sediment than a commercial anionic PAM. At 50 °C the ISR of the thermo-responsive starch

increased. This has potential for increased settling rates of cationic polymers, but the high temperatures used on an industrial scale would be energy intensive.

Amylopectin was also used as a natural polymer flocculant for the treatment of MFT [41,42]. In a study by Bazoubandi and Soares amylopectin was grafted with PAM with different graft lengths and frequencies and used to treat 5 wt.% MFT [41]. Longer PAM graft lengths were more effective flocculants and changing grafting frequency had minimal effect on flocculation performance. The amylopectin grafted with PAM also resulted in lower CST and higher solids content compared to PAM homopolymers.

Davey and Soares made flocculants from amylopectin with grafted poly(methyl acrylate) [42]. The grafted polymers were hydrolyzed to convert the methyl acrylate functional groups to methacrylic acid groups, making the polymer anionic. This study with amylopectin also found that higher ISR and lower CST was achieved with long graft lengths and low grafting frequency. This is attributed to longer graft chains leading to more efficient bridging flocculation.

Nanocrystalline cellulose has been investigated for its potential as a flocculant for kaolinite [43]. The form of this cellulose is referred to as hairy cationic nanocrystalline cellulose (CNCC), as first reported by Yang and van de Ven [44]. The CNCC synthesized was 4.7 ± nm wide and 380 ± 120 nm long. The term ‘hairy’ refers to the ends of the CNCC rod where amorphous polymer chains extend into solution, as depicted in Figure 2-8. Flocculation was monitored by FBRM and optical microscopy. Flocculation was most efficient close to the isoelectric point of the solution and also exhibited good re-flocculation efficiency indicating the primary mechanism was charge neutralization. The fractal dimension of the flocs was estimated from a chord length distribution data using a recently developed machine learning algorithm [43,45]. The fractal dimension of the kaolinite flocs changed depending on the dose of CNCC used and re-flocculation resulted in a higher fractal dimension due to compaction of flocs.

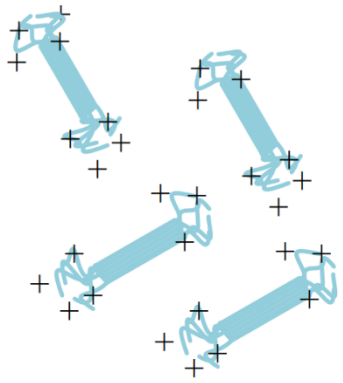

Figure 2-8: Representation of hairy cationic nanocrystalline cellulose (CNCC), which consists of a crystalline rod-like body and amorphous polymer chains at the ends [43].

2.3.3 FLOCCULATION USING A TWO-STEP POLYMER TREATMENT

The use of two polymers for flocculation, typically of opposite charges has been studied for enhanced water treatment in a number of fields such and mineral tailings and most extensively in papermaking [20,46]. In the first study using a dual polymer system for oil sands tailings treatment, Lu *et al*. used a commercial anionic PAM (Magnafloc-1011, 17500 kg/mol, 27% charged) in combination with chitosan (60 – 80 kg/mol, cationic). They found that adding chitosan to the PAM treated tailings improved supernatant turbidity with only a moderate impact on aggregate settling rate [47]. They proposed a mechanism where the PAM acts as a bridging flocculant and the addition of chitosan further consolidated the flocs through charge neutralization. They also characterized the adhesion force using a surface forces apparatus where the combination of PAM with chitosan resulted in stronger attractive forces [47].

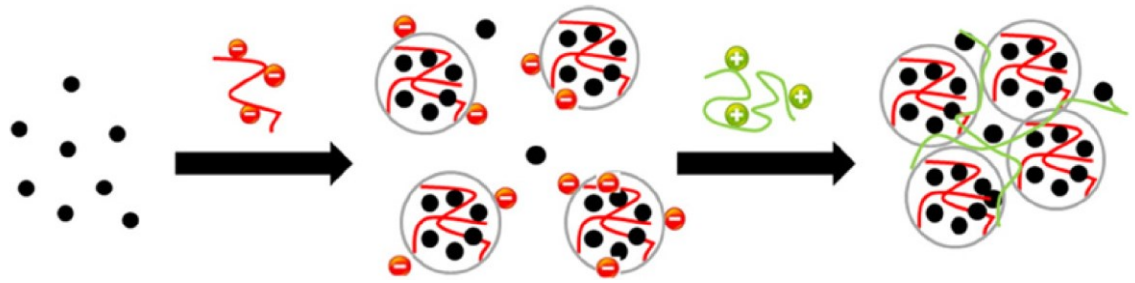

Figure 2-9: Two-step flocculation mechanism using anionic then cationic polymer [47].

A pair of studies using an anionic PAM and cationic poly(diallyldimethylammonium chloride) (polyDADMAC) investigated the performance of the combination of the two polymers in MFT dewatering [48,49]. In the first study, the anionic PAM (SNF A3335, 17000 kg/mol, 30% charge density) and the cationic polyDADMAC (BASF Alcomer 7115, 200 – 400 kg/mol, cationic) were used in sequence with the cationic polymer first [48]. The cationic dose was varied and capillary suction time (CST) and specific resistance to filtration (SRF) of the flocculated tailings was measured. Using the two polymers together performed better than either one alone, and the best CST and SRF performance was observed when the cationic polymer dose was higher. Solids content in the filter cake reached up to 64%. In the second study, the order of polymer addition was switched to PAM then polyDADMAC [49]. By changing the order of the polymer addition, the performance for CST and SRF was improved. Replacing polyDADMAC with a neutral PEO (8000 kg/mol) was also investigated [49]. Using PAM and PEO also resulted in better flocculation than either polymer alone. They found that PAM and polyDADMAC had faster dewatering as measured by CST, but PAM with PEO had better filtration performance, due to the ability of the high MW PEO to withstand shear.

In a recent work by Zhou *et al*., a combination of commercial anionic PAM (17500 kg/mol, 30% charge) with a hybrid $Al(OH)_3$-PAM (5000 – 6000 kg/mol, cationic) was used for the flocculation of MFT [50]. The sequential addition of PAM then $Al(OH)_3$-PAM resulted in fast settling rates and better sediment solids content over a single polymer alone when flocculating 10 wt.% MFT. Additionally, this group looked at how this dual polymer system would perform in a composite tailings treatment method where coarse sands are

added to MFT to help promote aggregation and sedimentation. They found that adding the sand to MFT was a better way to improve solids consolidation that increasing the dose of the dual polymer system [50].

In the reports related to MFT, the addition of an anionic polymer followed by a cationic polymer was consistently found to have better performance. This is not universally true when it comes to flocculation of other systems. Early reports on dual polymer flocculation of alumina showed that flocculation was insensitive to polymer order as long as they were added sequentially using polystyrene sulfonate and a cationic polyacrylamide [51]. Another study on alumina using polyacrylic acid and polyDADMAC added the anionic polymer first [52]. A study on iron ore tailings used a neutral or anionic PAM first with a cationic PAM second for optimal flocculation [53]. In a flocculation test of kaolinite, chitosan grafted with acrylamide and DADMAC was used before an anionic PAM [54]. Cationic polyelectrolytes are used extensively in the papermaking industry where they are added before a second flocculant, which can be anionic or cationic [20]. These differences illustrate that the interactions that make one addition order better than another will change depending on the specifics of the chemistry involved.

2.4 Reversible addition – fragmentation chain transfer (RAFT) polymerization

Reversible deactivation radical polymerization (RDRP), also called controlled radical polymerization (CRP), are a class of polymerization reactions where there is a rapid equilibrium between dormant and active radical chains. The dormant chains are more abundant in the reaction thereby minimizing the number of termination reactions that can occur, allowing the active chains a long lifetime in solution. The rapid conversion between dormant and active chains allows for each chain to grow at a similar rate leading to predictable chain lengths and low dispersity in a polymer sample. Two popular RDRP techniques are atom transfer radical polymerization (ATRP) and reversible addition – fragmentation chain transfer (RAFT) polymerization. ATRP reactions usually involve an

alkyl halide initiator and a transition metal catalyst, typically copper, where the main equilibrium is the transfer of the halogen atom to a propagating polymer chain [55]. RAFT polymerization relies on a chain transfer agent, typically a thiocarbonylthio compound, where the main equilibrium is between a propagating polymer chain and a dormant macro chain transfer agent [56]. This section will focus on RAFT polymerization because it was used to make polymers in Chapter 3 and Chapter 5 of this thesis.

RAFT polymerization, first reported in 1998 [57], is similar to free radical polymerization but done in the presence of a chain transfer agent that facilitates a degenerative transfer between dormant and active polymer chains. A typical reaction scheme is shown in Figure 2-10.

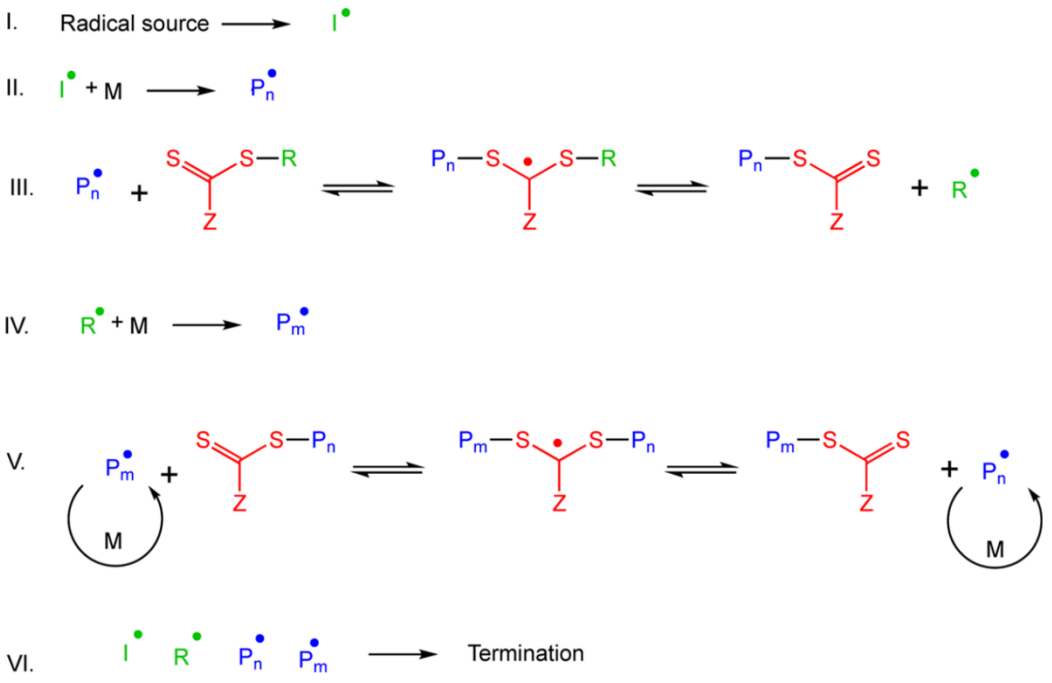

Figure 2-10: Reaction scheme for a typical RAFT polymerization [56].

Like in free radical polymerization, a source of radicals is needed to initiate the reaction (Figure 2-10, I and II). A RAFT pre-equilibrium step occurs when a radical species reacts with the chain transfer agent (Figure 2-10, III). The R group on the chain transfer agent

may undergo the reverse reaction with the transfer agent or react with a monomer in reinitiation (Figure 2-10, IV). The main RAFT equilibrium reaction (Figure 2-10, V) involves a rapid, reversible chain transfer reaction via the transfer agent intermediate. To maintain a controlled reaction, the addition/fragmentation equilibrium reactions should be faster than the propagation rate of the polymer, so on average less than one monomer is added to the polymer chain before chain transfer [56]. Termination reactions occur as they would in a free radical polymerization (Figure 2-10, VI), by combination or disproportionation reactions depending on the polymer. An appropriate RAFT chain transfer agent is key to a good level of control and the selection of R and Z groups will depend on the monomer and solvent used for the reaction.

RAFT methods, like many RDRP methods, has struggled to synthesize high molecular weight polymers with good control on dispersity, making their applications limited when it comes to the requirements for flocculation. However, relatively recently some monomers with high reactivity, including acrylamide, have successfully been synthesized with molecular weights above 1 million g/mol [58–60]. These innovations along with some polymer reaction engineering techniques have the potential to allow the synthesis of high molecular weight polymers, copolymers, and block copolymers with well-defined molecular weight distributions [61–64].

Chapter 3 MOLECULAR WEIGHT DISTRIBUTION EFFECTS OF POLYACRYLAMIDE FLOCCULANTS ON CLAY AGGREGATE FORMATION

This work investigates the effect of polyacrylamide dispersity (broad and narrow molecular weight distributions) on their flocculation performance in a system of kaolinite clay suspended in water. A series of uniform chain length (dispersity, Đ = 1.04 – 1.35) polyacrylamide flocculants were synthesized using reversible addition-fragmentation chain-transfer polymerization. These uniform polyacrylamides were used individually, as low dispersity flocculants, and in blends, as high dispersity flocculants. Flocculation of the kaolinite suspension was monitored using a focused beam reflectance measurement system where the chord-length distribution of the clay aggregates could be recorded in real-time. Polyacrylamide flocculants with lower dispersities made larger clay aggregates than those with higher dispersities at equal doses. In the polymer blends, the fraction of the high molecular weight component was the best indicator of aggregate size formation; the low molecular weight fraction influenced less the final aggregate size. These findings suggest that polymers with narrow molecular weight distributions can be used in lower dosages than standard high dispersity flocculants with a similar concentration of high molecular weight polymer chains.

3.1 INTRODUCTION

Polymer flocculants are extensively used to separate solids from aqueous suspensions in wastewater and mine tailings [22]. They work by two primary mechanisms: polymer bridging, wherein adsorbed polymer chains form bridges between particles and hold them together, or charge neutralization, in which a partially charged polymer or polyelectrolyte destabilizes a suspension by coagulation and/or adsorption through electrostatic attraction or charge patching [19,25]. These two mechanisms are affected by polymer charge and

molecular weight. In the case of bridging flocculation, longer polymer chains facilitate the formation of larger particle aggregates [25].

Common commercial flocculants are synthesized from water soluble monomers via free-radical polymerization in solution, bulk, or emulsion processes. They are classified according to their average molecular weights and, if ionic monomers are used, by their charge densities [22]. Since free-radical polymerization makes polymers with broad molecular weight distributions (dispersity, $Đ \geq 1.5\text{-}2.0$), uniform polymer samples with dispersities below 1.5 can only be produced by post-polymerization fractionation. This limits the potential to fine tune polymers for specific applications and may hinder some detailed studies on structure-property relationships [22].

Synthetic polymers are statistical materials that have distributions of chain lengths. Therefore, a polymer population consists of chains having different molecular weights, typically characterized by one or more average molecular weights. While we know how the average molecular weight of polymers affects their flocculation performances, the effect of the polymer molecular weight distribution (MWD) on flocculation performance has been hardly explored in the literature. One study examined the competitive adsorption of polyacrylamide (PAM) samples of low and high molecular weight averages on silica particles. The authors found that high molecular weight PAM favorably adsorbed, and even displaced, the previously adsorbed low molecular weight PAM [65]. This finding is relevant for flocculation because the bridging mechanism relies on the adsorption of polymer chains onto the particles that need to be flocculated. Even though the monomeric units of homopolymers like PAM are chemically identical, the adsorption of PAM on suspended solids depends on chain length because of differences in translational entropy upon adsorption on the surface: Even though the adsorption energy per monomeric unit is the same in shorter or longer chains, the adsorption of longer chains is favored because they lose less entropy when they are adsorbed from the solution [21,66]. This may lead to differential adsorption on the particle surfaces, as has been demonstrated with PAM absorbed on quartz [65]. A study on the flocculation of polystyrene latex particles with polyethylene oxide has also shown that the particle suspension transitions from stable to

unstable forms more sharply with low dispersity polymer samples as a function of the polymer dose [67].

Since flocculation performance and settling rate depend on polymer molecular weight, and polymer chains of different lengths compete to be adsorbed onto the particles, it is reasonable to expect that differences in the distribution of polymer chain lengths may affect flocculation performance. We tested this hypothesis by synthesizing a series of PAM samples with narrow MWDs by reversible addition fragmentation chain transfer (RAFT) [58,68]. Controlled radical polymerization techniques, such as RAFT and atom transfer radical polymerization, are methods that make polymers with more uniform distributions [55,56]. These methods are often limited in the size of the polymer chains they can produce, but some polymerization techniques can make polymers with molecular weights in excess of 10^6 Da [59,62].

In this investigation, room-temperature RAFT was used to synthesize high molecular weight PAM samples with low dispersities. These narrow MWD polymers were then used in flocculation experiments with kaolinite, a clay that is the major component in the solids suspended in oil sands tailings ponds [8]. To emulate the high dispersity PAM samples that would typically be used in industrial flocculations, blends of the narrow MWD PAM samples synthesized via RAFT were prepared and then evaluated for their flocculation performances. We chose PAM because it is the most common polymer used in flocculation. To isolate the effect of MWD on clay aggregate formation from the equally important effect of ionic charge, we used only neutral PAM samples in this investigation.

3.2 Materials And Methods

3.2.1 Materials

Acrylamide, methyl 2-[methyl(4-pyridinyl)carbamothioylthio]propionate (RAFT agent), 2,2′-Azobis(2-methylpropionamidine) dihydrochloride (V-50), Hydroxymethanesulfinic acid monosodium salt dihydrate (NaFS), ammonium persulfate (APS), kaolinite, and ethanol were purchased from Sigma-Aldrich and used without further purification.

3.2.2 METHODS

3.2.2.1 Synthesis of PAM-RAFT Agent Oligomer

A PAM oligomer was first synthesized with the RAFT agent to ensure good solubility in water for the subsequent polymerization of high molecular weight PAM [58]. The RAFT agent, methyl 2-[methyl(4-pyridinyl)carbamothioylthio]propionate, was first dissolved in a 1:1 solution of ethanol and water. Acrylamide was also dissolved in the solution at a molar ratio of 7:1 (acrylamide:RAFT agent). Oxygen was removed from the solution by purging with nitrogen. The solution was then heated to 60 ˚C and the initiator, V-50, was injected into the solution with a final concentration of 2.5×10^{-3} M. The reaction was stirred at 60 ˚C for 4 h. Ethanol was evaporated and the product was freeze-dried. The structure of the PAM-RAFT agent oligomer was confirmed with ^{1}H NMR. The molecular weight was calculated from NMR to be 697 Da, which corresponds to 6 acrylamide units per oligomer molecule.

3.2.2.2 Synthesis of PAM

The low-dispersity high molecular weight PAM was synthesized at room temperature via RAFT polymerization using a redox initiator [58]. The RAFT agent oligomer was added to a 10 wt% solution of acrylamide in water so that the ratio of monomer to RAFT agent conformed to the desired target molecular weight. The monomer solution was adjusted to a pH of 6 and purged with nitrogen for 45 minutes before the initiator was injected. The polymerization was carried out at room temperature using a NaFS/APS redox initiator system. An equimolar amount of NaFS and APS were used, at a concentration of 60 ppm APS relative to the acrylamide concentration. After the initiator was injected, the solution was stirred at room temperature overnight to ensure complete conversion. The polymer formed was then precipitated in acetone and freeze-dried. The freeze-dried polymer was then analyzed by gel permeation chromatography (GPC) and prepared for flocculation experiments.

3.2.2.3 Polymer Characterization

The polymer samples were characterized by gel permeation chromatography (GPC, Agilent 1260 Infinity Multi-Detector Suite). The triple detection GPC system included two columns (TSK-GEL G6000PWxl-CP) in series with a differential refractive index detector,

a dual angle light scattering detector, and a viscometer. The GPC was calibrated using polyethylene oxide standards. All samples were analyzed in a solution of 0.2 M sodium nitrate.

3.2.2.4 Kaolinite Characterization

The kaolinite clay used in the flocculation experiments was characterized by x-ray powder diffraction (XRD) with a Rigakau Ultima IV using a Co Kα radiation at 38 kV and 38 mA. Scans were from 5° to 90° (2θ). The particle size of the kaolinite suspensions in water before flocculation was measured by laser diffraction using a Malvern Mastersizer 3000.

3.2.2.5 Flocculation Experiments

Flocculation experiments were performed on kaolinite suspensions prepared at 2.5 wt% in deionized water under pH = 8.0, adjusted using NaOH. The suspensions were mixed for at least 72 h to ensure a consistent particle suspension for all experiments. The flocculation experiments were performed in 100 mL batches and monitored using a focused-beam reflectance measurement (FBRM) probe (FBRM G400, Mettler Toledo), where the chord-length distribution of the clay particle sizes was recorded continuously. All PAM solutions were prepared at a concentration of 2 mg/mL and allowed to mix overnight to ensure complete dissolution of the polymer before use in experiments. All polymer doses are reported in ppm, defined as mg polymer/kg solids content. Chord length distributions and mean chord length of the aggregating particles was recorded in 2 s intervals during the flocculation process. The FBRM probe can report data using primary or macro mode. Data was collected in macro mode, as it was determined to be more appropriate for the large flocs formed [69].

3.3 Results and Discussion

3.3.1 Kaolinite Characterization

The kaolinite suspension was characterized by laser diffraction. The volume average particle size distribution was bimodal with one population below 1 μm and a second population between 1 and 10 μm, as depicted in Figure 3-1a. The bimodal population is a result of clay aggregates naturally forming and may change depending on how the

suspensions are prepared [70]. The D10, D50, and D90 averages were 0.658 µm, 1.60 µm, and 5.16 µm, respectively. The XRD pattern of the kaolinite clay (Figure 3-1b) is consistent with the characteristic peaks of kaolinite reported in the literature [71].

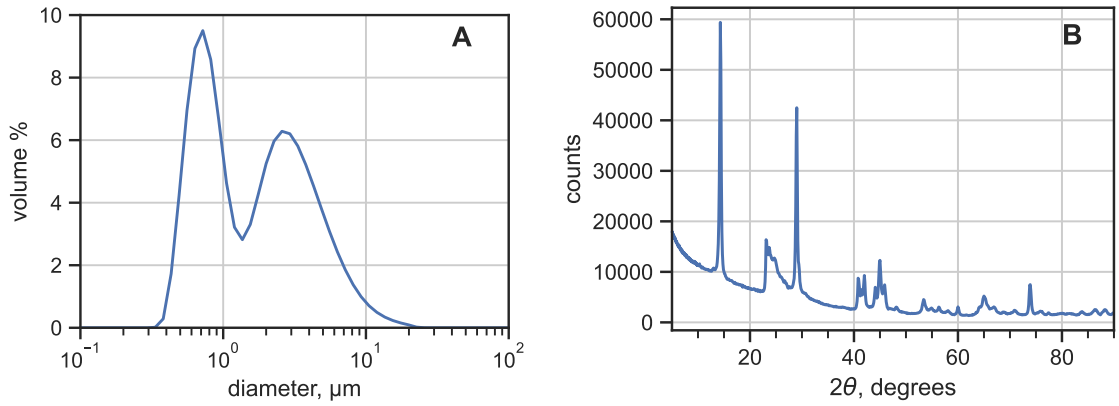

Figure 3-1: a) Particle size distribution of the kaolinite suspension before flocculation (D50 = 1.60 µm, D90 = 5.16 µm), b) XRD pattern of kaolinite.

3.3.2 Polymer Molecular Weight Distributions

Four PAM samples of distinct molecular weight averages were synthesized via RAFT polymerization. The molecular weight averages of each sample are summarized in Table 3-1, with the full MWD compared in Figure 3-2. Lower molecular weight samples were synthesized with dispersities as low as 1.04, but the dispersity increased as the molecular weight of the polymer increased. This is expected for RAFT polymerizations at high conversions because the higher viscosity of the polymer solution may hinder the RAFT agent transfer rates, leading to a broadening of the MWD [56,58]. Nonetheless, the dispersity of the sample with the highest molecular weight ($Đ$ = 1.35) is still substantially smaller than for PAMs synthesized by conventional free radical polymerization ($Đ$ > 1.5).

Table 3-1: Molecular weight averages of the PAM samples used in the flocculation experiments.

Sample	M_n (Da)	M_w (Da)	M_z (Da)	Đ
PAMs1	3.06×10^5	3.11×10^5	3.16×10^5	1.04
PAMs2	8.79×10^5	9.26×10^5	9.70×10^5	1.05
PAMs3	2.60×10^6	2.86×10^6	3.11×10^6	1.10
PAMs4	2.63×10^6	3.55×10^6	4.39×10^6	1.35

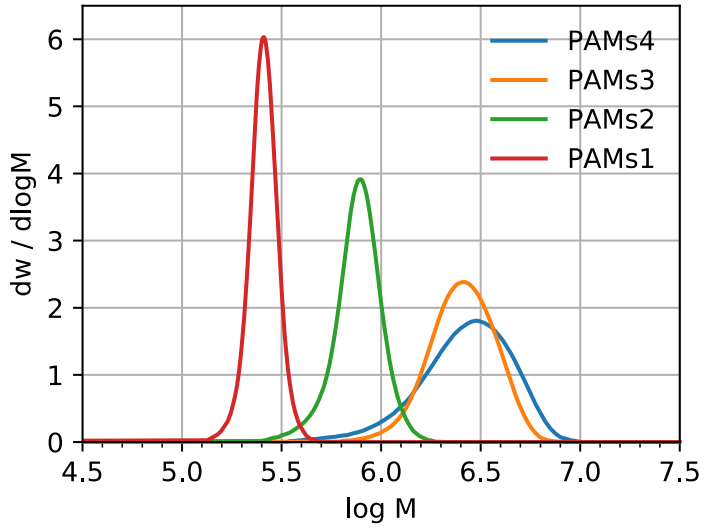

Figure 3-2: Molecular weight distributions of the narrow PAM samples used for flocculation.

A series of broad MWD samples were prepared as blends of the uniform MWD PAM samples. Binary and ternary were made by mixing equal mass fractions of the narrow PAM samples to create the blends. Their molecular weight averages and dispersities are summarized in Table 3-2. These samples were prepared to create broad MWD polymer samples to be used in comparative flocculation experiments.

Table 3-2: Molecular weight averages of PAM blends used in the flocculation experiments. Binary blends are made in 50/50 wt% ratios, and ternary blends in 33/33/33 wt% ratios.

Sample	M_n (Da)	M_w (Da)	M_z (Da)	Đ
PAMb12	3.78×10^5	6.23×10^5	8.02×10^5	1.65
PAMb13	4.77×10^5	1.58×10^6	2.84×10^6	3.32
PAMb23	1.06×10^6	1.89×10^6	2.59×10^6	1.78
PAMt123	5.28×10^5	1.37×10^6	2.42×10^6	2.59
PAMb24	1.06×10^6	2.24×10^6	3.68×10^6	2.11
PAMb34	2.54×10^6	3.20×10^6	3.84×10^6	1.26
PAMt234	1.32×10^6	2.45×10^6	3.47×10^6	1.86

Each sample in this study was labeled PAMs for single, narrow dispersity, polymer samples, PAMb for binary mixtures, and PAMt for ternary mixtures. The numbers after the label correspond to the single sample polymers.

3.3.3 Flocculation of Kaolinite

Polymer flocculation was tested using a model system consisting of kaolinite suspended in water (2.5 wt%) with 1000 ppm $CaCl_2$ (0.2 mM). FBRM data was continuously recorded in 2 s intervals for the duration of the experiment. An example of the dynamic change in aggregate size is shown in Figure 3-3. The mean aggregate size increased rapidly after the addition of polymer to the suspension. After polymer addition, the aggregates size was allowed to equilibrate for 2 minutes before an average aggregate size was recorded, based on the chord length data collected for a 2-minute interval after steady-state was reached.

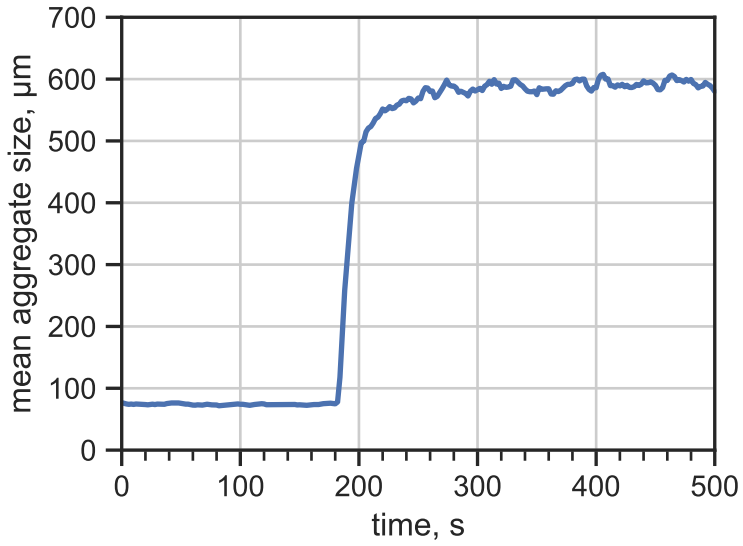

Figure 3-3: Change in kaolinite aggregate size over time due to flocculation with PAM. The flocculant addition at 180s (PAMt123, 2500 ppm) was followed by a rapid increase in particle size, as measured by FBRM.

The mean aggregate sizes are presented in Figure 3-4 and Figure 3-6, based on the mean square chord length measured via FBRM, which correlates with the volume average diameter of an aggregate as measured via laser diffraction [69].

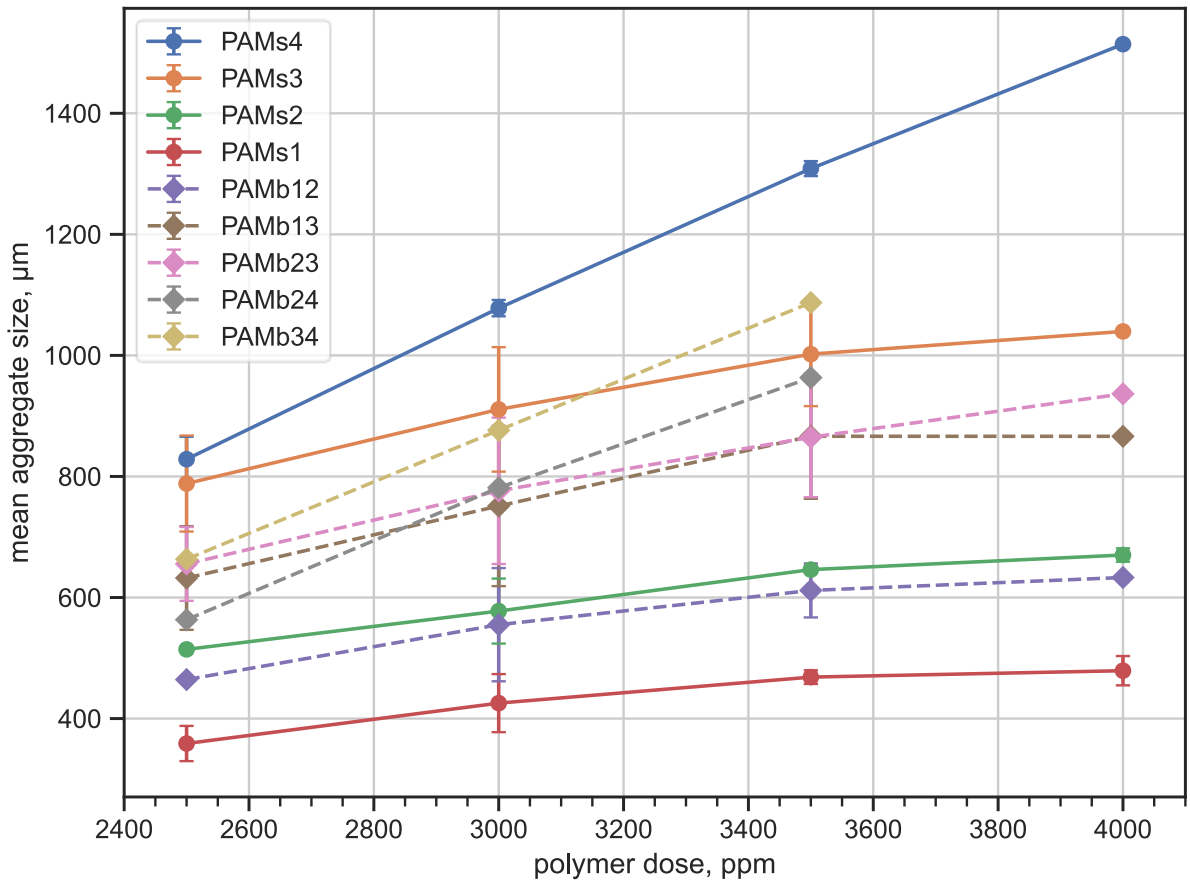

Figure 3-4: Mean aggregate size formed after the addition of PAM at different doses. Binary PAM blends are compared to single low dispersity PAM samples.

Figure 3-4 compares the aggregate sizes formed with the addition of the PAM flocculant as either single narrow-MWD homopolymers or broad-MWD binary blends. For all cases, the mean aggregate size increases with PAM molecular weight and polymer dose. Aggregate sizes begins to level off for dosages of about 3500 ppm for all samples, except for those containing the highest molecular weight sample, PAMs4. This leveling off effect is consistent with the flocculation literature: a plateau in optimum polymer dose is reached before the aggregate sizes start declining due to overdosing [12,72], which is attributed to an excess of adsorbed polymers sterically stabilizing the particles and preventing the formation of additional polymer bridges [25].

The mean aggregate sizes formed using single PAM samples (PAMs series) were always higher than those formed with the binary blends (PAMb series), with the size difference ranging between 20 and 120 μm. The polymer blends formed clay aggregates with sizes that fell in between the sizes formed from the single PAMs components (except for PAMb34, which formed smaller aggregates than PAMs3 at low doses). Even though an equal mass fraction of each PAMs component was used to make the binary PAMb blends, the size of the formed clay aggregates was not the average of the sizes formed with each PAMs component, but followed more closely the trends of the high MW component in the blend. This is apparent when comparing PAMb13 and PAMb23: both blends share the same high MW component (PAMs3) but have different low MW components (PAMs1 and PAMs2, respectively). The average sizes of the aggregates formed with the blends are similar, but they are smaller than those made with PAMs3 (PAMs3 > PAMb13 ≈ PAMb23 > PAMs2 > PAMs1). This suggests that the high MW component in the blend is responsible for most of the flocculation, likely because the polymer flocculants perform better when their MW increase [22,25]. Because the high MW fraction of a polymer sample affects more its flocculation performance, a narrow MWD polymer flocculant will have a larger effective dose of the high MW component than a broad MWD polymer that have overlapping MWDs. Figure 3-5 illustrates this point: both narrow and wide MWD polymers have chains with high MW, but the wide MWD polymer also contains a significant fraction of low MW chains that are not effective flocculants and, thereby, a lower dose of the more effective high MW chains.

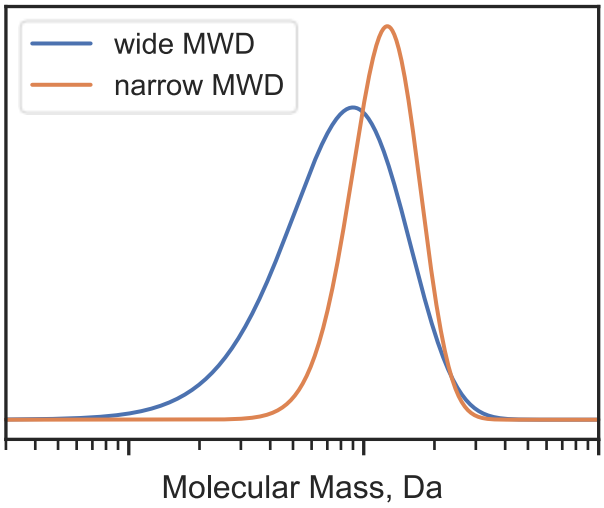

Figure 3-5: Representation of a molecular weight distributions from two polymer samples, one with a wide MWD and one with a narrow MWD. Both samples contain high molecular weight polymer, but the wide MWD sample has a large fraction of shorter polymer chains that do not contribute as much to flocculation.

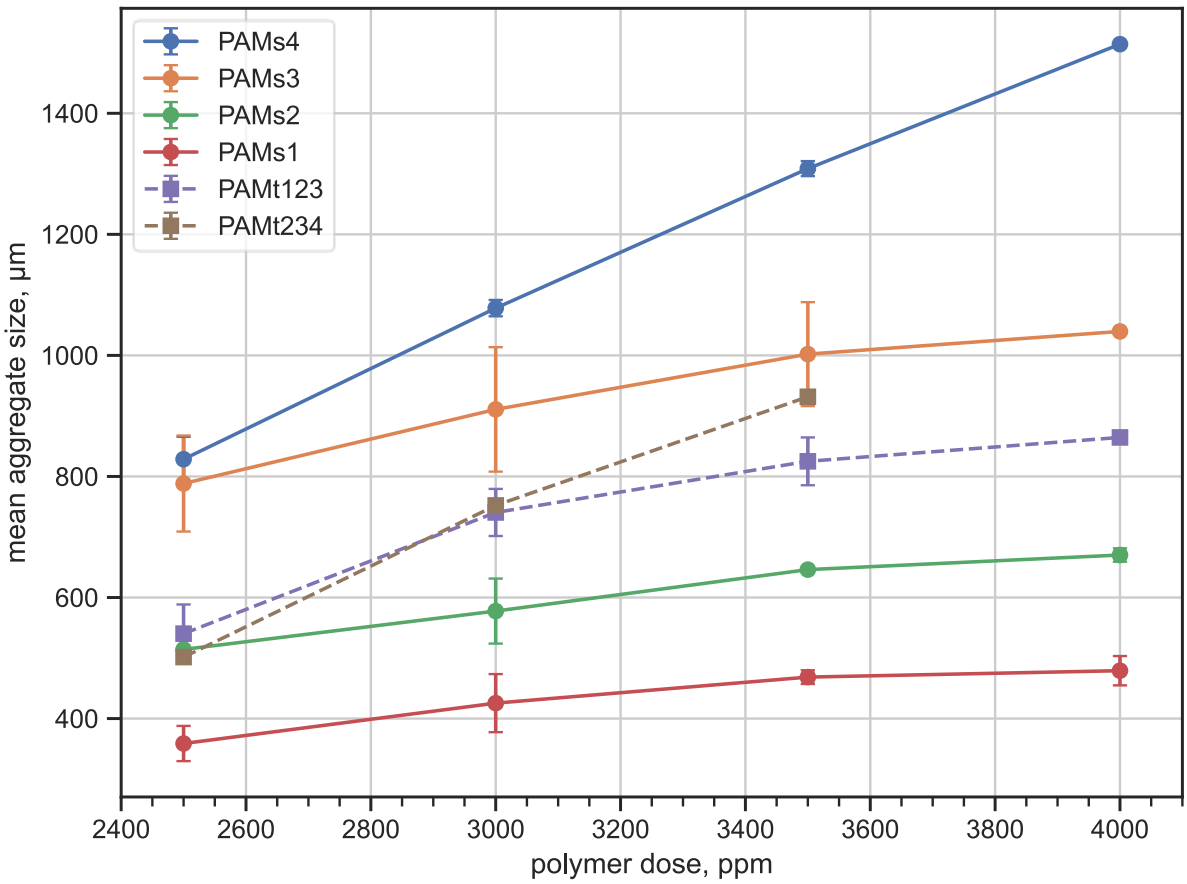

Figure 3-6: Mean aggregate size formed after the addition of PAM at different doses. Ternary PAM blends are compared to the single low dispersity PAM samples.

Figure 3-6 compares the mean aggregate sizes formed with PAM ternary mixtures (PAMt series) and the narrow PAMs series. The results are similar to those found for the binary mixtures. The narrow PAMs flocculants made larger aggregates than the ternary PAMt blends. For the ternary mixtures, the difference in aggregate size formed between their narrow components and the mixtures at the same dose was even more pronounced. The difference between the mean aggregate size of the highest MW homopolymer and the ternary mixtures was at least 200 µm.

To quantify the contribution the high MW fraction in each polymer blend has on the aggregate size, a required dose to get the same aggregate size as the blends using the single

low dispersity samples (PAMs series) was calculated from the linear regression of the PAMs samples. The ratio of the required dose to the actual dose used for the blends indicates what reduced dose may be used if only the high MW, low dispersity samples were used. It may also be thought of as the fraction of the polymer blend required to have chain lengths found in the high MW portion of the blend when maintain the same high dose. The required dose was determined and the ratios between the required and actual dose for the polymer blend experiments are summarized in Table 3-3.

Table 3-3: Ratio of the required dose to achieve the same aggregate size formation using low dispersity PAMs samples to the actual dose used in experiments with the polymer blends.

	Required Dose : Experimental Dose		
Sample	***2500 ppm***	***3000 ppm***	***3500 ppm***
PAMb12	0.79	0.94	0.95
PAMb13	0.58	0.72	0.81
PAMb23	0.64	0.77	0.81
PAMt123	0.37	0.70	0.74
PAMb24	0.76	0.79	0.79
PAMb34	0.85	0.86	0.87
PAMt234	0.70	0.77	0.77

From Table 3-3, the ratio of the required dose of the narrow MWD polymer to the dose used in the experiments with the polymer blends are all below unity. This quantifies what was discussed regarding Figure 3-4 and Figure 3-6, using the low dispersity homopolymers you can achieve the same mean aggregate size with a lower dose. Each ratio is higher than the mass fraction of the high molecular weight present in the blend, further demonstrating that the high MW chains of the polymer samples contribute more to the aggregate size formation than the low MW fraction of the sample. By using more narrowly dispersed

polymer blends you can get similar aggregate size formation at a reduced polymer mass dosage.

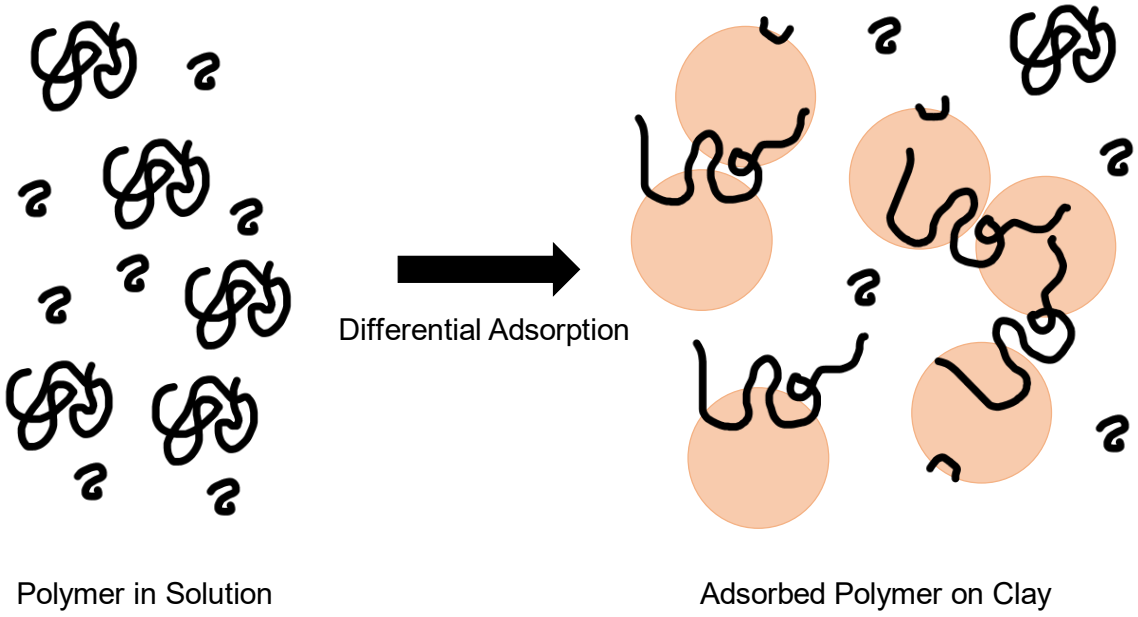

Figure 3-7: Illustration of the process of polymer differential adsorption in polydisperse samples. Longer polymer chains are more abundant on the particle surface and extend further into solution.

Two explanations may be proposed for these observations, as illustrated in the scheme shown in Figure 3-7. First, as the polymers adsorb onto the particle surface, the longer chains will form larger loops and longer tails [21,73]. Because the longer polymer chains will extend further out from the particle surfaces, they are more likely to initiate flocculation. Consequently, the formed aggregate structures will more closely resemble those made with the long, high MW polymer chains. Second, due to a reduced entropic penalty, the high MW chains will more favorably adsorb onto the particle surfaces than the shorter chains; consequently, the fraction of long polymer chains on the surface is higher than in solution [21,23,66]. This differential adsorption was also seen on a similar system with PAM and quartz particles [65]. This will result in clay aggregates that more closely match the characteristics of aggregates made with high molecular weight flocculants.

Aggregates formed with the high dispersity flocculants approached, but never reached, the mean aggregate sizes formed when low dispersity polymers were used alone because there was a lower effective dose of the high MW fraction in solution along with the presence of shorter chains which still adsorb in some amount.

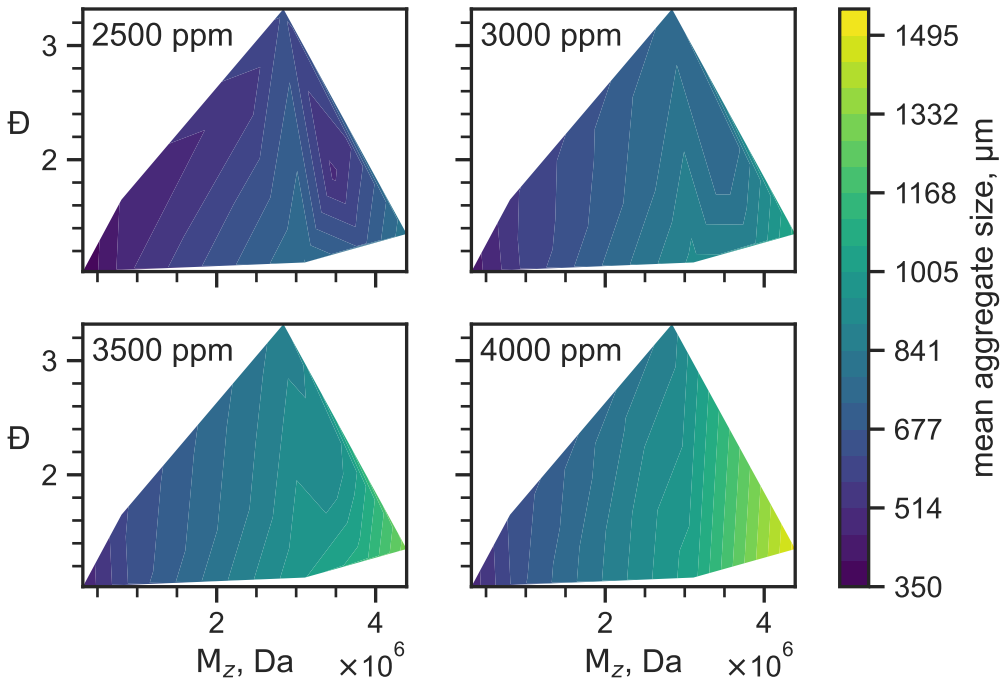

Figure 3-8: Contour plot of PAM dispersity versus z-average molecular weight for different PAM doses. Contour levels indicate mean clay aggregate size.

The experimental findings in the present study are evidence that the MWD of the polymer flocculant does influence the size of clay aggregates. In particular, the longer polymer chains have a greater influence on flocculation than the shorter chains. To further illustrate this point, Figure 3-8 shows the mean clay aggregate sizes formed as a function of both z-average molecular weight, M_z, and dispersity, $Đ$ (M_z was used because the largest polymer chains in a sample are those that control the flocculation, making this average more suitable in distinguishing between the samples). The mean aggregate size increases as polymer dose and M_z increase, as also demonstrated in Figure 3-4 and Figure 3-6. Adding dispersity as a third dimension reveals how the MWD also influences aggregate size. The largest

aggregates appear at low dispersity and high average molecular weight with the trend becoming more pronounced at higher doses where optimal flocculation is occurring.

3.4 CONCLUSIONS

This work looked at the role the molecular weight distribution of polymer flocculants has on the size of aggregates of clay particles. Polyacrylamide samples of different dispersities synthesized via RAFT polymerization were used in the flocculation of kaolinite particles suspended in water. Low dispersity PAM samples formed larger clay aggregates than those made with to broad molecular weight distribution samples at the same dose, or formed the same size aggregates as the broad MWD PAM made from the low dispersity samples at lower doses. The high molecular weight fraction of a polymer sample was determined to be the best indicator of aggregate size formed. This study with a model clay system is the first step toward understanding how tuning the MWD of flocculants can affect more complex industrial samples that contain clays. Recent work on how to control the shape of a polymer MWD during synthesis is a potential path to achieve even more control on the polymer size distribution [74–76]. Further work to test polymer flocculants with well controlled molecular weight distributions on industrial mineral tailings samples is desired, as the potential for reducing the amount of material required for the separation process is promising.

Chapter 4 DUAL ANIONIC AND CATIONIC POLYMER FLOCCULANTS FOR THE TREATMENT OF OIL SANDS TAILINGS - A STUDY OF DOSE AND CHARGE DENSITY

A two-step flocculation process using oppositely-charged polymers to treat oil sands mature fine tailings (MFT) was investigated using anionic hydrolyzed polyacrylamides (HPAM) and cationic poly(vinylbenzyl trimethylammonium chloride) (PVBTMAC). The effects charge density of HPAM and dosage combinations of HPAM and PVBTMAC were studied to achieve maximum dewatering of the MFT and minimum turbidity in the supernatant water. Using two flocculants resulted in better performance at lower doses compared to using each flocculant individually. HPAM with a charge density near 32 % led to the fastest initial settling rates and higher solids content in the sediment, but charge densities above 38 % were best for dewatering of the sediment by filtration or as measured by CST. Cationic PVBTMAC neutralized the anionic charges in the MFT slurry and the clearest supernatants were found when the zeta potential approached 0 mV. Undiluted MFT was flocculated with HPAM and PVBTMAC and then filtered at low-pressure (69 kPag), resulting in a filter cake consisting of 61 % solids. This study demonstrates the potential of two polymer flocculant systems for the treatment of MFT and the flexibility offered when optimizing with two polymers to improve flocculation performance.

4.1 INTRODUCTION

The extraction of bitumen from oil sands deposits is an energy and water-intensive process that produces a tailings byproduct that contains sands, clays, water and residual bitumen [3,4]. In-situ extraction processes can consume about 0.2 barrels of non-saline water per barrel of oil produced and surface mining operations can require up to 2.5 barrels of water per barrel of oil produced [2]. Water recycling is extensively used in the industry, but challenges remain in the treatment and recovery of water from mature fine tailings ponds [4,5]. Mature fine tailings (MFT) are what remains after the slurry from the water

extraction process is allowed to settle. Once the coarse particles settle out, the remaining material forms a stable suspension that will not separate from water [5,15].

MFT consists of fine clays, sand, and residual bitumen suspended in water. The solids typically make up 30 – 40 % of MFT by weight and bitumen below 5 %; the remaining mass is water. Treatment of mineral tailings, including MFT, using polymer flocculants is a widely used approach to dewater tailings, allowing for further consolidation and water recovery [22,46]. The most common flocculants used to treat MFT are anionic polyacrylamide (PAM), but their effectiveness as the sole treatment method is limited when it comes to the thick MFT slurries due to their tendency to retain water [4,6,12]. Modifications of PAM and novel polymeric materials have been investigated to improve the dewatering of MFT with positive results, but often are limited by high dose requirements [6,22,46].

Recent studies on the use of two polymer flocculants for the treatment of MFT show that they can outperform single polymers [46,47,49–51,54,77–79]. Lu *et al.* (2016) used a commercial anionic PAM flocculant with the natural cationic polymer chitosan to treat of oil sands tailings. The dual polymer combination achieved faster particle settling rates than with only chitosan, and better supernatant clarity than with anionic polyacrylamide alone [47]. Loerke *et al*. (2017) treated MFT with dual polymer flocculants followed by a filter press operation to enhance dewatering. They studied both the combination of an anionic PAM with the cationic polydiallyldimethylammonium chloride (polyDADMAC) and with a neutral polyethylene oxide and found that the dual polymer system increased the solids content in the flocculated material compared to any of the polymers alone [49]. Recently Zhou *et al.* (2021) used a dual system of anionic PAM with a hybrid aluminum hydroxide-PAM to treat MFT slurries with different sands to fine solids ratios [50]. They found that the use of dual polymers reduced the total polymer dose required and that higher solids content could be achieved in the sediment with the addition of larger sand particles [50].

The mechanism of flocculation using two oppositely-charged polymers has been attributed to the complementary roles the anionic and cationic polymers have in flocculation. Large anionic polymers act as bridging flocculants, bringing the solids together; the subsequent addition of the cationic polymer induces charge neutralization in the solution, which further

consolidates the flocs and helps remove fines, producing a clear supernatant [47,50,53]. The use of dual polymer systems for the flocculation of MFT is a promising innovation that allows us to reduce polymer dosage and increase water release from tailings. But the addition of a second polymer also adds complexity when optimizing the process for MFT treatment, since both polymers must be optimized for molecular weight, charge density, and dosage. And performance may also be affected by other factors such as how the polymers and MFT are mixed and the complex chemical and physical composition of MFT.

Many of the dual polymer systems previously studied rely on oppositely-charged polymers, with the addition of the cationic polymer required for charge neutralization in mineral tailings flocculation. Naturally, the dosage required for each polymer is dictated, in part, by the charge density of the polymers if charge-neutralization flocculation is to be achieved. The charge density of the polymer used in a dual polymer flocculation system has been underexplored in the literature to date. In this paper, we used a response surface method (RSM) experimental design to study three factors in the flocculation of MFT using two oppositely-charged polymers: anionic polymer dose, cationic polymer dose, and anionic polymer charge density. A series of anionic, hydrolyzed PAM samples were synthesized with the same chain length but varying degrees of anionic charge and used with the cationic poly(vinylbenzyl trimethylammonium chloride) to flocculate diluted MFT (10 wt % solids) and undiluted MFT. Optimal factors were determined based on initial settling rate, capillary suction time (CST), solids content of the sediment, and supernatant turbidity. We also demonstrated that at optimum polymer doses, a low pressure filter press can be used with undiluted MFT to achieved high solids content in the filter cake.

4.2 Materials and Methods

4.2.1 Materials

Acrylamide, (vinylbenzyl)trimethylammonium chloride, 2,2′-Azobis(2-methylpropionamidine) dihydrochloride (V-50), sodium chloride, potassium chloride,

magnesium chloride, calcium chloride, and acetone we purchased from MilliporeSigma. Mature fine tailings samples were provided through the Institute for Oil Sands Innovation.

4.2.2 METHODS

4.2.2.1 Synthesis of PVBTMAC

Poly(vinylbenzyl trimethylammonium chloride) (PVBTMAC) was synthesized via free-radical polymerization. A 0.5 M solution of (vinylbenzyl)trimethylammonium chloride was prepared in deionized water and purged with nitrogen gas for 45 minutes before the initiator, V-50, was added to a final concentration of 1 mM in the reaction solution. The reaction was stirred overnight at 50 ˚C. The polymer product was precipitated in acetone and freeze-dried before use in flocculation experiments.

4.2.2.2 Synthesis of PAM and HPAM

A single batch of polyacrylamide (PAM) was made via free-radical polymerization from which all hydrolyzed PAM samples were created. A 0.5 M solution of acrylamide monomer was prepared in deionized water and purged with nitrogen for 1 hour. The initiator, V-50, was then added to make a 0.05 mM concentration in the solution. The reaction was mixed overnight at 50 ˚C. The PAM product was then precipitated in acetone and freeze-dried.

Five samples of hydrolyzed PAM (HPAM) were prepared via base hydrolysis from the PAM previously synthesized. PAM solutions were prepared at a concentration of 10 mg/mL in deionized water. Once the polymer was dissolved, the temperature was raised to 70 ˚C and the reaction flask was purged with nitrogen. Five HPAM samples were then hydrolyzed with 1.79, 5.63, 11.3, 16.9, and 20.7 mmol of NaOH using a 1M stock solution. The reaction was stirred for 16 h at 70 ˚C. The polymer products were precipitated in acetone and freeze dried before characterization.

4.2.2.3 Polymer Characterization

All polymer samples were characterized by gel permeation chromatography (GPC, Agilent 1260 Infinity Multi-Detector Suite). The triple detection GPC system included two columns in series with a differential refractive index detector, a dual angle light scattering detector, and a viscometer. The GPC was calibrated using polyethylene oxide standards.

The PVBTMAC samples used the TSK-GEL G6000PWxl-CP column (Tosoh Bioscience) with a mobile phase consisting of 300 mM sodium sulfate, 50 mM acetic acid, and 2 mM sodium acetate. The PAM and HPAM samples used the PL aquagel-OH MIXED-H column (Agilent) with a 200 mM sodium nitrate mobile phase. The HPAM samples were further characterized with ATR-FTIR (Agilent Cary 660 FTIR spectrometer) and CHNS elemental analysis (Thermo Flash 2000 Elemental Analyzer) to determine the degree of hydrolysis for each sample.

4.2.2.4 MFT Characterization

The solids, water, and bitumen content in MFT samples were determined using a Dean Stark apparatus [80]. MFT was weighed in an extraction thimble and water and bitumen were separated from the solids using boiling toluene. The water was collected and weighed and mass of the remaining solids after extraction was also measured. Bitumen content was calculated from the difference between the mass of the MFT sample and the combined mass of the water and solids collected after extraction. The major cation concentration in the MFT sample was determined by ICP-OES (Thermo iCAP6300 Duo ICP-OES). Dried MFT solids were characterized by X-ray powder diffraction (XRD) with a Rigakau Ultima IV using a Co Kα radiation at 38 kV and 38 mA. Scans were from 5° to 90° (2θ). Major mineral components were identified and quantified using the reference intensity ratio (RIR) method.

4.2.2.5 Flocculation Experiments

Flocculation of diluted MFT and undiluted MFT was done using a dual polymer flocculation procedure. All diluted MFT samples were prepared to a final solids content of 10 wt %. The MFT was diluted with a salt solution prepared to match the salt content of the undiluted MFT sample to avoid changing the ionic strength of the solution when diluting the samples. The high ionic strength will additionally improve dewatering performance [81]. This salt solution consisted of 33.8 mM sodium chloride, 2.1 mM potassium chloride, 1.4 mM magnesium chloride, and 0.4 mM calcium chloride in deionized water. The same salt solution was used to prepare 2 mg/mL polymer flocculant solutions. Flocculation experiments were carried out in a 250 mL beaker using a four arm, pitch blade impeller. The MFT samples were stirred at 250 rpm for 2 minutes followed by the addition of the anionic HPAM, the solution was mixed for 1 minute and then the

cationic PVBTMAC was added. The solution was mixed for an additional 2 minutes to allow for floc formation and the particle size to stabilize. The flocculated sample was then evaluated based on the initial settling rate of the flocs, the capillary suction time of the flocs formed, the turbidity of the supernatant, zeta potential of the supernatant, and the solids content of the floc sediment. Undiluted MFT samples were evaluated based on the solids content of the sample after filtration and drying.

Initial settling rate tests were performed in 100 mL graduated cylinders. The flocculated MFT sample was carefully transferred to the cylinders then the cylinder were sealed and inverted three times before being placed on a level surface. The settling of the flocs was recorded and the height of the mudline was documented for the first 20 minutes and a final sediment height was recorded 24 hours after the start of the settling rate test. Capillary suction time was measured using a Triton Electronics Type 319 Multi-purpose CST, each test was repeated in triplicate with 5 mL of the flocculated sample. 24 hours after the settling rate test the supernatant of the flocculated solution was collected and the turbidity was recorded in nephelometric turbidity units (NTU) using a Hach 2100AN turbidimeter. The zeta potential of the supernatant was also measured with a Malvern Zetasizer Nano ZS. The sediment of the flocculated sample was poured over a 1 mm screen to separate free water from the solid sample. The sample was then weighed and dried at 65 ˚C for 24 hours. The dry mass of the sediment was recorded and the solids content was calculated. For undiluted MFT samples the flocculated sample was filtered under 69 kPag (10 psig) of pressure using compressed air for 5 minutes (OFI Testing Equipment Low Pressure Filter Press). Flocculation followed by filtration has been demonstrated as an effective method for improved dewatering of MFT [6,31,49,78]. The filtered sample was then collected weighed, and dried at 65 ˚C for 24 hours.

4.2.2.6 Experimental Design

Flocculation experiments were carried out using a three-factor, rotatable central composite design consisting of a 2^3 factorial design with 6 axial points and 3 centre points. The factors were the dose of the anionic HPAM, dose of the cationic PVBTMAC, and charge density of the anionic HPAM. A multiple linear regression model was used to evaluate the relationship between the factors and the flocculation responses: initial settling rate (ISR), capillary suction time (CST), solids content, and zeta potential. The general form of the

multiple regression model is described by Equation (4-1), where Y_i is the i^{th} predicted response, β_0 is a constant parameter, and β_i, β_{ii}, and β_{ij} are coefficients for the coded independent variables X_i and X_j.

$$Y_i = \beta_0 + \sum_{i=1}^{n} \beta_i X_i + \sum_{i=1}^{n} \beta_{ii} X_i^2 + \sum_{i=1}^{n-1} \sum_{j=i+1}^{n} \beta_{ij} X_i X_j \qquad (4\text{-}1)$$

The model fit was evaluated using the analysis of variance method and the surface response was plotted using significant coefficients of the model.

4.3 Results and Discussion

4.3.1 Polymer Synthesis and Characterization

The molecular weight of PVBTMAC and HPAM was determined by GPC with the averages summarized in Table 4-1 and the full molecular weight distribution in Figure 4-1. The weight average molecular weight for PAM and PVBTMAC was 1.21 × 10^6 g/mol and 2.82 × 10^6 g/mol, respectively. The dispersity of each sample is characteristic of polymers synthesized via free radical polymerization.

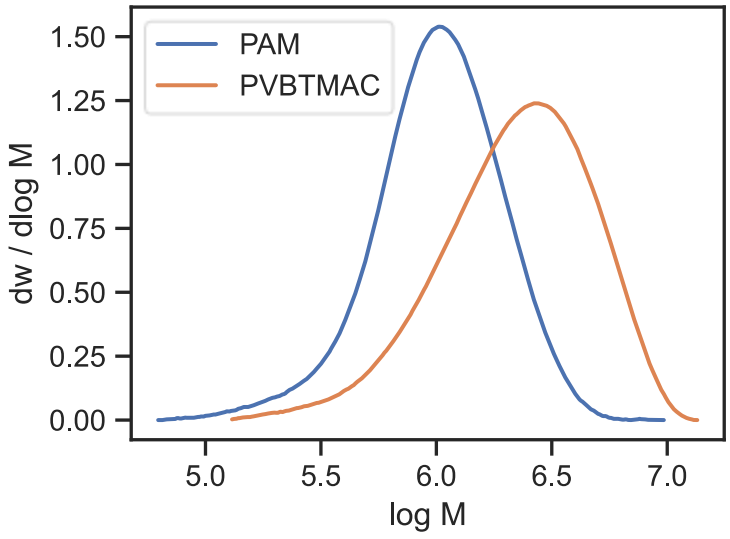

Figure 4-1: Molecular weight distribution of PAM and PVBTMAC.

Table 4-1: Molecular weight averages of PAM and PVBTMAC

Sample	$\mathbf{M_n}$ (g/mol)	$\mathbf{M_w}$ (g/mol)	$\mathbf{M_w / M_n}$	**Zeta Potential** (mV)
PAM	8.16×10^5	1.21×10^6	1.5	0.6 ± 0.6
PVBTMAC	1.62×10^6	2.82×10^6	1.7	61 ± 7

Hydrolyzed PAM samples (HPAM) were made using a single batch of PAM to ensure the same molecular weight of the polymer backbone. Partial conversion of acrylamide functional groups to acrylic acid functional groups was confirmed with FTIR spectroscopy and CHN elemental analysis. The degree of hydrolysis, defined as the percentage of functional groups converted to acrylic acid, was calculated from the C:N ratio in the elemental analysis. Additionally, the zeta potential of each HPAM sample was measured while in the salt solution used in all flocculation experiments (33.8 mM NaCl, 2.1 mM KCl, 1.4 mM $MgCl_2$, and 0.4 mM $CaCl_2$). The degree of hydrolysis and zeta potential values are summarized in Table 4-2.

Table 4-2: Degree of hydrolysis and zeta potential of HPAM samples

Sample	**Degree of Hydrolysis** (%)	**Zeta Potential** (mV)
HPAM1	8.6 ± 0.5	-18 ± 3
HPAM2	20.6 ± 0.1	-31 ± 5
HPAM3	37.0 ± 0.1	-33 ± 5
HPAM4	45.4 ± 0.1	-36 ± 8
HPAM5	49.3 ± 0.1	-38 ± 7

As expected, the zeta potential decreases with increasing degree of hydrolysis. The fraction of hydrolyzed functional groups decreases at higher doses of NaOH, deviating more from full stoichiometric conversion, likely due to mass transfer limitations during the reaction – the high molecular weight polymer solution was viscous and not all functional groups would be accessible during the reaction. Declining reaction rates with increased conversion have also been observed with the based catalyzed reaction at high pH [82–84]. Evidence

of hydrolysis is further confirmed via the FTIR spectra of the HPAM samples (Figure 4-2): the amide carbonyl stretch at 1650 cm^{-1} and the NH bending peak at 1600 cm^{-1} decrease as the carboxylate symmetric stretch peak increases with hydrolysis at 1556 cm^{-1}.

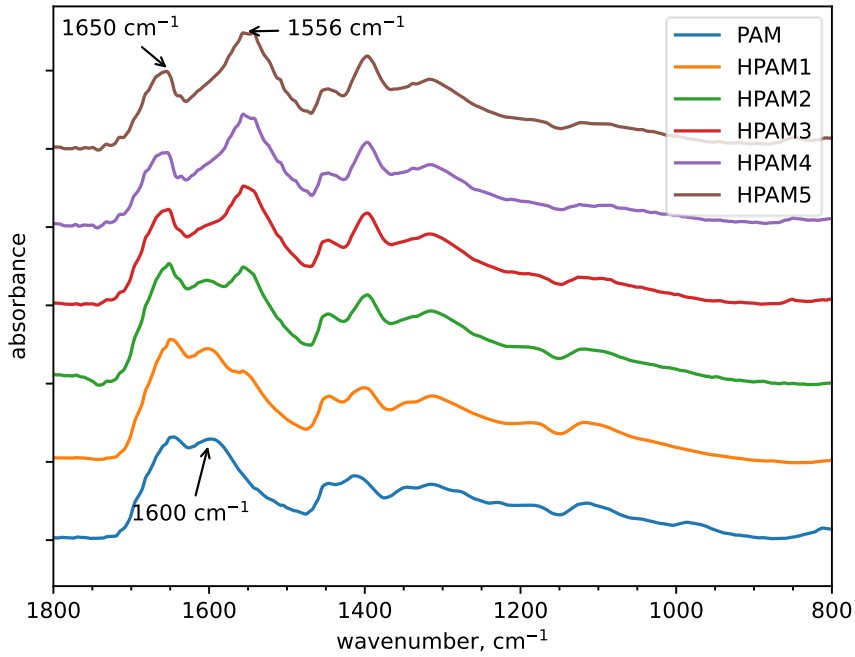

Figure 4-2: ATR-FTIR spectra of the PAM samples. Carboxylate peak at 1556 cm^{-1} increases with increased degree of hydrolysis.

4.3.2 MFT CHARACTERIZATION

The solids, water, and bitumen fraction of the MFT sample used in this study was estimated after Dean-Stark extraction. The average solids composition was 32.5 wt %, the water content was 64.2 wt %, and the residual bitumen was 3.3 wt %. Major cations in the water were measured by ICP-OES. In order of abundance, Na^{+}, K^{+}, Mg^{2+}, and Ca^{2+} were present in concentrations of 777, 83.8, 33.3, and 17.4 mg/L, respectively. Dried solids from the MFT sample were also analyzed by XRD (Figure 4-3), where the major phases were identified and the reference intensity ratio (RIR) method was used to estimate the relative abundance of the minerals: quartz (61 %) was the major component, followed by kaolinite

(17 %), and muscovite (13 %) as the major clay fractions. Minor components included hydroxylapatite (3 %), anatase (2 %), and rutile (1 %).

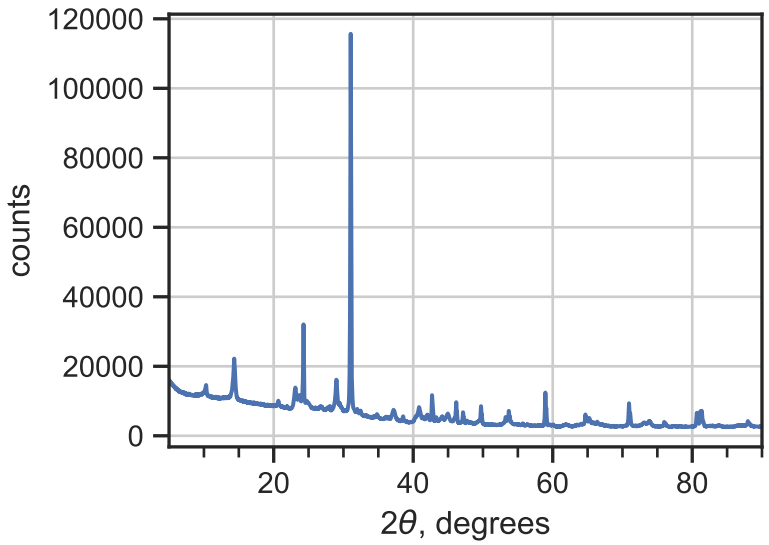

Figure 4-3: XRD pattern of dried MFT.

4.3.3 Flocculation Experiments

Preliminary experiments were done to determine the order of dosing the cationic and anionic polymers. Equal doses of 1500, 2500, and 3500 ppm (g polymer / kg solids) were evaluated for the case of anionic polymer first and the cationic polymer second. Then the reverse, the cationic polymer followed by the anionic polymer. HPAM4 and VBTMAC were the polymers used in the initial screening. Figure 4-4 depicts a settling test 24 hours after flocculation. In each case, adding the anionic polymer first produced a more compact sediment and a more clear supernatant than adding the cationic polymer first. Therefore, in the full experimental design the anionic HPAM polymers were added first.

Control experiments using only HPAM or PVBTMAC were also done. For both polymers, the single flocculant experiments did not perform as well as the dual polymer system within the same dose range. HPAM4 at 1500, 3500, and 5500 ppm resulted in an ISR of 1.2, 0.3, and 0.1 m/h, a CST of 74, 168, and 195 s, and a solids content of 31 %, 30 %, and 27 %,

respectively. PVBTMAC HPAM4 at 1500, 3500, and 5500 ppm resulted in a CST of 198, 128, and 13 s, and a solids content of 20 %, 12 %, and 18 %, respectively. IST was not measurable in the case of the PVBTMAC flocculation at 1500 and 3500 ppm; at 5500 ppm it was 0.2 m/h.

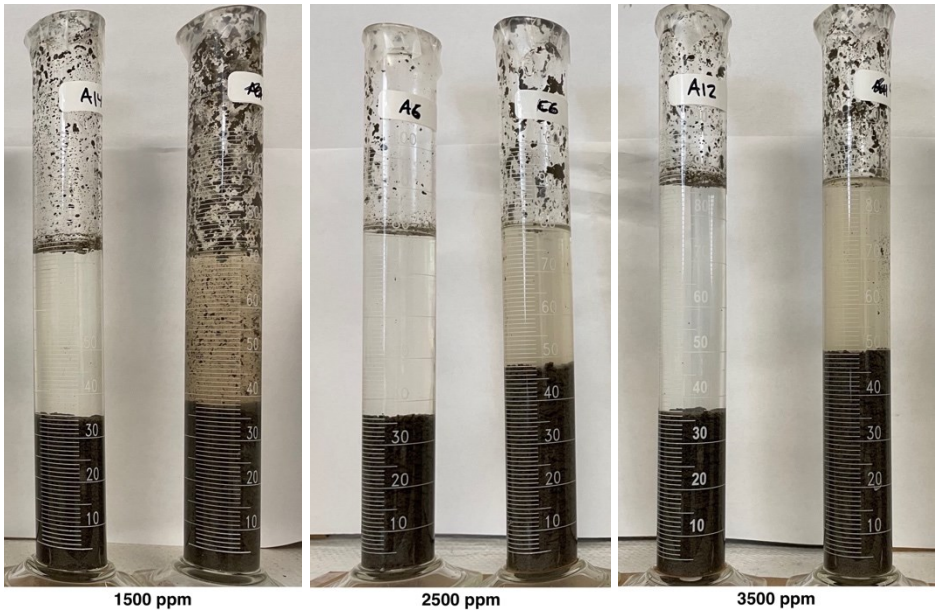

Figure 4-4: Screening test for order of polymer addition at 1500, 2500, and 3500 ppm doses of anionic and cationic flocculants. The left cylinder for each dose is when HPAM4 was added first. The right cylinder for each dose is when PVBTMAC was added first. Pictures were taken 24 hours after flocculation.

A central composite design with three factors – anionic polymer dose, anionic polymer charge, and cationic polymer dose – was used to study the initial settling rate, supernatant turbidity, solids content of the sediment, and the supernatant zeta potential. A summary of all the flocculation results can be found in Table C-1, Table C-2, and in the supporting information.

4.3.3.1 Initial Settling Rate

The initial settling rate (ISR) of MFT diluted to 10 wt % solids was measured after flocculation over a range of HPAM and PVBTMAC doses from 818 ppm to 4182 ppm, and charge density of HPAM from 9 % to 49 %. Data from these experiments are

summarized in Table C-1 and the statistical analysis of the parameter estimates can be found in Table C-4. The maximum observed ISR was 27.2 m/h when the HPAM charge density was 21 % and the treatment dose of 3500 ppm HPAM and PVBTMAC was used. Significant parameters evaluated at the 95% confidence interval ($p < 0.05$) were used in the regression model, Equation (4-2), and a summary of the ISR results are in Figure 4-5.

$$ISR = 20.46 + 3.54X_{HPAM} - 2.87X_{Charge} - 5.81X_{Charge}^2 \quad (4\text{-}2)$$

The ISR of the flocculated MFT was influenced by both the HPAM dose and charge density. The dose of PVBTMAC was not a significant factor in changing ISR. This is likely because cationic flocculants make smaller flocs than those formed using PAM [85]. Since the rate of particle setting is proportional to particle size, a flocculant that makes larger floc sizes lead to higher settling rates. In this case, the presence of the PVBTMAC did not influence flocculant size, but the dose of HPAM was positively correlated with ISR. From the regression model, the charge density of HPAM has an optimum around 30 %. Increasing the charge density of a polymer will cause the polymer to adopt a more extended conformation in solutions making bridging flocculation more efficient, but if the charge density is too high, the negative charges on the polymer chain and on the clays begin to hinder polymer adsorption [22].

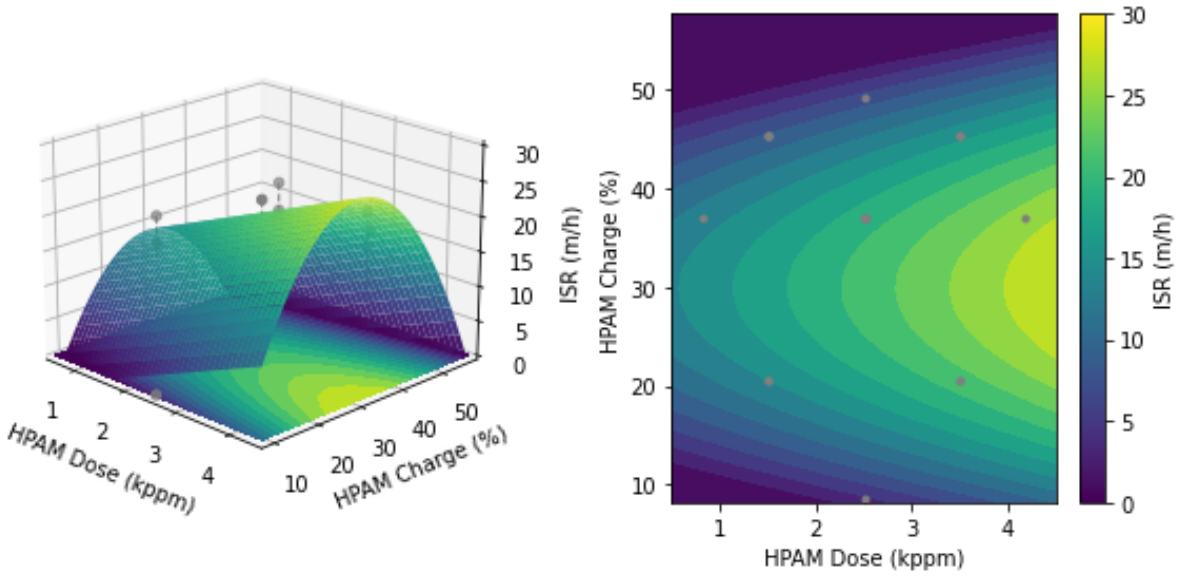

Figure 4-5: Surface plot and contour plot of the regression model describing the ISR of flocculated MFT as a function of HPAM dose and charge density.

4.3.3.2 Capillary Suction Time

Capillary suction time (CST) of the settled flocs from treated MFT was measured and the data is tabulated in Table C-1. The summary of the statistical analysis of the parameter estimates in the regression model are in Table C-5. The logarithm of the CST was used as the response variable for improved model fit. Significant parameters ($p < 0.05$) were used to fit the model described in Equation (4-3).

$$\log(CST) = 1.03 + 0.15X_{HPAM} - 0.16X_{PVBTMAC} - 0.19X_{HPAM}X_{PVBTMAC} - 0.12X_{Charge} + 0.14X_{Charge}^2 \quad (4\text{-}3)$$

All three tested factors – HPAM dose, PVBTMAC dose, and HPAM charge density – influenced CST; therefore, three figures were needed to depict the surface response. Figure 4-6 summarizes the model response to HPAM dose and charge density at a fixed PVBTMAC dose. The CST increased with HPAM dose. A minimum in CST was found when the HPAM charge density was around 38 %. Increase in the HPAM concentration, resulting in longer CST values, suggests that the hydrophilic HPAM chains retain water and slow down the dewatering process.

Figure 4-7 is the model response to the HPAM and PVBTMAC dose, where the HPAM charge was fixed at 37 %. Here the two-factor interaction between HPAM and PVBTMAC dose is apparent. Increasing the PVBTMAC dose improves CST, especially at higher doses of HPAM. PVBTMAC alone has been demonstrated to have improved dewatering capabilities over PAM [78], but in this case, at low doses of HPAM, the CST is not as low as for higher doses of PVBTMAC and HPAM together. It seems that the combination of improved dewaterability of PVBTMAC with the larger floc formation achieved from HPAM results in faster CSTs.

Figure 4-8 is the surface response from PVBTMAC dose and HPAM charge. In this case, we learn that CST decreases with PVBTMAC dose and that CST reaches a minimum when the HPAM charge density is 38 %.

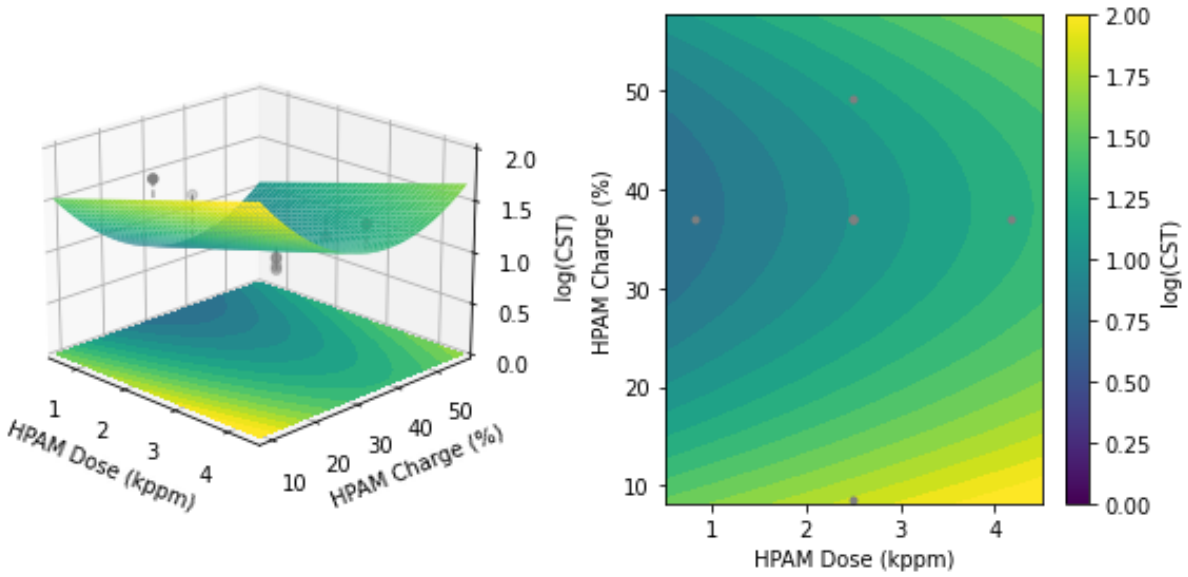

Figure 4-6: Surface plot and contour plot of model response due to HPAM dose and HPAM charge density (PVBTMAC dose = 2.5 kppm) on CST.

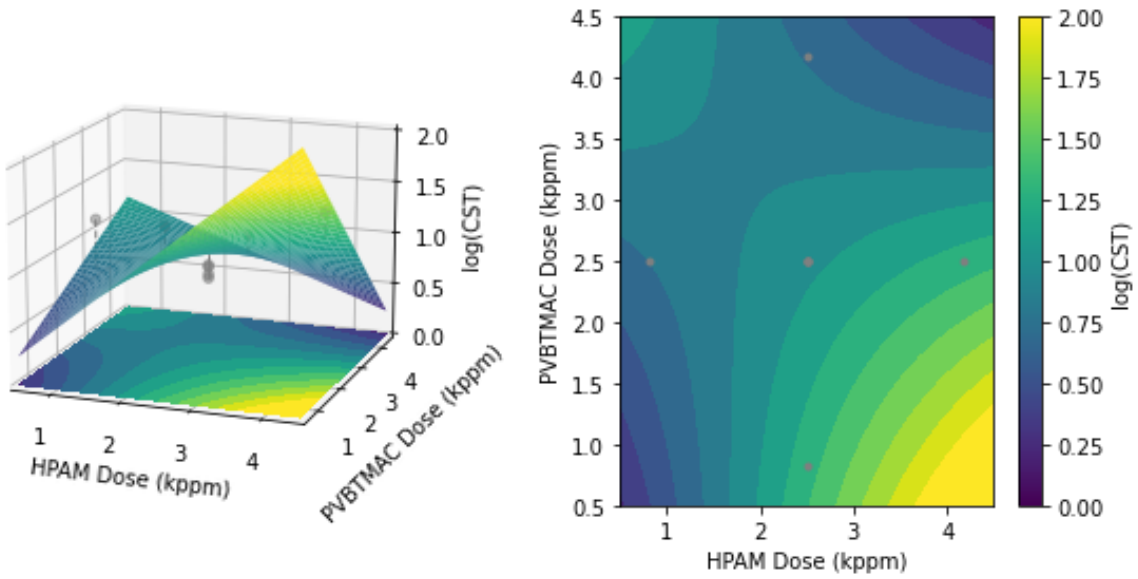

Figure 4-7: Surface plot and contour plot of model response due to HPAM dose and PVBTMAC dose (PVBTMAC charge density = 37 %) on CST.

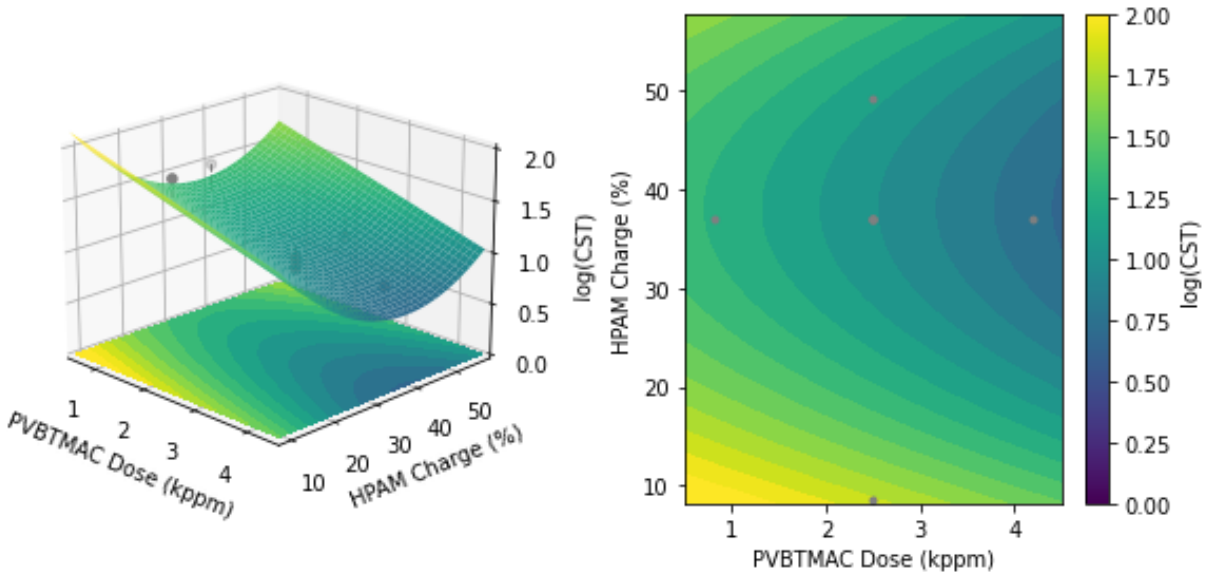

Figure 4-8: Surface plot and contour plot of model response due to HPAM charge density and PVBTMAC dose (HPAM dose = 2.5 kppm) on CST.

4.3.3.3 Solids Content

After the flocculated MFT was allowed to settle for 24 hours, the sediment was collected and dried. The fraction of the sediment that contained solids was calculated after drying. The data is summarized in Table C-1 and the statistical analysis of the parameter estimates is summarized in Table C-6. A regression model based on HPAM dose and HPAM charge density is described in Equation (4-4).

$$\%\, solids = 31.28 + 1.01X_{HPAM} - 0.28X_{Charge} - 1.95X_{Charge}^2 \qquad (4\text{-}4)$$

The solids content ranged from 21 wt % to 32 wt %, all an increase over the 10 wt % in the diluted MFT before flocculation. Solids content increased slightly with HPAM dose and a maximum in the surface response at a charge density of 32 % (Figure 4-9). The dose of PVBTMAC was not found to significantly affect the solids content of the sediment. The response surface for solids content is relatively flat, suggesting a wide dose window for the polymer combination used in the study. This gives flexibility to optimize for other factors, such as supernatant turbidity while keeping solids content relatively stable.

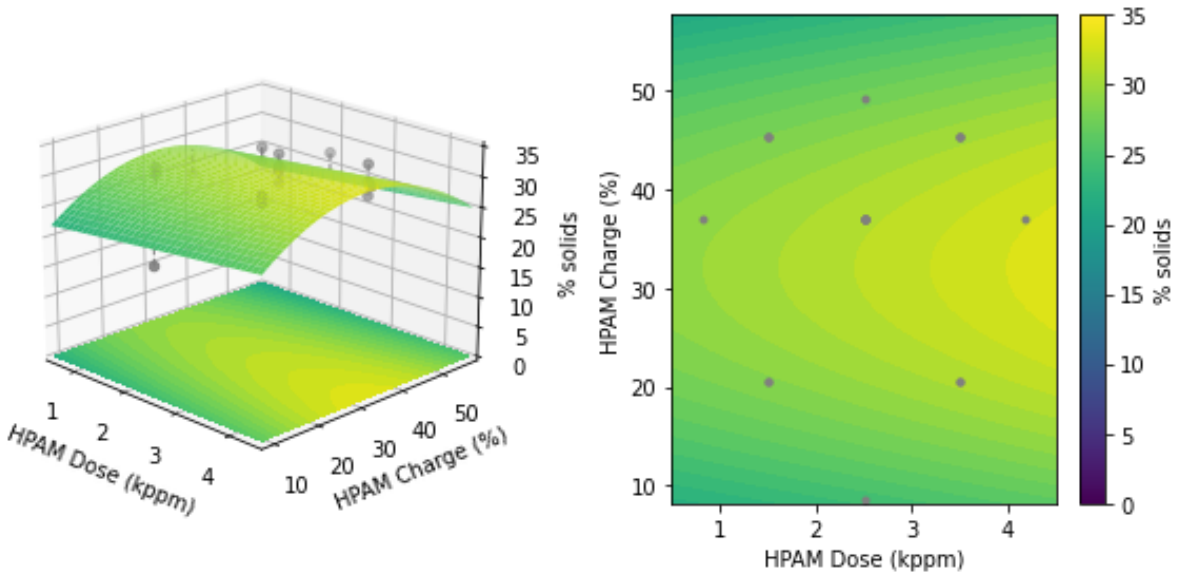

Figure 4-9: Surface plot and contour plot of HPAM dose and charge density effects on solids content in flocculated MFT sediment.

4.3.3.4 Turbidity

The turbidity of the water in the supernatant after flocculation and 24 hours of settling was measured and shown in Table C-2. The summary statistics of the parameter estimates for the regression model are in Table C-7. The final model is described by Equation (4-5). The charge density of HPAM did not have a significant effect on turbidity, it was likely confounded with HPAM dose.

$$Turbidity = 38.81 + 21.72X_{HPAM} - 12.38X_{PVBTMAC} - 34.87X_{HPAM}X_{PVBTMAC} + 26.00X_{PVBTMAC}^2 \quad (4\text{-}5)$$

Figure 4-10 shows how HPAM and PVBTMAC doses affected turbidity. Turbidity increased with an increase in the HPAM and PVBTMAC doses but remained low if HPAM and PVBTMAC doses were increased together. This was likely due to the need to keep the charge of the fine particles in the supernatant close to 0 to ensure that the solution was destabilized enough to support coagulation and sedimentation. This hypothesis is supported by the zeta potential data in Figure 4-11.

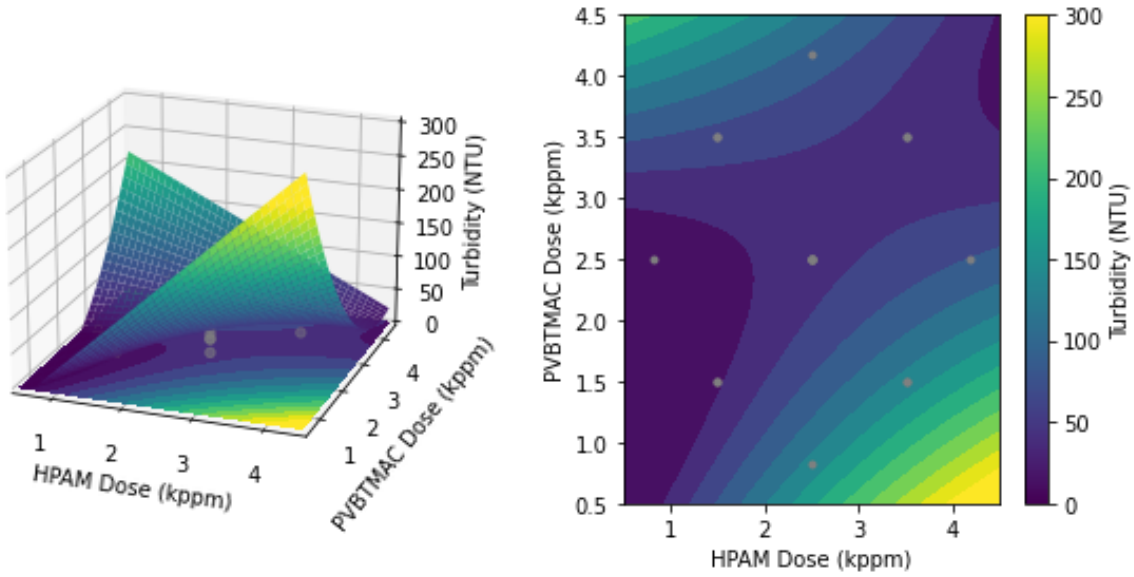

Figure 4-10: Surface plot and contour plot of HPAM dose and PVBTMAC dose effects on the turbidity of the flocculated MFT supernatant.

4.3.3.5 Zeta Potential

The zeta potential of the supernatant was measured 24 hours after flocculation and sedimentation of the MFT samples. Data from the zeta potential measurements can be found in Table C-2 and the summary statistics of the parameter estimates for the regression model are in Table C-8. The final model is described by Equation (4-6). The HPAM charge density was not a significant factor in the zeta potential model; it was likely confounded with HPAM dose.

$$zeta\ potential = 7.54 - 18.89X_{HPAM} + 20.38X_{PVBTMAC} \quad (4\text{-}6)$$

Figure 4-11 shows the relationship between the zeta potential and the dose of HPAM and PVBTMAC. The change in zeta potential in the supernatant is additive: add more cationic PVBTMAC and the zeta potential increases, add more HPAM and the zeta potential decreases.

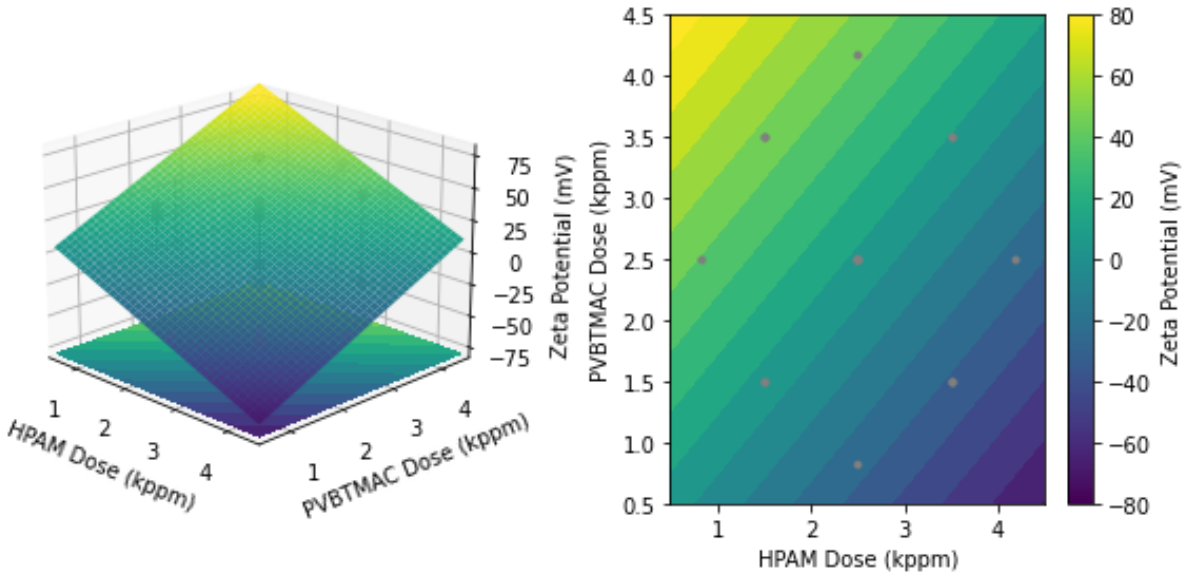

Figure 4-11: Surface plot and contour plot of HPAM dose and PVBTMAC dose effects on the zeta potential of the flocculated MFT supernatant.

From the turbidity and zeta potential data, a relationship between the two becomes beautifully simple: approaching a zeta potential of 0 mV results in low supernatant turbidity (Figure 4-12). This is consistent with literature and classic DLVO theory, where suspended particles may become unstable and aggregate when the zeta potential of the surface is near zero. This highlights the importance of balance the anionic and cationic polymer dose and charge density to ensure that the magnitude of the zeta potential of the flocculated suspension will be minimized.

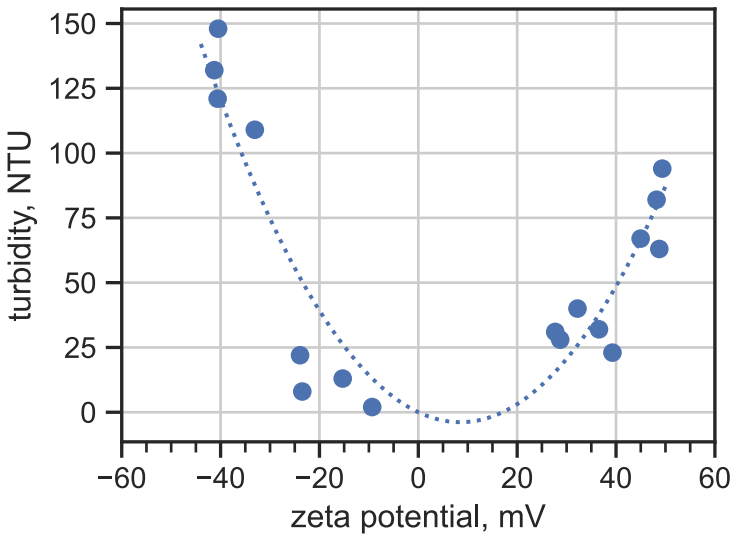

Figure 4-12: Turbidity vs zeta potential of the supernatant after flocculation of MFT with HPAM and PVBTMAC.

4.3.4 UNDILUTED MFT

Treatment of MFT that was not diluted beforehand was also investigated using the dual polymer flocculant system. If MFT can be treated without dilution, there is potential savings in terms of energy costs and freshwater resource usage. The MFT was treated with the polymers the same way as in the undiluted solids, but instead of settling rate tests, the treated MFT was filtered at 69 kPag and the solids content of the remaining material was measured. Flocculation followed by filtration has been demonstrated as an effective method for enhanced dewatering of MFT [6,49]. Table C-3 contains the data from these experiments and Table C-9 is the summary of the statistical analysis of the model parameters. Equation (4-7) is the resulting regression model with the significant parameters with the surface response plotted in Figure 4-13.

$$\%\, solids = 36.36 - 7.54X_{HPAM} + 5.35X_{Charge} \qquad (4\text{-}7)$$

Solids content of up to 61 % were observed after filtration in the case of high HPAM charge density and low HPAM dose. An image of the flocculated MFT before and after filtration is shown in Figure 4-14. PVBTMAC dose, while still important to achieve flocculation,

did not result in a significant change in solids content over the range of doses tested. Similar to the case of CST in the diluted MFT treatment, where increasing HPAM dose increased the CST, here increasing HPAM dose results in lower solids content after filtration. The mechanism is likely due to the hydrophilic HPAM retaining water in the sample during filtration.

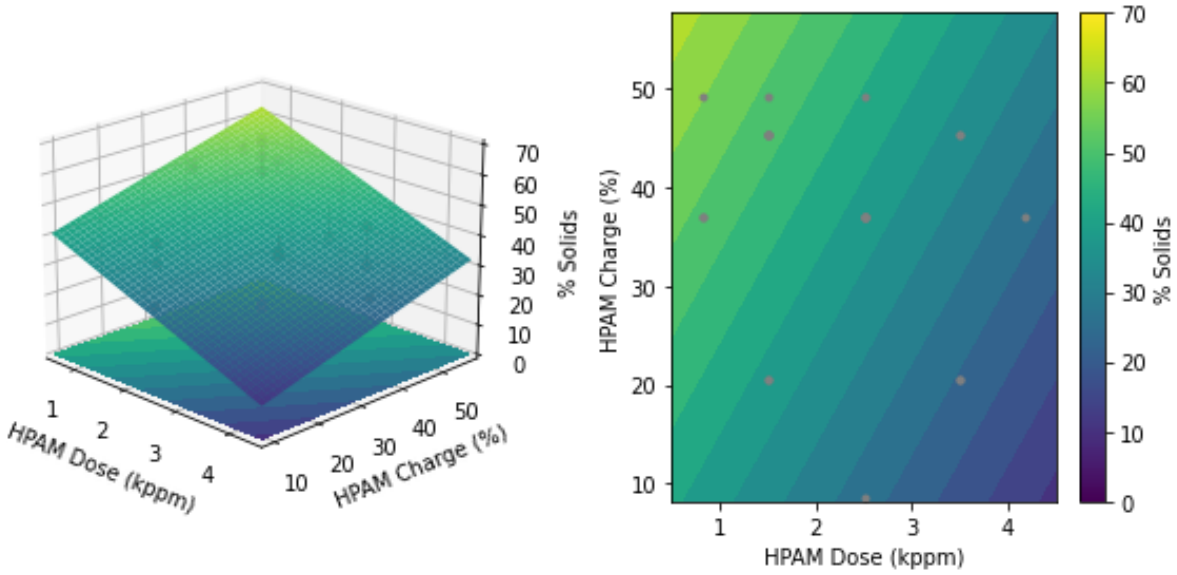

Figure 4-13: Surface plot and contour plot of HPAM dose and HPAM charge density effects on the solids content of flocculated undiluted MFT after filtration.

High charge density of HPAM produced filer cakes with higher solids content. This contrasts with the experiments with diluted MFT, where the solids content reached an optimum with a HPAM charge density near 32 %. The additional dewatering step via filtration can account for this difference. A high charge density can result in reduced adsorption efficiency for anionic polymers and high turbidity [85], which was also seen in this study when looking at the ISR and solids content of the 10 wt % MFT slurry, where the optimum charge density was approximately 30 %. But when it comes to a floc structure that allows for good dewatering, it appears that higher charge densities are preferred. The CST data has a higher optimum charge density of HPAM at 38 % compared to 30 % and 32 % for ISR and solids content, respectively. It has been demonstrated with kaolinite that cationic polymers and higher charge density anionic polyacrylamides form stronger flocs

under yield stress. These stronger, more open flocs, may allow for better dewatering when filtered [85].

Figure 4-14: Flocculated MFT without predilution (HPAM4 = 1500 ppm, PVBTMAC = 3500 ppm). Left: Before filtration. Right: After filtration.

The cationic polymer PVBTMAC may not play a strong role in the final solids content in the MFT filter cake, but it does play a role in the clarity of the water filtrate. For instance, the left image in Figure 4-15 is the filtrate after flocculation with HPAM4 at 1500 ppm and PVBTMAC at 3500 ppm and the right image uses the same dose of HPAM4 but only 1500 ppm of PVBTMAC; the addition of more PVBTMAC resulted in a clearer filtrate.

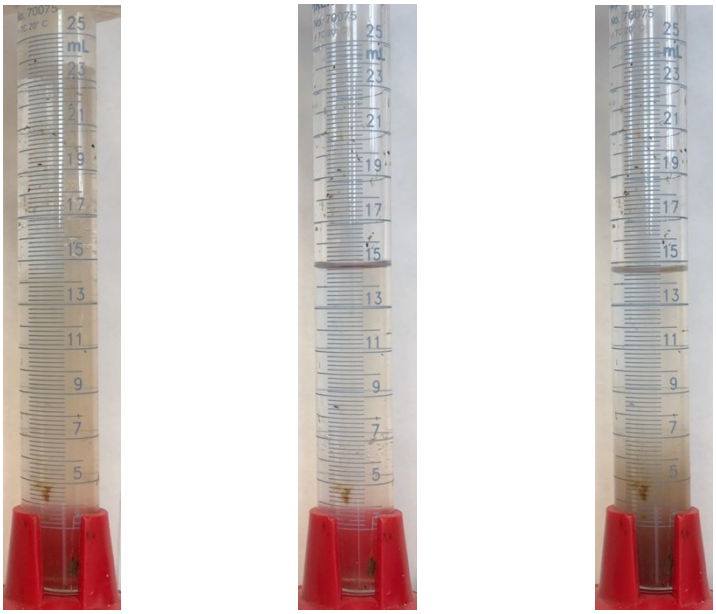

Figure 4-15: Filtrate water from filtered MFT. Left: HPAM4 = 1500 ppm, PVBTMAC = 3500 ppm. Middle: HPAM3 = 818 ppm, PVBTMAC = 2500 ppm. Right: HPAM4 = 1500 ppm, PVBTMAC = 1500 ppm.

4.4 CONCLUSIONS

A dual flocculation process using anionic PAM and cationic PVBTMAC was studied by varying the charge density of the HPAM and the dose of each polymer. Using a combination of the two polymers resulted in better performance at lower doses compared to each flocculant individually. HPAM and PVBTMAC play complementary roles in the flocculation of MFT. HPAM dose and charge density plays a large role in settling rate and final solids contents in the sediment, with a charge density optimum around 30 %. However, for CST and the solids content in undiluted MFT after low pressure filtration, higher charge densities resulted in better outcomes. The PVBTMAC played a large role in removing fines from the supernatant: doses that reduced the magnitude of the zeta potential of the suspension destabilized fines in the suspension and lowered the turbidity. The combination of HPAM with PVBTMAC and low-pressure filtration could achieve a solids content in the filtered MFT of up to 61 wt % with a clear filtrate.

The use of two polymers adds more flexibility in optimizing flocculation performance. The complementary roles of the anionic and cationic polymers allow each of them to be optimized for dose and charge density with more flexibility than in a single polymer flocculant system. The high solids content achieved with low-pressure filtration merits further investigation for feasibility on the industrial scale and further studies on how molecular weight of each flocculant affects flocculation performance would also be of interest.

Chapter 5 USING POLYMER ADSORPTION DATA AND A POPULATION BALANCE MODEL TO ESTIMATE HOW POLYMER DOSAGE AFFECTS THE FLOCCULATION OF MINERAL TAILINGS

Population balance models can describe how particles aggregate and fragment during the flocculation of mineral tailings. We used a new population balance model to describe the flocculation of oil sands mature fine tailings with poly(vinylbenzyl trimethylammonium chloride). Different from previous models, the polymer adsorption data onto the particles suspended in the tailings were used as a fundamental parameter to relate polymer dosage to the mean diameter of the aggregates formed during flocculation. This model is another step toward a quantitative understanding of how polymer properties affect the flocculation of mineral tailings.

5.1 INTRODUCTION

Population balances have been used to describe how particle size distributions change during crystallization [86,87], polymerization [88,89], and flocculation [90,91] processes because these distributions influence material properties or solid-liquid separation operations. For flocculation, polymers are commonly used to aggregate the solids suspended in mineral tailings. Understanding the dynamics of this process and how to predict aggregate sizes formed under different conditions would be useful to design more efficient or novel tailings treatment methods.

Population balances have been developed to model the flocculation of different particle types, including calcite [92], kaolinite and quartz [93], latex microparticles [94], fine tailings slurries [95], and oil sands tailings [26]. Modelling particle size changes during flocculation involves two main events: 1) aggregation, in which particles collide, stick together, and form larger flocs, and 2) fragmentation, during which shear forces break

larger aggregates into smaller particles. The frequencies of these two events anchor the development of population balance models.

Flocculation dynamics can be incredibly complex, leading to models that rely on many adjustable empirical parameters: the structure, chemical composition, and concentration of the polymer, the sizes, composition, and loading of the suspended particles, and the water chemistry, in addition to mixing, shear rate, and viscosity effects [91]. Despite these challenges, population balances can help understand the flocculation process and have been incorporated into computational fluid dynamics (CFD) models to better predict larger scale operations [91,95–97].

In this article, we used a population balance model to describe the aggregation of oil sands mature fine tailings (MFT) using the cationic flocculant poly(vinylbenzyl trimethylammonium chloride) (PVBTMAC). This model rests on the shoulders of the previous model by Vajihinejad and Soares (2018) [26], but adds a new fundamental feature: experimental adsorption data to describe how MFT aggregates respond to changes in the flocculant dosage.

Mature fine tailings is a by-product of oil sands mining. Tailings are pumped into ponds after bitumen is extracted from oil sands ores to allow for the suspended solids to settle out of the water. Larger mineral particles separate quickly, but the fine particles (with diameters less than 44 μm) remain in suspension indefinitely. The typical composition of MFT is 30-40 % solids by weight, 1-5 % bitumen, and 60-70 % water, with a pH around 8. Tailings also containing several inorganic salts [5,7]. Polymer flocculants – typically polyacrylamide – are frequently used to treat MFT, but they do not perform well enough to allow for the fast remediation of tailings ponds. This study is a small, but theoretically sound step, toward the quantification of MFT treatment with polymer flocculants.

5.2 Materials and Methods

5.2.1 Materials

Acrylamide, (vinylbenzyl)trimethylammonium chloride (VBTMAC), methyl 2-[methyl(4-pyridinyl)carbamothioylthio]propionate (RAFT agent), 2,2′-azobis(2-

methylpropionamidine) dihydrochloride (V-50), hydroxymethanesulfinic acid monosodium salt dihydrate (NaFS), ammonium persulfate (APS), kaolinite, and ethanol were purchased from Sigma-Aldrich. Mature fine tailings (MFT) samples from Alberta oil sands were provided through the Institute for Oil Sands Innovation.

5.2.2 METHODS

5.2.2.1 Synthesis of RAFT Agent Oligomer

A polyacrylamide oligomer was first synthesized with the RAFT agent to ensure good solubility in water for the subsequent polymerization of PVBTMAC. The RAFT agent, methyl 2-[methyl(4-pyridinyl)carbamothioylthio]propionate, was dissolved in a 1:1 solution of ethanol and water. Acrylamide was also dissolved in the solution at a molar ratio of 7:1 (acrylamide:RAFT agent). The solution was purged with nitrogen and then heated to 60 ˚C. The initiator, V-50, was injected into the solution with a final concentration of 2.5×10^{-3} M. The reaction medium was stirred at 60 ˚C for 4 h. Ethanol was evaporated, and the product was freeze-dried. The structure of the RAFT agent oligomer was confirmed with ^{1}H NMR. The molecular weight was calculated from NMR to be 697 g/mol, which corresponds to 6 acrylamide units per oligomer molecule.

5.2.2.2 Synthesis of PVBTMAC

PVTMAC was synthesized at room temperature via RAFT polymerization to make low-dispersity polymer samples. The RAFT agent oligomer was added to a 10 wt% solution of VBTMAC in deionized water with the required ratio of monomer to RAFT agent to reach the desired molecular weight. The monomer solution was adjusted to a pH of 6 and was then purged with nitrogen to create an oxygen-free environment. The polymerization was initiated using the NaFS/APS redox initiator system. An equimolar amount of NaFS and APS were used at a concentration of 60 ppm APS relative to the VBTMAC concentration. The polymerization was carried out overnight under constant stirring. The polymer was precipitated in acetone, and then freeze-dried.

5.2.2.3 Polymer Characterization

The molecular weight distributions of the PVBTMAC samples were measured by gel permeation chromatography (GPC, Agilent 1260 Infinity Multi-Detector Suite). The

triple detection GPC system included two columns (TSK-GEL G6000PWxl-CP) in series with a differential refractive index detector, a dual angle light scattering detector, and a viscometer. The GPC was calibrated using polyethylene oxide standards. All samples were analyzed in a solution of 300 mM sodium sulfate, 50 mM acetic acid, and 2 mM sodium acetate.

5.2.2.4 Adsorption Experiments

Mature fine tailings samples were diluted to a final solids content of 2.5 wt% using deionized water. A 30 mL sample of the diluted MFT was mixed with an appropriate dose of a 2 mg/mL solution of the synthesized PVBTMAC. The MFT sample was mixed for 60 minutes and then centrifuged at 3000×g (RCF) for 20 minutes. The supernatant was then collected, and the concentration of polymer was determined by UV-Vis spectrometry. A calibration curve for the concentration of PVBTMAC was made using its peak absorbance at 224 nm. The mass of the adsorbed polymer was calculated from the difference between the initial polymer concentration and the concentration of the polymer in the supernatant.

5.2.2.5 Flocculation Monitoring

Flocculation of the MFT was monitored using focused-beam reflectance measurement (FBRM) probe (FBRM G400, Mettler Toledo). The chord-length distribution of the particle aggregates was recorded every two seconds. Experiments were done in 100 mL batches, consisting of MFT diluted to 2.5 wt% in deionized water. The polymer flocculant, PVBTMAC, was prepared as a 2 mg/mL solution 24 hours before the flocculation experiment to ensure complete dissolution. The MFT suspension was mixed at 200 rpm with a pitched 4-blade impeller for 5 minutes before the addition of PVBTMAC. The dynamic changes in the aggregate sizes were continuously monitored under stirring at 200 rpm for 10 minutes. The FBRM probe can report data using primary or macro modes. Macro mode data was used for population balance modelling, as it was determined to be more appropriate for the large flocs formed under dilute conditions where particle overlap is minimal [26,98].

5.3 MODEL DEVELOPMENT

Flocculation is a dynamic process that involves the aggregation and breakage of flocs of different sizes. This process can be modelled using a population balance for aggregates described in Equation (5-1) [99],

$$\frac{\partial n(v,t)}{\partial t} = \frac{1}{2}\int_0^v Q(v-v',v')n(v-v',t)n(v',t)\,dv' + \int_v^\infty \Gamma(v,v')S(v')n(v',t)\,dv' - \int_0^\infty Q(v,v')n(v,t)n(v',t)\,dv' - S(v)n(v,t) \qquad (5-1)$$

where $n(v,t)$ is the number of aggregates of volume v per unit volume at time t, $Q(v,v')$ is the aggregation kernel for aggregates of size v and v', $S(v)$ is the breakage kernel for aggregates of size v, and $\Gamma(v,v')$ is the breakage distribution function. The first term in Equation (5-1) describes the formation of aggregates of size v from smaller aggregates of size v' and $v-v'$. The second term is the formation of aggregates of size v from the breakage of larger aggregates. The third term describes the loss of aggregates of size v due to their combination with a second aggregate. The last term is the breakage of aggregates of size v into smaller aggregates.

Several different methods may be used to solve the population balance equations, including discretization [26,91,100–102], quadrature method of moments [94,103,104], and Monte Carlo simulations [105–108]. We used the discretization method, where the aggregate sizes are on a geometric grid ($v_{i+1} = 2v_i$) [100,101]. After discretization, the population balance becomes,

$$\frac{dN_i}{dt} = \sum_{j=1}^{i-2} 2^{j-i+1}Q_{i-1,j}N_{i-1}N_j + \frac{1}{2}Q_{i-1,i-1}N_{i-1,i-1}^2 - N_i\sum_{j=1}^{i-1}2^{j-i}Q_{i,j}N_j - N_i\sum_{j=i}^{i_{max,1}}Q_{i,j}N_j - S_iN_i + \sum_{j=i}^{i_{max,2}}\Gamma_{i,j}S_jN_j \qquad (5-2)$$

The aggregation and breakage phenomena are described by their respective kernels. The aggregation kernel is defined as the product of the collision frequency, β, and collision efficiency, α,

$$Q_{i,j} = \alpha_{i,j}\beta_{i,j} \qquad (5-3)$$

The shear-induced collision frequency under isotropic turbulence (orthokinetic aggregation) has been described by Saffman and Turner [109],

$$\beta_{i,j} = 0.162G\left(d_i + d_j\right)^3 \qquad (5-4)$$

where G is the average shear rate, and d_i and d_j are the effective diameters for aggregates i and j. Aggregation from Brownian diffusion and particle sedimentation were not considered in the model because the system studied was under constant mixing. The effective diameters are calculated from the mass fractal dimension because the aggregates are fractal objects, not perfect spheres,

$$d_i = d_1\left(2^{i-1}\right)^{\frac{1}{D_f}} \qquad (5-5)$$

where d_1 is the primary particle diameter, which all the aggregates are composed of, and D_f is the mass fractal dimension.

The average shear rate was used in the current model and may be calculated as [110],

$$G = \left(\frac{\epsilon}{\nu}\right)^{1/2} \qquad (5-6)$$

where ν is the kinematic viscosity and ϵ is the average energy dissipation rate. For stirred tanks [111],

$$\epsilon = \frac{N_p N^3 D^5}{V} \qquad (5-7)$$

where N_p is the impeller power number, N is the rotational speed of the impeller, D is the length of the impeller blade, and V is the volume of the stirred suspension.

Since not every collision will result in aggregation, a collision efficiency must be used in the aggregation kernel. Frequently, the collision efficiency is an adjustable parameter, but there have been many attempts to add physical meaning to it. Selomulya *et al*. developed an empirical model based on the work of Kusters and the trajectory analysis of Adler to define the capture efficiency as a function of two fitted parameters [102,112–114],

$$\alpha_{i,j} = \frac{\exp\left(-x\left(1-\frac{i}{j}\right)^2\right)}{(ij)^y}\alpha_{max} \qquad (5-8)$$

where *x* and *y* are fitted parameters and *i* and *j* are the aggregate size bins of the discretized particle size distribution.

In the flocculation of mineral tailings, the aggregate sizes often change with time, which needs to be accounted for in the population balance model. Vajihinejad and Soares, quantified these dynamic changes by incorporating an exponential decay term in the capture efficiency parameter,

$$\alpha = (\alpha_{max} - \alpha_{min})e^{-k_d t} + \alpha_{min} \qquad (5-9)$$

where α_{max} and α_{min} are the maximum and minimum values of the capture efficiency and k_d is the aggregate size decay rate constant [26].

One limitation of the previous models is that they do not incorporate polymer dosage into the capture efficiency. Some early work by Hogg, later extended by Swerin, proposed a model for collision efficiency based on surface coverage of the particles [115,116]. Equation (5-10) describes how bridging flocculation affects capture efficiency, with a maximum efficiency when the effective surface coverage, θ, is 50 %.

$$\alpha_{bridging} = 2\theta(1-\theta) \qquad (5-10)$$

The authors further theorized that the thickness of the polymer adsorbed on the particles would also improve the flocculation efficiency because the effective particle diameter would increase. An additional term to describe the capture efficiency, which included the

growth in average layer thickness with increased surface coverage, was proposed by Swerin in Equation (5-11), where λ and ω are fitted parameters.

$$\alpha_{layer} = \lambda\left(1 - e^{-\omega\theta}\right) \qquad (5-11)$$

We were inspired by the idea of incorporating polymer surface coverage and a temporal component to account for aggregate rearrangement. The capture efficiency we are proposing in this study is described in Equation (5-12),

$$\alpha = a\left((1-h)e^{-k_d t} + h\right)\left(2\theta(1-\theta) + \frac{1}{1+e^{-b(\theta-\theta_{max})}}\right) \qquad (5-12)$$

where θ is the effective surface coverage, θ_{max} is the surface coverage when the aggregate sizes are the highest, h is a parameter between 0 and 1 related to the time dependence of the aggregate size caused by polymer and floc rearrangement, k_d is the aggregate size decay constant, and a and b are fitted parameters. The exponential decay portion of Equation (5-12) is related to Equation (5-9), instead of a maximum and minimum value of α we normalized the scale so the maximum value would be 1 and the minimum value is h. The second part of Equation (5-12) incorporates the adsorbed amount. $2\theta(1-\theta)$ assumes peak efficiency at 50% coverage with equal efficiency at low or high polymer dose, so sigmoid curve is added to take into account that overdosing with polymer will result in larger aggregate sizes compared to low doses.

The breakage rate is modelled by a shear-induced power law breakage kernel proposed by Pandya and Spielman [117], where s_1 and s_2 are empirical constants, and d_i is the diameter of the breaking aggregate,

$$S_i = s_1 G^{s_2} d_i \qquad (5-13)$$

The breakage distribution in this model is a binary breakage function. Admittedly, this is a simple model, but it gives reliable results when we are only interested in simulating average particle sizes [101,118].

$$\Gamma_{ij} = \frac{v_j}{v_i} \qquad (5-14)$$

5.4 Results and Discussion

5.4.1 Polymer Synthesis and Characterization

Three low dispersity cationic polyelectrolytes were synthesized from VBTMAC. The molecular weight averages of each sample were measured by GPC (Table 5-1). We used polymers with a narrow molecular weight distribution to minimize the effect of dispersity on polymer adsorption and flocculation [65,119].

Table 5-1: Molecular weight averages of PVBMTAC samples

Sample	M_n	M_w	M_w/M_n
VB13	0.85×10^6	1.27×10^6	1.50
VB14	1.10×10^6	1.38×10^6	1.26
VB24	1.73×10^6	2.42×10^6	1.40

5.4.2 PVBTMAC Adsorption

PVBTMAC adsorption onto MFT solids was determined for the three samples listed in Table 5-1. Figure 5-1 illustrates how the mass of polymer adsorbed on MFT changes with the initial solution concentration. At low concentrations, the masses of all polymers are about the same, but as the dose increases, they reach different plateaus. This plateau region, for the purposes of flocculation, can be considered the effective maximum amount of polymer that can be adsorbed, corresponding to $\theta = 1.0$ [115,116,120]. From Figure 5-1, the polymer with the lowest molecular weight, VB13, plateaus at the highest adsorbed amount; the polymer with the highest molecular weight, at the lowest adsorbed amount. This phenomenon has been reported in the literature for some flocculants adsorbed on clays [121,122] and may be related to intraparticle mass transfer resistance or competitive adsorption with other components present in MFT. The polyelectrolytes VB13, VB14, and VB24 reach their adsorption plateaus at 12 mg/g, 10.4 mg/g, and 8.2 mg/g, respectively.

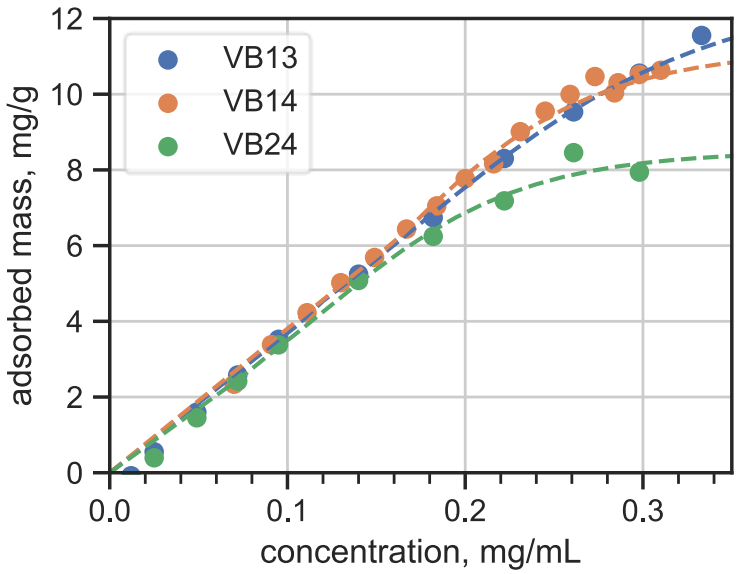

Figure 5-1: Adsorption of PVBTMAC onto suspended solids in MFT. Concentration is the initial concentration of PVBTMAC in solution.

The value of θ for each dose and polymer sample can be calculated from Figure 5-1 for a given polymer dose used to flocculate MFT. Values of θ used in this study are summarized in Table 5-2.

Table 5-2: Calculated adsorbed fraction for each polymer and dose

Dose, mg/kg	**Concentration, mg/mL**	**θ**		
		VB13	**VB14**	**VB24**
4000	0.095	0.29	0.33	0.41
6000	0.140	0.45	0.49	0.62
8000	0.182	0.56	0.62	0.76
10000	0.222	0.69	0.75	0.88

5.4.3 *FLOCCULATION EXPERIMENTS*

Flocculation of diluted MFT using three different samples of PVBTMAC were carried out at doses of 4000, 6000, 8000, and 10000 ppm (mg of polymer per kg of solids in the MFT suspension). The mixing speed was 200 rpm for all experiments to keep the shear rate constant. The chord length distribution of the aggregates was continuously recorded. It was then discretized to generate the initial population of particles in the population balance simulation. The initial number concentration, $N_{0,i}$, for each binned particle volume, $V_{0,i}$, was calculated from the interpolation of the experimental volume fractions,

$$N_{0,i} = \frac{\phi v(d_{0,i})}{V_{0,i}} \qquad (5-15)$$

where ϕ is the volume fraction of particles in suspension, and $v(d_{0,i})$ is the volume fraction of particles with diameter d_i. Following the geometric grid pattern for discretization, the volume of particles in the i^{th} bin is,

$$V_{0,i} = 2^{i-1}V_1 \qquad (5-16)$$

where V_1 is the volume of the primary particle.

Equation (5-17) is the interpolation method used to calculate the particle volume fractions,

$$v(d_{0,i}) = \frac{v(d_{i+1}^{exp}) - v(d_{i-1}^{exp})}{d_{i+1}^{exp} - d_{i-1}^{exp}}(d_{0,i} - d_{i-1}^{exp}) + v(d_{i-1}^{exp}) \qquad (5-17)$$

Figure 5-2 shows a sample of the MFT particle size distribution before and after discretization.

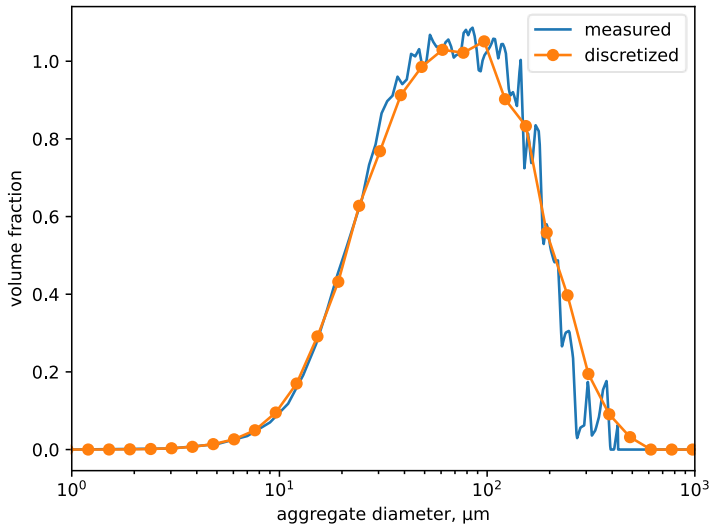

Figure 5-2: Particle size distribution of the MFT sample. Measured values in blue and the discretized distribution used in the population balance model in orange.

The population balance equations were solved using an implicit Runge-Kutta method for stiff ODEs (TRBDF2 in the DifferentialEquations.jl software package [123]). Model parameters were estimated by minimizing the objective function, Equation (5-18), for each dose of the polymer sample simultaneously,

$$F(s_1, s_2, k_d, h, a, b) = \sum_{t=0}^{t_{final}} \left(d_{exp} - d_{model}\right)^2 \qquad (5-18)$$

where d is the volume average diameter of the MFT aggregates, d_{exp} comes from experimental data, and d_{model} is defined in Equation (5-19),

$$d_{model} = \frac{\sum_{i=1}^{max} N_i d_i^4}{\sum_{i=1}^{max} N_i d_i^3} \qquad (5-19)$$

Three metrics were reported to evaluate the fit of the model: the coefficient of determination (R^2), to measure how well the model fits the experiment,

$$R^2 = 1 - \frac{\sum_{i=1}^{max}\left(d_{exp,i} - d_{model,i}\right)^2}{\sum_{i=1}^{max}\left(d_{exp,i} - \bar{d}_{exp,mean}\right)^2} \qquad (5-20)$$

the Pearson correlation coefficient (ρ), to determine the linear correlation between the model and the experiment,

$$\rho = \frac{\sum_{i=1}^{max}\left(d_{exp,i} - \bar{d}_{exp,mean}\right)\left(d_{model,i} - \bar{d}_{model,mean}\right)}{\left(\sum_{i=1}^{max}\left(d_{exp,i} - \bar{d}_{exp,mean}\right)^2 \sum_{i=1}^{max}\left(d_{model,i} - \bar{d}_{model,mean}\right)^2\right)^{\frac{1}{2}}} \qquad (5-21)$$

and the mean absolute percentage error (MAPE), as a measure of the prediction accuracy of the model,

$$MAPE = \frac{100}{i_{max}} \sum_{i=1}^{i_{max}} \left| \frac{d_{exp,i} - d_{model,i}}{d_{exp,i}} \right| \qquad (5-22)$$

A mass fractal dimension of 2.4 was used in the model based on an estimation by Vajihinejad and Soares done with microscopy image analysis [26]. This fractal dimension was considered an adequate estimate because both their study and ours used PVBTMAC as the flocculant and both treated diluted MFT samples.

Model parameters were fit for PVBTMAC samples of different molecular weights. Figure 5-3 illustrates how each parameter was used in the model: shared between all experiments, polymer dependent, or dose dependent. The fraction of absorption sites occupied on the MFT particles, θ, was calculated for each polymer dose based on the predicted adsorbed mass and the plateau absorbed mass from Figure 5-1. The parameters related to aggregate breakage, s_1 and s_2, and related to the time dependence of the aggregate size, k_d and h, were shared between all polymer samples and doses (see Table 5-3, Table 5-5, and Table 5-7). The parameters b and θ_{max} were the same for all polymer doses within the same sample. The adjustable parameter, a, was modified to fit the data for each dose. Earlier attempts at parameter fitting kept a the same across doses within the polymer sample, like b and θ_{max}. The overall trends were correct, but the predicted average aggregate sizes were not as accurate.

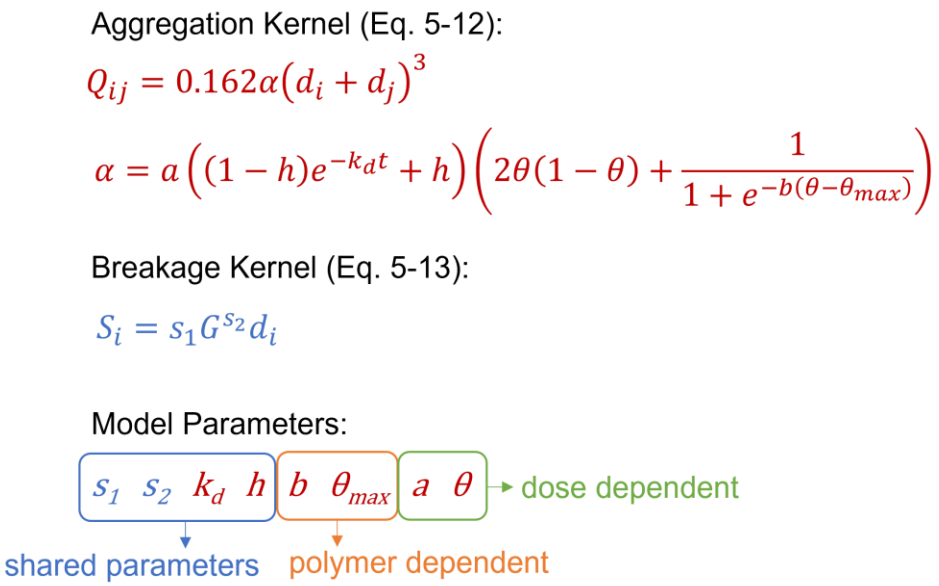

Figure 5-3: Schematic diagram of model parameter dependence on polymer sample and dose.

The mean aggregate size formed when MFT was treated with VB13 is depicted in Figure 5-4. The fitted parameters shared between all experiments with the same polymer sample are in Table 5-3 and the individual statistics and parameters for each dose are in Table 5-4. The fraction of absorbed polymer was calculated for each dose from Figure 5-1 and summarized in Table 5-4. It ranges from $\theta = 0.29$ to 0.69 (Table 5-4). A dose of 6000 ppm resulted in larger aggregates compared to all the other doses for both VB13 (Figure 5-4) and VB14 (Figure 5-5). For VB13, the experiments with 8000 and 10000 ppm doses resulted in very similar mean aggregate sizes over the course of the experiments. At 4000 ppm, the peak aggregate size after initial injection of polymer was lower than for the other samples, but the average aggregate size after the floc rearrangement was similar to the 8000 and 10000 ppm experiments.

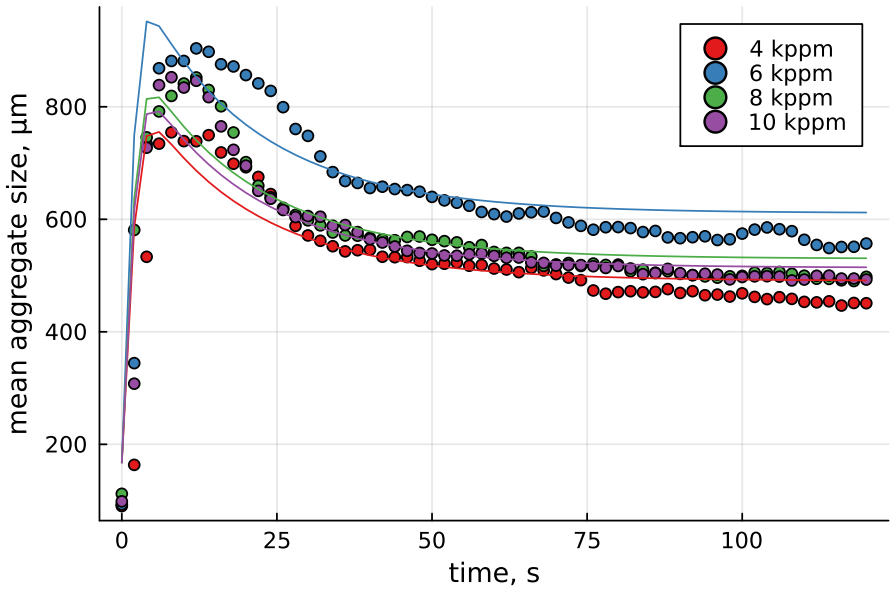

Figure 5-4: Average aggregate size of MFT after addition of VB13 for different doses. Circles are experimental data points, lines are from the population balance model.

Table 5-3: Shared parameters for each flocculation experiment with VB13.

s_1	s_2	d_F	k_d	h	b	θ_{max}
0.24	1.92	2.4	0.05	0.8	0.01	0.45

Table 5-4: Model fit statistics and parameters, θ and a, for each dose of VB13.

Dose, mg/kg	θ	a	R^2	ρ	**MAPE**
4000	0.29	0.0028	0.64	0.81	10.6
6000	0.45	0.0028	0.71	0.86	9.0
8000	0.56	0.00265	0.90	0.96	5.3
10000	0.69	0.0028	0.81	0.92	5.9

The VB14 samples behaved similarly to the VB13 samples – the peak aggregate size was achieved at 6000 ppm with a comparable average floc size. This was expected because the

average molecular weights of both samples are comparable; their main difference is their dispersities (M_w / M_n = 1.5 for VB13 and 1.26 for VB14). The parameters for the fitted population balance model are summarized in Table 5-5 and Table 5-6. Unlike with VB13, where only the dose at 6000 ppm resulted in a different average aggregate size, with VB14 each dose resulted in a distinct mean aggregate size. This was also reflected in population balance model with the parameter b, from Equation (5-12), b = 0.01 for VB13 and 0.7 for VB14.

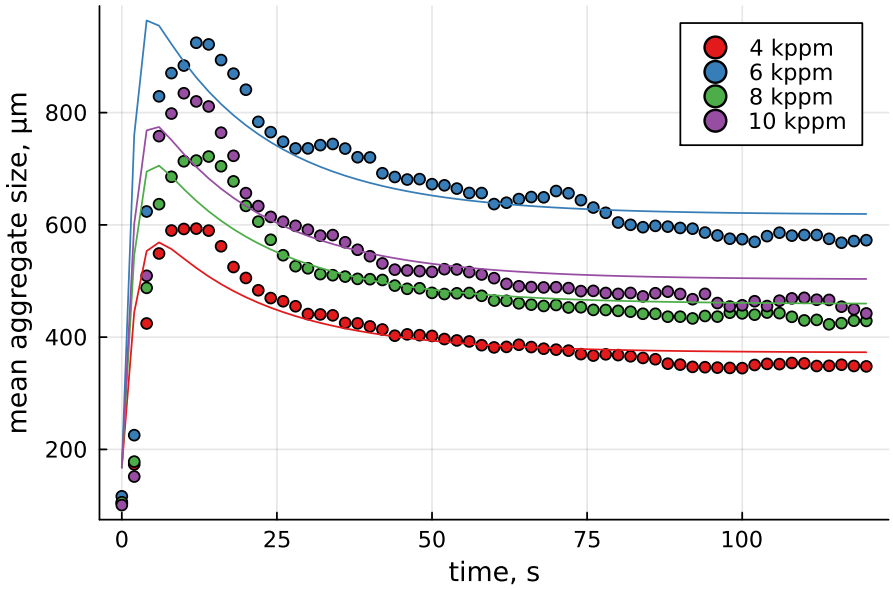

Figure 5-5: Average aggregate size of MFT after addition of VB14 for different doses. Circles are experimental data points, lines are model predictions.

Table 5-5: Shared parameters for each flocculation experiment with VB14.

s_1	s_2	d_F	k_d	h	b	θ_{max}
0.24	1.92	2.4	0.05	0.8	0.7	0.49

Table 5-6: Model fit statistics and parameters, θ and a, for each dose of VB14.

Dose, mg/kg	θ	a	R^2	ρ	MAPE
4000	0.33	0.0025	0.70	0.85	8.4
6000	0.49	0.0028	0.54	0.75	10.2
8000	0.62	0.0025	0.63	0.81	9.1
10000	0.75	0.0028	0.61	0.81	12.5

The higher molecular weight VB24 resulted in a larger peak aggregate size at an optimum dose of 8000 ppm (Figure 5-6). This optimum dose was higher than VB13 and VB14, which had a peak floc size at 6000 ppm. The calculated effective surface coverage, θ, for the optimum dose was also higher for VB24, θ = 0.76 at 8000 ppm, compared to VB13 and VB14 where θ = 0.45 and 0.46, respectively. The fitted parameters a and b, listed in Table 5-7 and Table 5-8, were higher with VB24 than the lower molecular weight samples to account for the larger aggregates formed in flocculation.

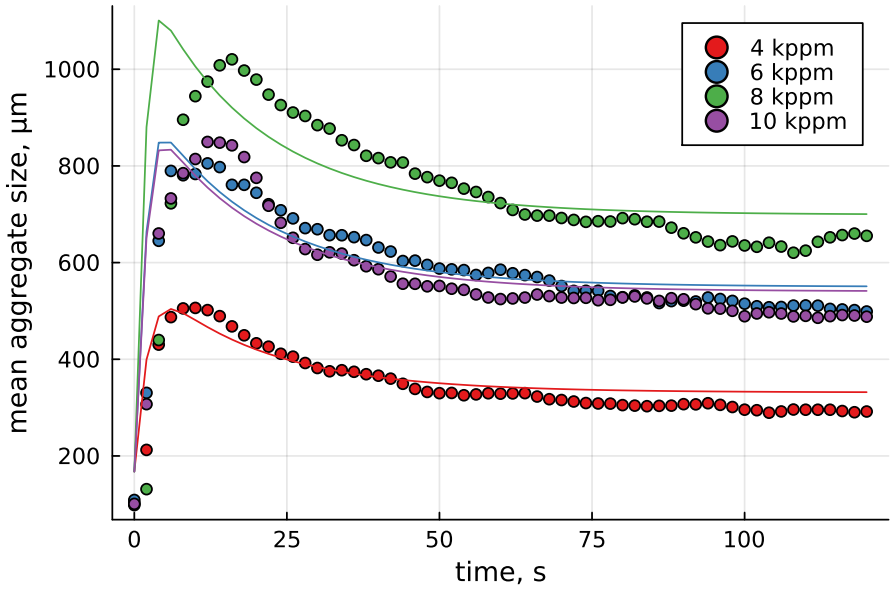

Figure 5-6: Average aggregate size of MFT after addition of VB24 for different doses. Circles are experimental data points, lines are model predictions.

Table 5-7: Shared parameters for each flocculation experiment with VB24.

s_1	s_2	d_F	k_d	h	b	θ_{max}
0.24	1.92	2.4	0.05	0.8	4.0	0.76

Table 5-8: Model fit statistics and parameters, θ and a, for each dose of VB24.

Dose, mg/kg	θ	a	R^2	ρ	MAPE
4000	0.41	0.0032	0.74	0.92	9.3
6000	0.62	0.0032	0.72	0.86	7.9
8000	0.76	0.0034	0.21	0.54	19.8
10000	0.88	0.0032	0.70	0.86	9.3

Overall, the population balance model described in this paper could capture how the mean aggregate size of mature fine tailings changed with polymer dosage. Using polymer adsorption data was enough to predict these changes. This approach adds a physically-sound parameter to the population balance model and suggests that smaller scale adsorption experiments may be used to predict dose response in flocculation if data from larger flocculation experiments are not available. The proposed model still has some limitations. It relies on empirical data and fitted parameters, but is another step toward a better understanding on how polymer properties can be used in population balance models to describe the flocculation of mineral tailings.

5.5 CONCLUSIONS

This study used a population balance modelling approach to describe the flocculation of oil sands mature fine tailings using the cationic polyelectrolyte PVBTMAC. Adsorption data of PVBTMAC onto MFT was used in the population balance model to predict how the mean aggregate size of flocs changed with the dose of the polymer flocculant. Trends were qualitatively predictive for three polymer samples of different molecular weights.

These findings suggest that polymer adsorption experiments can be used to develop more fundamental population balance models for the flocculation of mineral tailings and is another step towards quantifying how polymer type and dose effects MFT flocculation.

Chapter 6 CONCLUSIONS AND RECOMMENDATIONS

6.1 CONCLUSIONS

The goal of this thesis was to better understand how the structure of polymer flocculants affect the flocculation and dewatering of oil sands mature fine tailings. Three main studies looking at different aspects of polymers in flocculation were carried out. First, the role polymer molecular weight distribution (MWD) has on flocculation was studied with polyacrylamide and kaolinite, the most common clay fraction of MFT. High molecular weight polyacrylamides with narrow MWDs were synthesized via RAFT polymerization and broad MWD polymer samples were prepared from blends of the synthesized PAM. Aggregate size of the kaolinite was monitored using focused beam reflectance measurements. It was found that it is the high molecular weight fraction of a polymer blend that had most influence on the aggregate size of the flocs. This implies that the low molecular weight fraction in a polymer sample has little influence on the size of aggregates formed or the settling rate of the flocs. Flocculants with narrow MWDs could, therefore, be used in place of broad MWD polymers at a reduced dose.

The combination of anionic and cationic flocculants for the treatment of MFT was also systematically studied with a design of experiment method. Cationic PVBTMAC and anionic PAM were used to treat diluted and undiluted MFT. The combination of two oppositely-charged polymers in sequence, first anionic and second cationic, results in better flocculation performance as measured by settling rate, water turbidity, and CST. Supernatant turbidity was lowest as the zeta potential approached zero, something that could easily be achieved by adjusting the dose of the cationic polymer. At 30%, the charge density of the anionic polymer was optimal for settling rates, but higher charge densities were better for CST and solids content in the sediment. With the addition of a filtration step after flocculation, the solids content in undiluted MFT was measured as high as 61 wt.%.

The flocculation of MFT was also described using a population balance model. Aggregate formation of MFT using PVBTMAC as the flocculant was monitored using FBRM and the

adsorption of PVBTMAC onto MFT was also experimentally measured. A function dependent on polymer adsorption was introduced into the model to predict the dose dependence on aggregate size formation. The model was used to describe the flocculation over a range of polymer molecular weights and doses.

In addition to the main chapters of the thesis, related work was done as described in the Appendices. In Appendix A, a study trying to find a polymer flocculant for the capture and removal of solids in diluted bitumen was carried out. Challenges related to polymer solubility and molecular weight are also discussed in this appendix. Determination of reactivity ratios of poly(VBTMAC-co-acrylamide) and a polymerization rate for PVBTMAC is discussed in Appendix B.

6.2 RECOMMENDATIONS

With the findings of this thesis the following avenues of additional research are recommended:

High molecular weight polymers synthesized with controlled radical polymerization (CRP) techniques have been proven feasible for some water-soluble monomers. Further work investigating block copolymers, polymers with tunable molecular weight distributions, and polymers other that acrylamide with narrow molecular weight distributions could be investigated for flocculation performance. Although the molecular weights of polymers made by CRP do not reach the size of conventional polyacrylamide, molecular weight seems to mainly influence settling rate. When it comes to MFT, dewaterability of sediment is a major challenge and some amount of reduced settling rate would be an acceptable tradeoff if the sediments formed with high enough solids content that it could lead to land reclamation.

Dual polymer flocculation has been demonstrated as promising treatment option for MFT. Further studies on using this method with a polymer other that PAM is warranted. The combination of two polymers seems to consistently reduce the amount of polymer needed

for flocculation and some novel polymers that were promising replacements to PAM but required a high dose may warrant revisiting. Additionally, the use of the two-polymer system in combination with mechanical separation such as filtration or centrifugation may be worth testing on a larger scale.

Improving mathematical models describing the flocculation of MFT can be approached from several ways. First, a model describing the kinetics of polymer adsorption in combination with particle aggregation would be a way to account for the delay in flocculation after polymer addition. Another challenge with modelling flocculation is the accurate determination of the mass fractal dimension. Determining fractal dimension from 3D confocal microscopy data or with machine learning models and 2D optical microscopy data have both been recently demonstrated. Accurate fractal dimension data is essential to studying floc restructuring. Finally, using the flocculation models developed in larger scale CFD models would allow better flocculation prediction taking into account heterogeneous distribution of polymer flocculants and flow regimes.

BIBLIOGRAPHY

[1] K.A. Clark, D.S. Pasternack, Hot Water Separation of Bitumen from Alberta Bituminous Sand, Industrial & Engineering Chemistry. 24 (1932) 1410–1416. https://doi.org/10.1021/ie50276a016.

[2] Alberta Water Use Performance Report, Alberta Energy Regulator, 2021. https://www.aer.ca/protecting-what-matters/holding-industry-accountable/industry-performance/water-use-performance.

[3] A.K. Katta, M. Davis, V. Subramanyam, A.F. Dar, M.A.H. Mondal, M. Ahiduzzaman, A. Kumar, Assessment of energy demand-based greenhouse gas mitigation options for Canada's oil sands, Journal of Cleaner Production. 241 (2019) 118306. https://doi.org/10.1016/j.jclepro.2019.118306.

[4] J.H. Masliyah, J. Czarnecki, Z. Xu, Handbook on Theory and Practice of Bitumen Recovery from Athabasca Oil Sands, Kingsley Knowledge Publishing, 2011.

[5] J. Masliyah, Z.J. Zhou, Z. Xu, J. Czarnecki, H. Hamza, Understanding Water-Based Bitumen Extraction from Athabasca Oil Sands, The Canadian Journal of Chemical Engineering. 82 (2008) 628–654. https://doi.org/10.1002/cjce.5450820403.

[6] C. Wang, D. Harbottle, Q. Liu, Z. Xu, Current state of fine mineral tailings treatment: A critical review on theory and practice, Minerals Engineering. 58 (2014) 113–131. https://doi.org/10.1016/j.mineng.2014.01.018.

[7] L. Botha, J.B.P. Soares, The Influence of Tailings Composition on Flocculation, Canadian Journal of Chemical Engineering. 93 (2015) 1514–1523. https://doi.org/10.1002/cjce.22241.

[8] H.A.W. Kaminsky, T.H. Etsell, D.G. Ivey, O. Omotoso, Distribution of clay minerals in the process streams produced by the extraction of bitumen from athabasca oil sands, Canadian Journal of Chemical Engineering. 87 (2009) 85–93. https://doi.org/10.1002/cjce.20133.

[9] K.L. Konan, C. Peyratout, J.-P. Bonnet, A. Smith, A. Jacquet, P. Magnoux, P. Ayrault, Surface properties of kaolin and illite suspensions in concentrated calcium hydroxide medium, Journal of Colloid and Interface Science. 307 (2007) 101–108. https://doi.org/10.1016/j.jcis.2006.10.085.

[10] J.N. Israelachvili, Intermolecular and surface forces, 3rd ed., Academic Press, Burlington, MA, 2011.

[11] S.-J. Park, M.-K. Seo, Intermolecular Force, in: Interface Science and Technology, Elsevier, 2011: pp. 1–57. https://doi.org/10.1016/B978-0-12-375049-5.00001-3.

[12] D.R.L. Vedoy, J.B.P. Soares, Water-soluble polymers for oil sands tailing treatment: A Review, Canadian Journal of Chemical Engineering. 93 (2015) 888–904. https://doi.org/10.1002/cjce.22129.

[13] M.D. MacKinnon, J.G. Matthews, W.H. Shaw, R.G. Cuddy, Water Quality Issues Associated With Composite Tailings (CT) Technology for Managing Oil Sands Tailings, International Journal of Surface Mining, Reclamation and Environment. 15 (2001) 235–256. https://doi.org/10.1076/ijsm.15.4.235.7416.

[14] N.O. Ivanova, Z. Xu, Q. Liu, J.H. Masliyah, Surface forces in unconventional oil processing, Current Opinion in Colloid & Interface Science. 27 (2017) 63–73. https://doi.org/10.1016/j.cocis.2016.09.013.

[15] J.H. Piette, A. Abbasi Moud, J. Poisson, B. Derakhshandeh, Z.M. Hudson, S.G. Hatzikiriakos, Rheology of Mature Fine Tailings, Physics of Fluids. (2022) 5.0091505. https://doi.org/10.1063/5.0091505.

[16] J. Klein, Forces between mica surfaces bearing adsorbed macromolecules in liquid media, Journal of the Chemical Society, Faraday Transactions 1: Physical Chemistry in Condensed Phases. 79 (1983) 99. https://doi.org/10.1039/f19837900099.

[17] J. Klein, Forces between mica surfaces bearing layers of adsorbed polystyrene in cyclohexane, Nature. 288 (1980) 248–250. https://doi.org/10.1038/288248a0.

[18] J.N. Israelachvili, M. Tirrell, J. Klein, Y. Almog, Forces between two layers of adsorbed polystyrene immersed in cyclohexane below and above the θ temperature, Macromolecules. 17 (1984) 204–209. https://doi.org/10.1021/ma00132a015.

[19] J. Gregory, C.R. O'Melia, Fundamentals of flocculation, Critical Reviews in Environmental Control. 19 (1989) 185–230. https://doi.org/10.1080/10643389909388365.

[20] J. Gregory, S. Barany, Adsorption and flocculation by polymers and polymer mixtures, Advances in Colloid and Interface Science. 169 (2011) 1–12. https://doi.org/10.1016/j.cis.2011.06.004.

[21] G.J. Fleer, M.A.C. Stuart, J.M.H.M. Scheutjens, T. Cosgrove, B. Vincent, Polymers at Interfaces, Springer Netherlands, Dordrecht, 1998. https://doi.org/10.1007/978-94-011-2130-9.

[22] V. Vajihinejad, S.P. Gumfekar, B. Bazoubandi, Z. Rostami Najafabadi, J.B.P. Soares, Water Soluble Polymer Flocculants: Synthesis, Characterization, and Performance Assessment, Macromolecular Materials and Engineering. (2018) 1800526. https://doi.org/10.1002/mame.201800526.

[23] M.A.C. Stuart, G.J. Fleer, Adsorbed Polymer Layers in Nonequilibrium Situations, Annu. Rev. Mater. Sci. 26 (1996) 463–500. https://doi.org/10/dxhrfs.

[24] M. Elimelech, J. Gregory, X. Jia, R.A. Williams, Modelling of aggregation processes, in: Particle Deposition & Aggregation, Elsevier, 1995: pp. 157–202. https://doi.org/10.1016/B978-075067024-1/50006-6.

[25] E. Dickinson, L. Eriksson, Particle flocculation by adsorbing polymers, Advances in Colloid and Interface Science. 34 (1991) 1–29. https://doi.org/10.1016/0001-8686(91)80045-L.

[26] V. Vajihinejad, J.B.P. Soares, Monitoring polymer flocculation in oil sands tailings: A population balance model approach, Chemical Engineering Journal. 346 (2018) 447–457. https://doi.org/10.1016/j.cej.2018.04.039.

[27] A. Hethnawi, T. Karaki, Y.Z. Keteklahijani, M. Chehelamirani, A. Hassan, N.N. Nassar, Enhanced Settling and Dewatering of Oil Sands Mature Fine Tailings with Titanomagnetite Nanoparticles Grafted with Polyacrylamide and Lauryl Sulfate, ACS Appl. Nano Mater. (2022) acsanm.1c04566. https://doi.org/10.1021/acsanm.1c04566.

[28] S.P. Gumfekar, T.R. Rooney, R.A. Hutchinson, J.B.P. Soares, Dewatering Oils Sands Tailings with Degradable Polymer Flocculants, ACS Applied Materials & Interfaces. (2017) acsami.7b10302. https://doi.org/10.1021/acsami.7b10302.

[29] G.R. Younes, A.R. Proper, T.R. Rooney, R.A. Hutchinson, S.P. Gumfekar, J.B.P. Soares, Structure Modifications of Hydrolytically-Degradable Polymer Flocculant for

Improved Water Recovery from Mature Fine Tailings, Ind. Eng. Chem. Res. 57 (2018) 10809–10822. https://doi.org/10.1021/acs.iecr.8b02783.

[30] Z. Rostami Najafabadi, A.A. Omaña, E. Rivard, J.B.P. Soares, Ethylene/Propylene/Diene Terpolymers Grafted with Poly(methyl acrylate) by Reverse Atom Transfer Radical Polymerization, Macro Chemistry & Physics. 222 (2021) 2100189. https://doi.org/10.1002/macp.202100189.

[31] Z. Rostami Najafabadi, J.B.P. Soares, Flocculation and dewatering of oil sands tailings with a novel functionalized polyolefin flocculant, Separation and Purification Technology. 274 (2021) 119018. https://doi.org/10.1016/j.seppur.2021.119018.

[32] W. Zou, L. Gong, M. Pan, Z. Zhang, C. Sun, H. Zeng, Effect of salinity on adsorption and interaction forces of hydrophobically modified polyacrylamide on silica and alumina surfaces, Minerals Engineering. 150 (2020) 106280. https://doi.org/10/ggm6gz.

[33] W. Zou, L. Gong, J. Huang, Z. Zhang, C. Sun, H. Zeng, Adsorption of hydrophobically modified polyacrylamide P(AM-NaAA-C16DMAAC) on model coal and clay surfaces and the effect on selective flocculation of fine coal, Minerals Engineering. 142 (2019) 105887. https://doi.org/10.1016/j.mineng.2019.105887.

[34] V.H. Lim, Y. Adachi, Analysis of initial stage of colloidal particles flocculation induced by different degree branching polyelectrolytes, Colloids and Surfaces A: Physicochemical and Engineering Aspects. 625 (2021) 126986. https://doi.org/10/gmvxvn.

[35] B. Nguyen, J.B.P. Soares, Effect of the branching morphology of a cationic polymer flocculant synthesized by controlled reversible-deactivation radical polymerization on the flocculation and dewatering of dilute mature fine tailings, The Canadian Journal of Chemical Engineering. 100 (2022) 790–799. https://doi.org/10.1002/cjce.24329.

[36] V.H. Dao, N.R. Cameron, K. Saito, Synthesis of UHMW Star-Shaped AB Block Copolymers and Their Flocculation Efficiency in High-Ionic-Strength Environments, Macromolecules. 52 (2019) 7613–7624. https://doi.org/10/ghf4tx.

[37] V. Dao, K. Mohanarangam, P.D. Fawell, K. Simic, R. Iyer, N.R. Cameron, K. Saito, Enhanced Flocculation Efficiency in High Ionic Strength Environment by the

aid of Anionic ABA Triblock Copolymers, Langmuir. (2020). https://doi.org/10.1021/acs.langmuir.9b03689.

[38] L.-W. Zhang, J.-R. Hua, W.-J. Zhu, L. Liu, X.-L. Du, R.-J. Meng, J.-M. Yao, Flocculation Performance of Hyperbranched Polyethylenimine-Grafted Cellulose in Wastewater Treatment, ACS Sustainable Chem. Eng. 6 (2018) 1592–1601. https://doi.org/10.1021/acssuschemeng.7b02343.

[39] B. Zheng, S.D. Taylor, Nonthermoresponsive and Thermoresponsive Cationic Starch for the Flocculation of Oil Sands Mature Fine Tailings, Energy Fuels. 35 (2021) 5163–5171. https://doi.org/10.1021/acs.energyfuels.1c00031.

[40] B. Zheng, S.D. Taylor, Thermoresponsive Starch for the Flocculation of Oil Sands Mature Fine Tailings, Environ. Sci. Technol. 54 (2020) 13981–13991. https://doi.org/10.1021/acs.est.0c02576.

[41] B. Bazoubandi, Amylopectin-graft-polyacrylamide for the flocculation and dewatering of oil sands tailings, Minerals Engineering. (2020) 11. https://doi.org/10/gjpxvh.

[42] S. Davey, J.B.P. Soares, Amylopectin graft copolymers for oil sands tailings treatment, Can J Chem Eng. 100 (2022) 731–751. https://doi.org/10.1002/cjce.24290.

[43] C. Campano, P. Lopez-Exposito, A. Blanco, C. Negro, T.G.M. van de Ven, Hairy cationic nanocrystalline cellulose as a novel flocculant of clay, Journal of Colloid and Interface Science. 545 (2019) 153–161. https://doi.org/10.1016/j.jcis.2019.02.097.

[44] H. Yang, T.G.M. van de Ven, Preparation of hairy cationic nanocrystalline cellulose, Cellulose. 23 (2016) 1791–1801. https://doi.org/10.1007/s10570-016-0902-5.

[45] P. Lopez-Exposito, C. Negro, A. Blanco, Direct estimation of microalgal flocs fractal dimension through laser reflectance and machine learning, Algal Research. 37 (2019) 240–247. https://doi.org/10.1016/j.algal.2018.12.007.

[46] A. Abbasi Moud, Polymer based flocculants: Review of water purification applications, Journal of Water Process Engineering. 48 (2022) 102938. https://doi.org/10.1016/j.jwpe.2022.102938.

[47] Q. Lu, B. Yan, L. Xie, J. Huang, Y. Liu, H. Zeng, A two-step flocculation process on oil sands tailings treatment using oppositely charged polymer flocculants, Science

of the Total Environment. 565 (2016) 369–375. https://doi.org/10.1016/j.scitotenv.2016.04.192.

[48] Y. Zhu, X. Tan, Q. Liu, Dual polymer flocculants for mature fine tailings dewatering, The Canadian Journal of Chemical Engineering. 95 (2017) 3–10. https://doi.org/10.1002/cjce.22628.

[49] R. Loerke, X. Tan, Q. Liu, Dewatering of Oil Sands Mature Fine Tailings by Dual Polymer Flocculation and Pressure Plate Filtration, Energy Fuels. 31 (2017) 6986–6995. https://doi.org/10.1021/acs.energyfuels.7b00938.

[50] J. Zhou, H. Li, X. Zhang, Synergy between Dual Polymers and Sand-to-Fines Ratio for Enhanced Flocculation of Oil Sand Mature Fine Tailings, Energy Fuels. 35 (2021) 8884–8894. https://doi.org/10.1021/acs.energyfuels.1c00620.

[51] X. Yu, P. Somasundaran, Enhanced flocculation with double flocculants, Colloids and Surfaces A: Physicochemical and Engineering Aspects. 81 (1993) 17–23. https://doi.org/10.1016/0927-7757(93)80231-3.

[52] A. Fan, N.J. Turro, P. Somasundaran, A study of dual polymer flocculation, Colloids and Surfaces A: Physicochemical and Engineering Aspects. 162 (2000) 141–148. https://doi.org/10.1016/S0927-7757(99)00252-6.

[53] Y. Yang, A. Wu, B. Klein, H. Wang, Effect of primary flocculant type on a two-step flocculation process on iron ore fine tailings under alkaline environment, Minerals Engineering. 132 (2019) 14–21. https://doi.org/10.1016/j.mineng.2018.11.053.

[54] R. Xu, W. Zou, T. Wang, J. Huang, Z. Zhang, C. Xu, Adsorption and interaction mechanisms of Chi-g-P(AM-DMDAAC) assisted settling of kaolinite in a two-step flocculation process, Science of The Total Environment. 816 (2022) 151576. https://doi.org/10.1016/j.scitotenv.2021.151576.

[55] N.P. Truong, G.R. Jones, K.G.E. Bradford, D. Konkolewicz, A. Anastasaki, A comparison of RAFT and ATRP methods for controlled radical polymerization, Nat Rev Chem. (2021). https://doi.org/10/gm7qk2.

[56] S. Perrier, *50th Anniversary Perspective* : RAFT Polymerization—A User Guide, Macromolecules. 50 (2017) 7433–7447. https://doi.org/10.1021/acs.macromol.7b00767.

[57] J. Chiefari, Y.K. Chong, F. Ercole, J. Krstina, J. Jeffery, T.P.T. Le, R.T.A. Mayadunne, G.F. Meijs, C.L. Moad, G. Moad, E. Rizzardo, S.H. Thang, Living free-radical polymerization by reversible addition - Fragmentation chain transfer: The RAFT process, Macromolecules. 31 (1998) 5559–5562. https://doi.org/10.1021/ma9804951.

[58] E. Read, A. Guinaudeau, D. James Wilson, A. Cadix, F. Violleau, M. Destarac, Low temperature RAFT/MADIX gel polymerisation: access to controlled ultra-high molar mass polyacrylamides, Polymer Chemistry. 5 (2014) 2202. https://doi.org/10.1039/c3py01750h.

[59] R.N. Carmean, T.E. Becker, M.B. Sims, B.S. Sumerlin, Ultra-High Molecular Weights via Aqueous Reversible-Deactivation Radical Polymerization, Chem. 2 (2017) 93–101. https://doi.org/10.1016/j.chempr.2016.12.007.

[60] R.J. McBride, J.F. Miller, A. Blanazs, H.-J. Hähnle, S.P. Armes, Synthesis of High Molecular Weight Water-Soluble Polymers as Low-Viscosity Latex Particles by RAFT Aqueous Dispersion Polymerization in Highly Salty Media, Macromolecules. (2022). https://doi.org/10.1021/acs.macromol.2c01071.

[61] D.T. Gentekos, R.J. Sifri, B.P. Fors, Controlling polymer properties through the shape of the molecular-weight distribution, Nat Rev Mater. 4 (2019) 761–774. https://doi.org/10/gn84j8.

[62] Z. An, 100th Anniversary of Macromolecular Science Viewpoint: Achieving Ultrahigh Molecular Weights with Reversible Deactivation Radical Polymerization, ACS Macro Lett. 9 (2020) 350–357. https://doi.org/10/ghf4tw.

[63] N. Zaquen, M. Rubens, N. Corrigan, J. Xu, P.B. Zetterlund, C. Boyer, T. Junkers, Polymer Synthesis in Continuous Flow Reactors, Progress in Polymer Science. 107 (2020) 101256. https://doi.org/10.1016/j.progpolymsci.2020.101256.

[64] M.-N. Antonopoulou, R. Whitfield, N.P. Truong, D. Wyers, S. Harrisson, T. Junkers, A. Anastasaki, Concurrent control over sequence and dispersity in multiblock copolymers, Nat. Chem. 14 (2022) 304–312. https://doi.org/10.1038/s41557-021-00818-8.

[65] H. Bessaies-Bey, J. Fusier, M. Hanafi, S. Zhang, M. Destarac, S. Jouenne, N. Passade-Boupat, F. Lequeux, J.-B. d'Espinose de Lacaillerie, N. Sanson, Competitive

adsorption of PAM and HPAM on siliceous material, Colloids and Surfaces A: Physicochemical and Engineering Aspects. 579 (2019) 123673. https://doi.org/10.1016/j.colsurfa.2019.123673.

[66] G.J. Howard, S.J. Woods, Adsorption of polymers at the solution-solid interface. VIII. Competitive effects in the adsorption of polystyrenes on silica, Journal of Polymer Science Part A-2: Polymer Physics. 10 (1972) 1023–1028. https://doi.org/10.1002/pol.1972.160100606.

[67] E.G.M. Pelssers, M.A.C. Stuart, G.J. Fleer, Kinetic aspects of polymer bridging: Equilibrium flocculation and nonequilibrium flocculation, Colloids and Surfaces. 38 (1989) 15–25. https://doi.org/10.1016/0166-6622(89)80139-8.

[68] C. Barner-Kowollik, ed., Handbook of RAFT polymerization, Wiley-VCH, Weinheim, 2008.

[69] A.R. Heath, P.D. Fawell, P.A. Bahri, J.D. Swift, Estimating average particle size by focused beam reflectance measurement (FBRM), Particle and Particle Systems Characterization. 19 (2002) 84–95. https://doi.org/10.1002/1521-4117(200205)19:2<84::AID-PPSC84>3.0.CO;2-1.

[70] F. Franco, L.A. Pérez-Maqueda, J.L. Pérez-Rodríguez, The effect of ultrasound on the particle size and structural disorder of a well-ordered kaolinite, Journal of Colloid and Interface Science. 274 (2004) 107–117. https://doi.org/10.1016/j.jcis.2003.12.003.

[71] B. Ndlovu, S. Farrokhpay, E. Forbes, D. Bradshaw, Characterisation of kaolinite colloidal and flow behaviour via crystallinity measurements, Powder Technology. 269 (2015) 505–512. https://doi.org/10.1016/j.powtec.2014.09.029.

[72] J. Gregory, Rates of flocculation of latex particles by cationic polymers, Journal of Colloid And Interface Science. 42 (1973) 448–456. https://doi.org/10.1016/0021-9797(73)90311-1.

[73] B. O'Shaughnessy, D. Vavylonis, Non-equilibrium in adsorbed polymer layers, Journal of Physics: Condensed Matter. 17 (2005) R63–R99. https://doi.org/10.1088/0953-8984/17/2/R01.

[74] D.T. Gentekos, R.J. Sifri, B.P. Fors, Controlling polymer properties through the shape of the molecular-weight distribution, Nature Reviews Materials. (2019). https://doi.org/10.1038/s41578-019-0138-8.

[75] D.T. Gentekos, J. Jia, E.S. Tirado, K.P. Barteau, D.-M. Smilgies, R.A. DiStasio, B.P. Fors, Exploiting Molecular Weight Distribution Shape to Tune Domain Spacing in Block Copolymer Thin Films, J. Am. Chem. Soc. 140 (2018) 4639–4648. https://doi.org/10/gdc9x5.

[76] D.J. Walsh, D.A. Schinski, R.A. Schneider, D. Guironnet, General route to design polymer molecular weight distributions through flow chemistry, Nat Commun. 11 (2020) 3094. https://doi.org/10.1038/s41467-020-16874-6.

[77] W. Sun, H. Zeng, T. Tang, Synergetic adsorption of polymers on montmorillonite: Insights from molecular dynamics simulations, Applied Clay Science. 193 (2020) 105654. https://doi.org/10/ggw6cx.

[78] V. Vajihinejad, S.P. Gumfekar, D.V. Dixon, M.A. Silva, J.B.P. Soares, Enhanced dewatering of oil sands tailings by a novel water-soluble cationic polymer, Separation and Purification Technology. 260 (2021) 118183. https://doi.org/10.1016/j.seppur.2020.118183.

[79] M. Lapointe, B. Barbeau, Dual starch–polyacrylamide polymer system for improved flocculation, Water Research. 124 (2017) 202–209. https://doi.org/10.1016/j.watres.2017.07.044.

[80] Bulmer J.T., J. Starr, Syncrude analytical methods for oil sand and bitumen processing, 1979.

[81] M. Boshrouyeh Ghandashtani, A. Costine, M. Edraki, T. Baumgartl, The impacts of high salinity and polymer properties on dewatering and structural characteristics of flocculated high-solids tailings, Journal of Cleaner Production. 342 (2022) 130726. https://doi.org/10.1016/j.jclepro.2022.130726.

[82] K. Nagase, K. Sakaguchi, Alkaline hydrolysis of polyacrylamide, Journal of Polymer Science Part A: General Papers. 3 (1965) 2475–2482. https://doi.org/10.1002/pol.1965.100030706.

[83] H. Kheradmand, J. François, V. Plazanet, Hydrolysis of polyacrylamide and acrylic acid-acrylamide copolymers at neutral pH and high temperature, Polymer. 29 (1988) 860–870. https://doi.org/10.1016/0032-3861(88)90145-0.

[84] Q. Ma, P.J. Shuler, C.W. Aften, Y. Tang, Theoretical studies of hydrolysis and stability of polyacrylamide polymers, Polymer Degradation and Stability. 121 (2015) 69–77. https://doi.org/10.1016/j.polymdegradstab.2015.08.012.

[85] M.S. Nasser, A.E. James, The effect of polyacrylamide charge density and molecular weight on the flocculation and sedimentation behaviour of kaolinite suspensions, Separation and Purification Technology. 52 (2006) 241–252. https://doi.org/10.1016/j.seppur.2006.04.005.

[86] F. Puel, G. Févotte, J.P. Klein, Simulation and analysis of industrial crystallization processes through multidimensional population balance equations. Part 1: a resolution algorithm based on the method of classes, Chemical Engineering Science. 58 (2003) 3715–3727. https://doi.org/10.1016/S0009-2509(03)00254-9.

[87] C.B.B. Costa, M.R.W. Maciel, R.M. Filho, Considerations on the crystallization modeling: Population balance solution, Computers & Chemical Engineering. 31 (2007) 206–218. https://doi.org/10.1016/j.compchemeng.2006.06.005.

[88] C. Kiparissides, A. Alexopoulos, A. Roussos, G. Dompazis, C. Kotoulas, Population Balance Modeling of Particulate Polymerization Processes, Ind. Eng. Chem. Res. 43 (2004) 7290–7302. https://doi.org/10.1021/ie049901x.

[89] C. Kotoulas, C. Kiparissides, A generalized population balance model for the prediction of particle size distribution in suspension polymerization reactors, Chemical Engineering Science. 61 (2006) 332–346. https://doi.org/10.1016/j.ces.2005.07.013.

[90] V. Runkana, P. Somasundaran, P.C. Kapur, A population balance model for flocculation of colloidal suspensions by polymer bridging, Chemical Engineering Science. 61 (2006) 182–191. https://doi.org/10.1016/j.ces.2005.01.046.

[91] R.I. Jeldres, P.D. Fawell, B.J. Florio, Population balance modelling to describe the particle aggregation process: A review, Powder Technology. 326 (2018) 190–207. https://doi.org/10.1016/j.powtec.2017.12.033.

[92] A.R. Heath, P.A. Bahri, P.D. Fawell, J.B. Farrow, Polymer flocculation of calcite: Population balance model, AIChE Journal. 52 (2006) 1641–1653. https://doi.org/10.1002/aic.10749.

[93] G.R. Quezada, J. Ramos, R.I. Jeldres, P. Robles, P.G. Toledo, Analysis of the flocculation process of fine tailings particles in saltwater through a population balance model, Separation and Purification Technology. 237 (2020) 116319. https://doi.org/10/ghtpwd.

[94] M. Vlieghe, C. Coufort-Saudejaud, A. Liné, C. Frances, QMOM-based population balance model involving a fractal dimension for the flocculation of latex particles, Chemical Engineering Science. 155 (2016) 65–82. https://doi.org/10.1016/j.ces.2016.07.044.

[95] K. Pougatch, S. Delfel, M. Hosseini, B. Moyls, A. Sadighian, A. Revington, Population balance modelling of dense clay slurries flocculation, Chemical Engineering Science. 231 (2021) 116260. https://doi.org/10/ghtpwf.

[96] M. Shiea, A. Buffo, M. Vanni, D. Marchisio, Numerical Methods for the Solution of Population Balance Equations Coupled with Computational Fluid Dynamics, Annu. Rev. Chem. Biomol. Eng. 11 (2020) 339–366. https://doi.org/10/gmfctf.

[97] X. Wang, B. Cui, D. Wei, Z. Song, Y. He, A.E. Bayly, CFD-PBM modelling of tailings flocculation in a lab-scale gravity thickener, Powder Technology. (2021) S0032591021009359. https://doi.org/10/gnbt68.

[98] R. Hecker, L. Kirwan, P. Fawell, J. Farrow, J. Swift, A. Jefferson, Focused beam reflectance measurement for the continuous assessment of flocculant performance, in: UBC-McGill International Symposium on Fundamentals of Mineral Processing, Canadian Institute of Mining, Metallurgy and Petroleum, Montreal, Quebec, 1999: pp. 91–105.

[99] S. Kumar, D. Ramkrishna, On the solution of population balance equations by discretization—I. A fixed pivot technique, Chemical Engineering Science. 51 (1996) 1311–1332. https://doi.org/10.1016/0009-2509(96)88489-2.

[100] M.J. Hounslow, R.L. Ryall, V.R. Marshall, A discretized population balance for nucleation, growth, and aggregation, AIChE Journal. 34 (1988) 1821–1832. https://doi.org/10.1002/aic.690341108.

[101] P.T. Spicer, S.E. Pratsinis, Coagulation and fragmentation: Universal steady-state particle-size distribution, AIChE Journal. 42 (1996) 1612–1620. https://doi.org/10.1002/aic.690420612.

[102] K.K. Kusters, The influence of turbulence on aggregation of small particles in agitated vessels, (1991). https://doi.org/10.6100/IR362582.

[103] R. McGraw, Description of Aerosol Dynamics by the Quadrature Method of Moments, Aerosol Science and Technology. 27 (1997) 255–265. https://doi.org/10/d63zm3.

[104] D.L. Marchisio, R.D. Vigil, R.O. Fox, Quadrature method of moments for aggregation–breakage processes, Journal of Colloid and Interface Science. 258 (2003) 322–334. https://doi.org/10.1016/S0021-9797(02)00054-1.

[105] M. Smith, T. Matsoukas, Constant-number Monte Carlo simulation of population balances, Chemical Engineering Science. 53 (1998) 1777–1786. https://doi.org/10/dcwkst.

[106] K. Lee, T. Matsoukas, Simultaneous coagulation and break-up using constant-N Monte Carlo, Powder Technology. 110 (2000) 82–89. https://doi.org/10/cjqk37.

[107] Y. Lin, K. Lee, T. Matsoukas, Solution of the population balance equation using constant-number Monte Carlo, Chemical Engineering Science. 57 (2002) 2241–2252. https://doi.org/10/cm5zb3.

[108] H.H. Liu, S. Surawanvijit, R. Rallo, G. Orkoulas, Y. Cohen, Analysis of Nanoparticle Agglomeration in Aqueous Suspensions via Constant-Number Monte Carlo Simulation, Environ. Sci. Technol. 45 (2011) 9284–9292. https://doi.org/10/d8f4xt.

[109] P.G. Saffman, J.S. Turner, On the collision of drops in turbulent clouds, J. Fluid Mech. 1 (1956) 16. https://doi.org/10.1017/S0022112056000020.

[110] P.T. Spicer, S.E. Pratsinis, Shear-induced flocculation: The evolution of floc structure and the shape of the size distribution at steady state, Water Research. 30 (1996) 1049–1056. https://doi.org/10.1016/0043-1354(95)00253-7.

[111] D.C. Hopkins, J.J. Ducoste, Characterizing flocculation under heterogeneous turbulence, Journal of Colloid and Interface Science. 264 (2003) 184–194. https://doi.org/10.1016/S0021-9797(03)00446-6.

[112] C. Selomulya, G. Bushell, R. Amal, T.D. Waite, Understanding the role of restructuring in flocculation: The application of a population balance model, Chemical Engineering Science. (2003) 12. https://doi.org/10.1016/S0009-2509(02)00523-7.

[113] P.M. Adler, Interaction of Unequal Spheres, Journal of Colloid and Interface Science. 84 (1981) 13.

[114] P.M. Adler, Streamlines in and around porous particles, Journal of Colloid and Interface Science. 81 (1981) 531–535. https://doi.org/10.1016/0021-9797(81)90434-3.

[115] R. Hogg, Collision efficiency factors for polymer flocculation, Journal of Colloid and Interface Science. 102 (1984) 232–236. https://doi.org/10.1016/0021-9797(84)90215-7.

[116] A. Swerin, L. Ödberg, L. Wågberg, An extended model for the estimation of flocculation efficiency factors in multicomponent flocculant systems, Colloids and Surfaces A: Physicochemical and Engineering Aspects. 113 (1996) 25–38. https://doi.org/10/czrxbm.

[117] J.D. Pandya, L.A. Spielman, Floc breakage in agitated suspensions: Theory and data processing strategy, Journal of Colloid and Interface Science. 90 (1982) 517–531. https://doi.org/10.1016/0021-9797(82)90317-4.

[118] W. Chen, R.R. Fischer, J.C. Berg, Simulation of particle size distribution in an aggregation-breakup process, Chemical Engineering Science. 45 (1990) 3003–3006. https://doi.org/10.1016/0009-2509(90)80201-O.

[119] D.V. Dixon, J.B.P. Soares, Molecular weight distribution effects of polyacrylamide flocculants on clay aggregate formation, Colloids and Surfaces A: Physicochemical and Engineering Aspects. (2022) 129487. https://doi.org/10.1016/j.colsurfa.2022.129487.

[120] L. Besra, D.K. Sengupta, S.K. Roy, P. Ay, Influence of polymer adsorption and conformation on flocculation and dewatering of kaolin suspension, Separation and Purification Technology. 37 (2004) 231–246. https://doi.org/10.1016/j.seppur.2003.10.001.

[121] S.M.R. Shaikh, M.S. Nasser, I.A. Hussein, A. Benamor, Investigation of the effect of polyelectrolyte structure and type on the electrokinetics and flocculation behavior of bentonite dispersions, Chemical Engineering Journal. 311 (2017) 265–276. https://doi.org/10.1016/j.cej.2016.11.098.

[122] R. Denoyel, G. Durand, F. Lafuma, R. Audebert, Adsorption of cationic polyelectrolytes onto montmorillonite and silica: Microcalorimetric study of their conformation, Journal of Colloid and Interface Science. 139 (1990) 281–290. https://doi.org/10.1016/0021-9797(90)90463-X.

[123] C. Rackauckas, Q. Nie, DifferentialEquations.jl – A Performant and Feature-Rich Ecosystem for Solving Differential Equations in Julia, JORS. 5 (2017) 15. https://doi.org/10.5334/jors.151.

[124] K.A. Clark, D.S. Pasternack, Hot Water Seperation of Bitumen from Alberta Bituminous Sand, Industrial & Engineering Chemistry. 24 (1932) 1410–1416. https://doi.org/10.1021/ie50276a016.

[125] Lower Athabasca Region: Tailings Management Framework for Mineable Athabasca Oil Sands, 2015.

[126] L. Botha, J.B.P. Soares, The Influence of Tailings Composition on Flocculation, Canadian Journal of Chemical Engineering. 93 (2015) 1514–1523. https://doi.org/10.1002/cjce.22241.

[127] D.R.L. Vedoy, J.B.P. Soares, Water-soluble polymers for oil sands tailing treatment: A Review, Canadian Journal of Chemical Engineering. 93 (2015) 888–904. https://doi.org/10.1002/cjce.22129.

[128] F. Lin, S.R. Stoyanov, Y. Xu, Recent Advances in Nonaqueous Extraction of Bitumen from Mineable Oil Sands: A Review, Organic Process Research & Development. 21 (2017) 492–510. https://doi.org/10.1021/acs.oprd.6b00357.

[129] F. Rao, Q. Liu, Froth Treatment in Athabasca Oil Sands Bitumen Recovery Process: A Review, Energy & Fuels. 27 (2013) 7199–7207. https://doi.org/10.1021/ef4016697.

[130] G. Ngnie, D. Baitan, G.K. Dedzo, C. Detellier, Sedimentation of fine particles of kaolinite and polymer-coated kaolinite in cyclohexane: Implications for fines

removal from extracted bitumen in non-aqueous processes, Fuel. 234 (2018) 218–224. https://doi.org/10.1016/j.fuel.2018.07.032.

[131] J. Gregory, S. Barany, Adsorption and flocculation by polymers and polymer mixtures, Advances in Colloid and Interface Science. 169 (2011) 1–12. https://doi.org/10.1016/j.cis.2011.06.004.

[132] H. Li, J. Long, Z. Xu, J.H. Masliyah, Novel polymer aids for low-grade oil sand ore processing, The Canadian Journal of Chemical Engineering. 86 (2008) 168–176. https://doi.org/10.1002/cjce.20030.

[133] H. Li, J. Long, Z. Xu, J.H. Masliyah, Synergetic Role of Polymer Flocculant in Low-Temperature Bitumen Extraction and Tailings Treatment, Energy & Fuels. 19 (2005) 936–943. https://doi.org/10.1021/ef049744e.

[134] J. Long, H. Li, Z. Xu, J.H. Masliyah, Improving Oil Sands Processability Using a Temperature-Sensitive Polymer, Energy & Fuels. 25 (2011) 701–707. https://doi.org/10.1021/ef1012819.

[135] M.-H. Ese, J. Sjöblom, J. Djuve, R. Pugh, An atomic force microscopy study of asphaltenes on mica surfaces. Influence of added resins and demulsifiers, Colloid & Polymer Science. 278 (2000) 532–538. https://doi.org/10.1007/s003960050551.

[136] P. Tchoukov, F. Yang, Z. Xu, T. Dabros, J. Czarnecki, J. Sjöblom, Role of asphaltenes in stabilizing thin liquid emulsion films, Langmuir. 30 (2014) 3024–3033. https://doi.org/10.1021/la404825g.

[137] E. Pensini, D. Harbottle, F. Yang, P. Tchoukov, Z. Li, I. Kailey, J. Behles, J. Masliyah, Z. Xu, Demulsification Mechanism of Asphaltene-Stabilized Water-in-Oil Emulsions by a Polymeric Ethylene Oxide–Propylene Oxide Demulsifier, Energy & Fuels. 28 (2014) 6760–6771. https://doi.org/10.1021/ef501387k.

[138] J. Wu, Y. Xu, T. Dabros, H. Hamza, Effect of EO and PO positions in nonionic surfactants on surfactant properties and demulsification performance, Colloids and Surfaces A: Physicochemical and Engineering Aspects. 252 (2005) 79–85. https://doi.org/10.1016/j.colsurfa.2004.09.034.

[139] I. Szilagyi, G. Trefalt, A. Tiraferri, P. Maroni, M. Borkovec, Polyelectrolyte adsorption, interparticle forces, and colloidal aggregation, Soft Matter. 10 (2014) 2479. https://doi.org/10.1039/c3sm52132j.

[140] D.H. Napper, Flocculation studies of non-aqueous sterically stabilized dispersions of polymer, Transactions of the Faraday Society. 64 (1968) 1701. https://doi.org/10.1039/tf9686401701.

[141] V. Vajihinejad, S.P. Gumfekar, B. Bazoubandi, Z. Rostami Najafabadi, J.B.P. Soares, Water Soluble Polymer Flocculants: Synthesis, Characterization, and Performance Assessment, Macromolecular Materials and Engineering. 304 (2019) 1800526. https://doi.org/10.1002/mame.201800526.

[142] J. Long, H. Li, Z. Xu, J.H. Masliyah, Role of colloidal interactions in oil sand tailings treatment, AIChE Journal. 52 (2006) 371–383. https://doi.org/10.1002/aic.10603.

[143] Q. Lu, B. Yan, L. Xie, J. Huang, Y. Liu, H. Zeng, A two-step flocculation process on oil sands tailings treatment using oppositely charged polymer flocculants, Science of the Total Environment. 565 (2016) 369–375. https://doi.org/10.1016/j.scitotenv.2016.04.192.

[144] Y. Zhu, X. Tan, Q. Liu, Dual polymer flocculants for mature fine tailings dewatering, The Canadian Journal of Chemical Engineering. 95 (2017) 3–10. https://doi.org/10.1002/cjce.22628.

[145] H. Lu, L. Xiang, X. Cui, J. Liu, Y. Wang, R. Narain, H. Zeng, Molecular Weight Dependence of Synthetic Glycopolymers on Flocculation and Dewatering of Fine Particles, Langmuir. 32 (2016) 11615–11622. https://doi.org/10.1021/acs.langmuir.6b03072.

[146] L.G. Reis, R.S. Oliveira, T.N. Palhares, L.S. Spinelli, E.F. Lucas, D.R.L. Vedoy, E. Asare, J.B.P. Soares, Using acrylamide/propylene oxide copolymers to dewater and densify mature fine tailings, Minerals Engineering. 95 (2016) 29–39. https://doi.org/10.1016/j.mineng.2016.06.005.

[147] L. Botha, S. Davey, B. Nguyen, A.K. Swarnakar, E. Rivard, J.B.P. Soares, Flocculation of oil sands tailings by hyperbranched functionalized polyethylenes (HBfPE), Minerals Engineering. 108 (2017) 71–82. https://doi.org/10.1016/j.mineng.2017.02.004.

[148] H. Li, J. Zhou, R. Chow, A. Adegoroye, A.S. Najafi, Enhancing treatment and geotechnical stability of oil sands fine tailings using thermo-sensitive poly(n-

isopropyl acrylamide), Canadian Journal of Chemical Engineering. 93 (2015) 1780–1786. https://doi.org/10.1002/cjce.22276.

[149] H. Lu, Y. Wang, L. Li, Y. Kotsuchibashi, R. Narain, H. Zeng, Temperature- and pH-Responsive Benzoboroxole-Based Polymers for Flocculation and Enhanced Dewatering of Fine Particle Suspensions, ACS Applied Materials and Interfaces. 7 (2015) 27176–27187. https://doi.org/10.1021/acsami.5b09874.

[150] E. Dickinson, L. Eriksson, Particle flocculation by adsorbing polymers, Advances in Colloid and Interface Science. 34 (1991) 1–29. https://doi.org/10.1016/0001-8686(91)80045-L.

[151] S. Wang, L. Zhang, B. Yan, H. Xu, Q. Liu, H. Zeng, Molecular and surface interactions between polymer flocculant chitosan g polyacrylamide and kaolinite particles: Impact of salinity, Journal of Physical Chemistry C. 119 (2015) 7327–7339. https://doi.org/10.1021/acs.jpcc.5b00739.

[152] J. Gregory, Rates of flocculation of latex particles by cationic polymers, Journal of Colloid And Interface Science. 42 (1973) 448–456. https://doi.org/10.1016/0021-9797(73)90311-1.

[153] J.C. Berg, An Introduction to Interfaces and Colloids: The Bridge to Nanoscience, World Scientific, 2010.

[154] I.D. Morrison, Electrical charges in nonaqueous media, Colloids and Surfaces A: Physicochemical and Engineering Aspects. 71 (1993) 1–37. https://doi.org/10.1016/0927-7757(93)80026-B.

[155] B.J. Marlow, G.C. Sresty, R.D. Hughes, O.P. Mahajan, Colloidal stabilization of clays by asphaltenes in hydrocarbon media, Colloids and Surfaces. 24 (1987) 283–297. https://doi.org/10.1016/0166-6622(87)80235-4.

[156] S. Wang, J. Liu, L. Zhang, Z. Xu, J. Masliyah, Colloidal Interactions between Asphaltene Surfaces in Toluene, Energy & Fuels. 23 (2009) 862–869. https://doi.org/10.1021/ef800812k.

[157] A. Natarajan, J. Xie, S. Wang, J. Masliyah, H. Zeng, Z. Xu, Z. Xu, Understanding Molecular Interactions of Asphaltenes in Organic Solvents Using a Surface Force Apparatus, The Journal of Physical Chemistry C. 115 (2011) 16043–16051. https://doi.org/10.1021/jp2039674.

[158] C. Hansen, Hansen Solubility Parameters, CRC Press, 2007. https://doi.org/10.1201/9781420006834.

[159] H. Nikakhtari, L. Vagi, P. Choi, Q. Liu, M.R. Gray, Solvent screening for non-aqueous extraction of Alberta oil sands, The Canadian Journal of Chemical Engineering. 91 (2013) 1153–1160. https://doi.org/10.1002/cjce.21751.

[160] K. Pal, L.D.P. Nogueira Branco, A. Heintz, P. Choi, Q. Liu, P.R. Seidl, M.R. Gray, Performance of Solvent Mixtures for Non-aqueous Extraction of Alberta Oil Sands, Energy & Fuels. 29 (2015) 2261–2267. https://doi.org/10.1021/ef502882c.

[161] J.E. Mark, ed., Physical Properties of Polymers Handbook, Springer New York, New York, NY, 2007. https://doi.org/10.1007/978-0-387-69002-5.

[162] D. Mowla, A. Naderi, Experimental study of drag reduction by a polymeric additive in slug two-phase flow of crude oil and air in horizontal pipes, Chemical Engineering Science. 61 (2006) 1549–1554. https://doi.org/10.1016/j.ces.2005.09.006.

[163] C.P.P. Mazzeo, F.A. Stedille, C.R.E. Mansur, A.C.S. Ramos, E.F. Lucas, Flocculation of Asphaltenes by Polymers: Influence of Polymer Solubility Conditions, Energy & Fuels. 32 (2018) 1087–1095. https://doi.org/10.1021/acs.energyfuels.7b02577.

[164] T.C. Chung, W. Janvikul, R. Bernard, G.J. Jiang, Synthesis of ethylene-propylene rubber graft copolymers by borane approach, Macromolecules. 27 (1994) 26–31. https://doi.org/10.1021/ma00079a004.

[165] C.P.P. Mazzeo, F.A. Stedille, C.R.E. Mansur, A.C.S. Ramos, E.F. Lucas, Flocculation of Asphaltenes by Polymers: Influence of Polymer Solubility Conditions, Energy & Fuels. 32 (2018) 1087–1095. https://doi.org/10.1021/acs.energyfuels.7b02577.

[166] V. Vajihinejad, J.B.P. Soares, Monitoring polymer flocculation in oil sands tailings: A population balance model approach, Chemical Engineering Journal. 346 (2018) 447–457. https://doi.org/10.1016/j.cej.2018.04.039.

[167] S.P. Gumfekar, J.B.P. Soares, A novel hydrophobically-modified polyelectrolyte for enhanced dewatering of clay suspension, Chemosphere. 194 (2018) 422–431. https://doi.org/10.1016/j.chemosphere.2017.12.009.

[168] J.K. Gupta, S. Basu, Simultaneous aggregation and sedimentation of silica particles in the presence of surfactants, Colloids and Surfaces A: Physicochemical and Engineering Aspects. 255 (2005) 139–143. https://doi.org/10.1016/j.colsurfa.2004.12.010.

[169] A. Karkooti, Aggregation and Sedimentation of Fine Solids in Non-Aqueous Media, University of Alberta, 2014.

[170] L. He, F. Lin, X. Li, H. Sui, Z. Xu, Interfacial sciences in unconventional petroleum production: from fundamentals to applications, Chem. Soc. Rev. 44 (2015) 5446–5494. https://doi.org/10.1039/C5CS00102A.

[171] H.A.W. Kaminsky, T.H. Etsell, D.G. Ivey, O. Omotoso, Distribution of clay minerals in the process streams produced by the extraction of bitumen from athabasca oil sands, Canadian Journal of Chemical Engineering. 87 (2009) 85–93. https://doi.org/10.1002/cjce.20133.

[172] S. Hlushak, A. Kovalenko, Effective Interactions and Adsorption of Heterocyclic Aromatic Hydrocarbons in Kaolinite Organic Solutions Studied by 3D-RISM-KH Molecular Theory of Solvation, The Journal of Physical Chemistry C. 121 (2017) 22092–22104. https://doi.org/10.1021/acs.jpcc.7b06414.

[173] S. Hlushak, S.R. Stoyanov, A. Kovalenko, A 3D-RISM-KH Molecular Theory of Solvation Study of the Effective Stacking Interactions of Kaolinite Nanoparticles in Aqueous Electrolyte Solution Containing Additives, The Journal of Physical Chemistry C. 120 (2016) 21344–21357. https://doi.org/10.1021/acs.jpcc.6b03786.

[174] A.R. Heath, P.D. Fawell, P.A. Bahri, J.D. Swift, Estimating average particle size by focused beam reflectance measurement (FBRM), Particle and Particle Systems Characterization. 19 (2002) 84–95. https://doi.org/10.1002/1521-4117(200205)19:2<84::AID-PPSC84>3.0.CO;2-1.

[175] M. Abdollahi, F. Ziaee, P. Alamdari, H. Koolivand, A comprehensive study on the kinetics of aqueous free-radical homo- and copolymerization of acrylamide and diallyldimethylammonium chloride by online 1H-NMR spectroscopy, Journal of Polymer Research. 20 (2013). https://doi.org/10.1007/s10965-013-0239-9.

[176] J. Feng, O.O. Oyeneye, W.Z. Xu, P.A. Charpentier, In-Situ NMR Measurement of Reactivity Ratios for Copolymerization of Methyl Methacrylate and Diallyl

Dimethylammonium Chloride, Industrial & Engineering Chemistry Research. 57 (2018) 15654–15662. https://doi.org/10.1021/acs.iecr.8b04033.

[177] C. Preusser, R.A. Hutchinson, An In-Situ NMR Study of Radical Copolymerization Kinetics of Acrylamide and Non-Ionized Acrylic Acid in Aqueous Solution, Macromolecular Symposia. 333 (2013) 122–137. https://doi.org/10.1002/masy.201300048.

[178] D. Cuccato, G. Storti, M. Morbidelli, Experimental and Modeling Study of Acrylamide Copolymerization with Quaternary Ammonium Salt in Aqueous Solution, Macromolecules. 48 (2015) 5076–5087. https://doi.org/10.1021/acs.macromol.5b01148.

[179] P.C. Hiemenz, T.P. Lodge, Polymer Chemistry, 2nd ed., CRC Press, 2007.

Appendix A CHALLENGES IN DEVELOPING POLYMER FLOCCULANTS TO IMPROVE BITUMEN QUALITY IN NON-AQUEOUS EXTRACTION PROCESSES: AN EXPERIMENTAL STUDY

Western Canada's oil sands hold the third-largest hydrocarbon deposits in the world. Bitumen, a very heavy petroleum, is currently recovered by surface mining with warm water or *in situ*. Recovery processes that use organic solvents are being developed to reduce water usage and tailings production. While solvent-based methods can effectively extract bitumen, removal of residual fine solids from diluted bitumen product (DBP) to meet the pipeline transport requirement of <0.5 wt% solids and water in DBP remains a major challenge. We propose a novel area of application of polymer flocculants for fine solids removal from DBP. In principle, polymer flocculants can be applied to help remove these residual solids in conjunction with physical separation processes to increase process effectiveness and energy efficiency. Several polymers are selected and screened for flocculation behaviour using kaolinite suspended in DBP and toluene, as a model system. Focused beam reflectance measurements and force tensiometer techniques are used to determine flocculation and sedimentation in DBP. The observed flocculation and sedimentation rate enhancements indicate that the polymers tested have only minor effects, providing opportunities for advanced polymer development. These findings exemplify the challenges in identifying polymers that may be effective as flocculants in heavy petroleum media.

A.1 INTRODUCTION

For several decades, bitumen has been extracted from oil sands in Alberta by surface mining using variations of the modified Clark hot water extraction process [124]. This

process is energy intensive, as up to 10 volumes of water need to be heated per volume of bitumen produced. The process also yields fluid fine tailings (FFT) that are currently stored in tailings ponds for decades, and must undergo further intensive dewatering before the solids can be reclaimed as a dry landscape. Recent estimates show that tailing ponds (including dykes, berms, and beaches) already occupy over 220 km^2 of land in Alberta [125]. The remediation of tailings ponds is an area of active research, with polymeric flocculants being used in most commercial tailings treatment technologies [126,127].

Alternatives to the modified Clark process are actively being investigated, with the aim of reducing energy and water usage. Of particular interest are non-aqueous bitumen extraction processes based on organic solvents intended to eliminate water use and long-term tailings storage [128]. Non-aqueous extraction processes however, face challenges in solvent recovery and solids migration to the bitumen product [128]. Process aids, such as polymers, are one approach that may improve the efficiency of non-aqueous bitumen extraction processes [128].

Both commercial extraction processes and pilot-scale non-aqueous extraction processes currently require an additional solids removal step before the bitumen product can be transported by pipeline [128,129]. The use of polymers as flocculants in organic media and in oil applications, have been, to the authors' knowledge, largely underexplored as a means of flocculating solids in these media, with previous studies being restricted to model systems [130].

Polymer flocculants have been used successfully to remove solids at lower energy costs than mechanical separations in waste water treatment, mineral processing, pulp and paper [131], as well as in treatment of FFT from oil sand mining operations. Process aids consisting mainly of polyacrylamides (PAMs), have been investigated to improve the overall processing of low-grade ores [132–134]. Polymers are used in bitumen froth treatment as demulsifiers to facilitate the coalescence of water droplets and allow for bitumen-water phase separation [135–138]. Typically, polymer flocculation involves the adsorption of a polymer onto the surface of colloidal particles, where it can then act as a bridge between particles, resulting in aggregation and destabilization of the suspension. The flocculation process is sometimes enhanced via charge neutralization if the polymer

sub-units and the particles are oppositely charged [127,139]. Higher-molecular-weight polymers improve particle settling rates due to the formation of longer/multiple bridges between mineral particles. Most flocculation applications call for water-soluble polymers and polyelectrolytes that are insoluble in bitumen. However, the principles of aqueous flocculation should be applicable for the development and optimization of oil-soluble polymer flocculants for the removal of fines from diluted bitumen products [130,140].

Of particular interest are polymer flocculants that have been used in the oil sands industry to treat FFT and mature fine tailings (MFT), a topic covered in recent reviews [127,141]. Most flocculants used to treat FFTs are derived from PAMs, which can by synthesized as neutral, anionic, or cationic polymers [127,142–149]. This flexibility has allowed PAMs to be used in a variety of systems that may require different charge characteristics. Additionally, PAMs can be synthesized with exceptionally high molecular weights (>10^6 g/mol), which makes these polymers even more effective as bridging flocculants [127,131]. In polymer applications for flocculation of solids out of bitumen, a major challenge would be to select polymers that adsorb on mineral solids but that are also soluble in oil.

A.2 Polymer Flocculant Selection

Many of the properties that make a demulsifier surface-active are analagous for polymer flocculants. Surface-active components are required for efficient adsorption of the polymer chains onto the clay particle surfaces. However, unlike demulsifiers, flocculants must be composed of long polymer chains so that the free end of an adsorbed polymer molecule may attach to other particles and form large flocs [150]. To meet the requirement of less than 0.5 wt% solids and water in diluted bitumen, the ideal flocculant must be soluble in diluted bitumen, form dense flocs with mineral solids that will settle out of the bitumen phase, preferentially adsorb to clay and other mineral particles over bitumen, and lead to a sediment that dries easily. The latter characteristic would minimize the retention of solvent in the settled solids. Ideally, this should be accomplished at the lowest possible dosage and material cost.

Intermolecular interactions are central to understanding how solids migrate into bitumen and how polymer flocculants operate. To better understand the hierarchy of intermolecular forces acting in these systems, further knowledge of the chemical structures of the solids and polymer flocculant, and of solvation thermodynamics is needed. Electrostatic and dispersion forces play key roles in interactions among the system components. Moreover, an understanding of the mechanism of formation of polymer bridges between particles and the forces that arise due to the bridging interactions, as well as the mixing energy in the system, are required in order to describe the interactions in the system [150].

Polymer bridging is the process by which a polymer molecule adsorbs onto one particle, and then a tail or loop of the adsorbed polymer adheres to other particle(s). If the bridging force is sufficient, the particles will remain in close proximity and form a floc that can then settle out of the mixture. Attractive bridging forces have been measured for polymer flocculants used in tailings treatments [143,149,151]. While bridging is the main mechanism for polymer-mediated flocculation, electric double-layer forces may also play a significant role for electrostatically stabilized suspensions. These suspensions can often be flocculated through charge neutralization, electrostatic patching, or in combination with polymer bridging [150]. For these cases, polyelectrolytes are the most useful additives because they interact strongly with charged particles that need to be separated. Adsorbed polymers are more likely to stay attached to an oppositely charged surface, and the net surface charge of the polymer-coated surfaces may be neutralized at the right dosage of polyelectrolyte. Complete coating of a charged particle with an oppositely charged polymer is not necessary for flocculation. If only patches of opposite charge are formed, the enhanced electrostatic attraction between the particles may still create better opportunities for polymer bridging [150,152].

Electrostatic effects are prominent in aqueous solutions, where ions are readily soluble and hydronium cations may freely dissociate from some functional groups, stabilized by water and free ions. This is not the case in nonpolar solvents, where the dielectric constants are very low (~2). As a result, in nonpolar media, electrostatic interactions typically play a smaller role compared to other interactions such as polymer bridging, steric forces, and hydrophobic interactions [153,154].

The choice of solvent can have a significant effect on the stability of a mineral suspension and the performance of a polymer flocculant. The interactions among polymer, solids, solvent, and the interfacially-active components of bitumen, such as asphaltenes, all contribute to flocculation performance. Toluene is considered a good solvent for asphaltenes, the component of bitumen that is known to stabilize emulsions and suspended solids [155]. In toluene-based systems, asphaltenes at surfaces create a repulsive steric barrier between particles due to the swelling of the asphaltene layer [156,157]. In the presence of heptane, a poor solvent for asphaltenes, the asphaltene layers are not extended and there is only a small attractive force between asphaltene-coated surfaces [157].

Moreover, the choice of solvent in the diluted bitumen would have a substantial effect on the thermodynamics of polymer adsorption. As described by the mean field theories of polymer adsorption, and the Flory-Huggins solution theory, the quality of the solvent can affect the conformation of polymers and the energetic driving force behind adsorption. For good flocculation performance, the polymer would need to outcompete adsorption of both solvent and bitumen components that may also interact with mineral surfaces.

When choosing a class of polymers to work with, the use of solubility parameters may be helpful in guiding the selection of materials that are compatible with bitumen-solvent mixtures. The solubility parameter, first introduced by Hildebrand and Scott, is derived from the cohesive energy density of a pure substance and estimated using the following equation [158]:

$$\delta = \left(\frac{\Delta H_v - RT}{V}\right)^{\frac{1}{2}} \tag{A-1}$$

where δ is the Hildebrand solubility parameter, ΔH_v is the enthalpy of vaporization, R is the gas constant, T is the absolute temperature, and V is the molar volume. According to this theory, materials having similar solubility parameters are miscible with one another. This theory is limited when it comes to polymers because the enthalpy of vaporization cannot be measured in polymeric materials, as they degrade when heated. The solubility parameters of polymers can be calculated by indirect methods based on solvent testing,

swelling values, refractive index, intrinsic viscosity or inverse gas chromatography. These can still serve to qualitatively predict behaviour or guide experiments.

When selecting solvents for the extraction of bitumen, Pal et al. and Nikakhtari et al [159,160]. have come to close agreement on what solubility parameter would be ideal for solvent-bitumen mixtures. Pal et al. determined that the solvent solubility parameter should fall between 16.45 $MPa^{1/2}$ and 16.65 $MPa^{1/2}$ to minimize fines in bitumen, and Nikakhtari et al. determined that solubility parameters above 16.5 $MPa^{1/2}$ are best to reduce fines migration into bitumen [159,160]. A polymer selected in this range may also be soluble in diluted bitumen. Some polymers in this range include polyethylene (16.2–16.6 $MPa^{1/2}$), polyisoprene (15.8–16.68 $MPa^{1/2}$), and polyisobutene (16.06–16.47 $MPa^{1/2}$) [161]. These polymers all fall under the class of polyolefins, and have been used widely in the oil industry as drag reducers for pipelines. They share some characteristics with the desired attributes of polymers for flocculation of fine solids in the bitumen extraction process, namely, they should be of high molecular weight (greater than 10^6 g/mol), amorphous, and readily soluble in oil [162].

A purely oil-soluble hydrophobic polymer, however, cannot be used in flocculation applications because the polymer would favour remaining in the bulk oil phase instead of adsorbing onto clay or other mineral solids. These solids are negatively charged in water and would still be partially negatively charged in bitumen because clays could retain some water from the oil sand ore. Therefore, the target polymer flocculant would also require some polar end groups or blocks of hydrophilic polymer to facilitate adsorption onto fine solids. Figure A-1 illustrates some possible arrangements of hydrophilic and hydrophobic monomers. Systems, such as hydrolyzed polyethylene [147], blocks of PEO/PPO [137,146], or temperature-responsive changes in hydrophobicity [134,149], have all been used in the treatment of mineral tailings and have the potential to work in the removal of solids from bitumen in a non-aqueous extraction process.

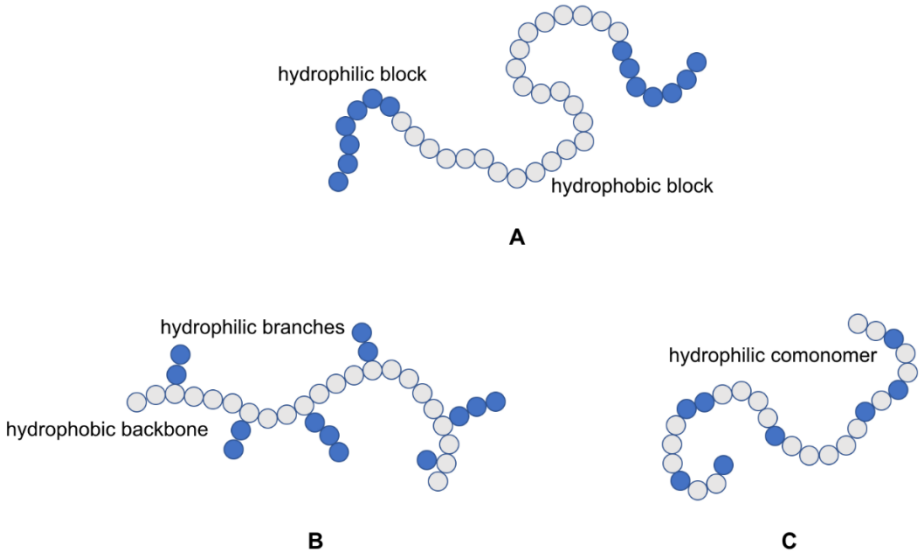

Figure A-1: Schematic diagram of possible polymer flocculant structures. A) block copolymer with hydrophobic chain and hydrophilic chain ends. B) hydrophobic polymer with hydrophilic branches. C) random copolymer with hydrophobic and hydrophilic monomers.

Herein, we explore the challenges faced when developing polymer flocculants to improve bitumen product quality and support the industrial implementation of non-aqueous recovery processes. An evaluation of several flocculant systems for solids removal is presented in the context of the challenges of observing fine solids settling in dark bitumen media. Moreover, criteria for the design of polymer flocculants to settle fine particles out of a diluted bitumen are outlined, based on knowledge gained from the use of flocculants in different stages of the modified Clark process.

A.3 Materials and Methods

A.3.1 Materials

Organic solvents used in this study, toluene and cyclohexane, were purchased from Sigma-Aldrich and used without further purification. Kaolinite was purchased from Acros Organics. Bitumen, free of solids, was obtained from an oil sands operator and used as is. Ethyl cellulose, poly(ethylene glycol)-block-poly(propylene glycol)-block-poly(ethylene glycol) (M_n ~ 5800), (Hydroxypropyl)methyl cellulose, poly(ethylene oxide) (M_w ~ 1M), polystyrene (M_w ~ 350000), methyl acrylate, amylopectin, and hydroxyethyl cellulose were purchased from Sigma-Aldrich. Hyper-branched functionalized polyethylene (HBfPE) (5% methyl acrylate) was synthesized in our group, as described elsewhere [147]. Polystyrene sulfonate was modified according to the procedure detailed in Mazzeo et al [163]. Ethylene-propylene-diene terpolymers (EPDM) (3 – 6% diene content) were supplied by DOW Chemical Co. and modified using 9-borabicyclo[3.3.1]nonane and hydroxylated with $NaOH/H_2O_2$ [164].

A.3.2 Solubility Screening

Polymer solubility was determined qualitatively based on cloud point observations at room temperature, at concentrations of 2 mg/mL [165]. Both toluene and cyclohexane were used as solvents to screen the viability of the polymer flocculants. Initially, the polymer solutions were mixed for up to 24 h at room temperature. If the polymer appeared insoluble, or if the solution remained cloudy, the temperature was raised to 50˚C and stirred for an additional 24 h. All solutions were cooled to room temperature before final observations were made.

A.3.3 Preparation of model suspensions

Kaolinite particles were prepared as a 2% w/w suspension in bitumen/toluene solution (10% w/w). This mixture was stirred at room temperature overnight at 250 rpm to ensure sufficient adsorption of bitumen on the kaolinite particles. The suspensions were then

sonicated for 1 min and mixed again for an additional 30 min. These suspensions were then used in particle size and sedimentation measurements.

A.3.4 FBRM MONITORING

Focused beam reflectance measurement (FBRM) is an optical technique for the characterization of particle sizes (chord lengths). It is useful for *in-situ* monitoring of particles ranging in size from 1 μm to 1 mm. The technique relies on the reflectance of a laser light, and can thus be used in dark or highly concentrated solutions, where absorbance or light scattering measurements are typically unreliable. In oil sands applications, the FBRM technique has been successfully used for the characterization and performance measurement of a number of flocculants used for mature fine tailings treatments [166,167].

Model suspensions were prepared and used for chord length distribution monitoring. The suspensions were mixed at 200 rpm in a 250 mL beaker and monitored in real-time with an FBRM probe. The polymer was added as a 2 mg/mL solution in toluene to the suspension under the same mixing conditions and the chord-length distribution of the particles were continuously recorded, as the polymer dose was increased from 500 mg polymer/kg solids up to 50000 mg polymer/kg solids.

A.3.5 SEDIMENTATION

A Krüss K100 force tensiometer with a sedimentation probe – a highly sensitive balance with a probe immersed in the solution where particles can accumulate on a dish – was used to measure mass accumulation over time. This technique has proved useful to monitor the sedimentation of silica microparticles in aqueous solutions and in organic media treated with bitumen [168,169]. Model suspensions were transferred to a dish in the force tensiometer and polymer was then added to the suspension under constant mixing for 1 min before mixing was stopped, and the sedimentation probe was immersed in the suspension to monitor mass accumulation. Figure A-2 depicts the experimental setup.

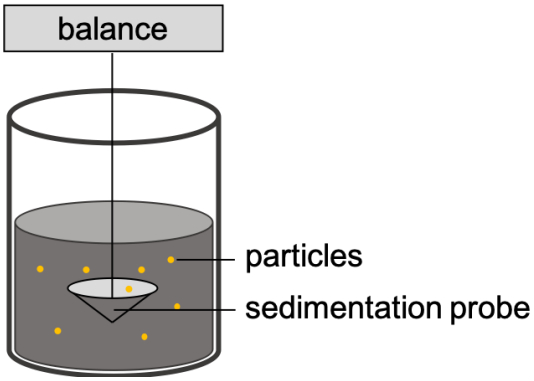

Figure A-2: Schematic diagram of force tensiometer with sedimentation probe.

A.4 Results and Discussion

A.4.1 Polymer Solubility Evaluation

The polymers in Figure A-3 were first evaluated for solubility in toluene and cyclohexane. A viable polymer for flocculation needs to be readily dispersible in diluted bitumen at operating temperatures. The first candidate was a recently developed HBfPE, a polyethylene copolymerized with methyl acrylate having a hyperbranched structure.[147] This polymer was selected because it had been developed as a flocculant to treat MFT and, being polyethylene-based, would be more easily soluble in oil. The HBfPE used to treat MFT had a methyl acrylate content above 35%, to allow for dispersion in water, but for an oil-soluble variant a lower methyl acrylate content was desired. Analogous to HBfPE, where a hydrophobic polymer was functionalized with a more hydrophilic monomer, a second type of polymer based on the synthetic rubber EPDM was modified to add hydroxyl functionality (EPDM-OH). A third type of polymer chosen for screening was a triblock poly(ethylene oxide)-poly(propylene oxide)-poly(ethylene oxide) (PEO-PPO-PEO). Polymers of this class are used as surfactants and demulsifiers. In fact, many PEO-PPO-PEO linear and star polymers are used in oil sands froth treatment to break emulsions [170]. Our hypothesis was that the surface-active nature of these polymers and the ability to tune their hydrophobicity by changing the ratio of PEO to PPO could make them good candidates if they could be synthesized with sufficiently high molecular weights. Poly(methyl acrylate) (PMA) homopolymer was also tested for solubility. PMA has been

used as part of grafted copolymers of PAMs and EPDMs, as mentioned above. This screening was conducted to determine if the PMA homopolymer could act as a flocculant in this system. Poly(styrene sulfonate) (PSS) was also tested with 7% of the sub-units sulfonated. Polystyrene is oil soluble, and its sulfonated derivative is highly charged, improving solubility in water at high degrees of sulfonation; at low degrees of sulfonation the polymer remains soluble in toluene. A number of natural polymers that have been used in the oil industry as demulsifiers—ethyl cellulose (EC), hydroxypropyl methyl cellulose (HPMC), amylopectin (AMP), and hydroxyethyl cellulose (HEC)—were also included in these screening experiments [170].

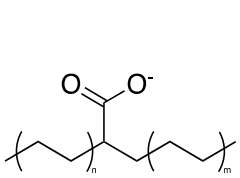

HBfPE

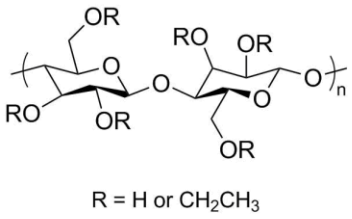

EC

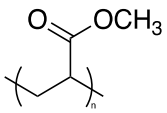

PMA

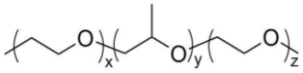

PEO-PPO-PEO

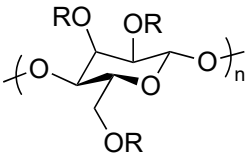

HPMC

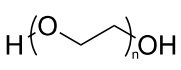

PEO

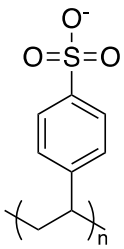

PSS

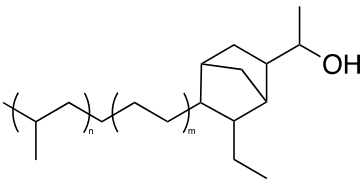

EPDM-OH

Figure A-3: Polymer structures for the screening experiments: hyperbranched functionalized polyethylene (HBfPE), ethyl cellulose (EC), hydroxypropyl methyl cellulose (HPMC), poly(methyl acrylate) (PMA), polystyrene sulfonate (PSS),

hydroxylated ethylene propylene diene (EPDM-OH), poly(ethylene oxide)-poly(propylene oxide)-poly(ethylene oxide) (PEO-PPO-PEO), and poly(ethylene oxide) (PEO).

Among these polymers, three were found to be soluble (clear solution at room temperature) in toluene, and five were found to be slightly soluble (cloudy solution at room temperature, but soluble at elevated temperatures) in toluene (Table A-1). Only HBfPE was completely soluble in cyclohexane, one of the more effective solvents for non-aqueous extraction processes [159]. These findings further demonstrate the challenge in identifying polymers that may be effective in oil-based media. Even at low degrees of polar functionalization, many of the tested polymers become difficult to disperse in toluene and are insoluble in cyclohexane. The eight toluene-soluble polymers were used in further tests to evaluate the flocculation and sedimentation of kaolinite using the FBRM and force tensiometer techniques.

Table A-1: Solubility of 2 mg/mL of polymer in toluene and cyclohexane.

Polymer	**Description**	**Toluene soluble**	**Cyclohexane soluble**
HBfPE	hyperbranched functionalized polyethylene	Yes	Yes
EC	ethyl cellulose	Yes	Sparingly
PMA	poly(methyl acrylate)	Sparingly	No
PEO-PPO-PEO	poly(ethylene oxide)-*block*-poly(propylene oxide)-*block*-poly(ethylene oxide)	Yes	Sparingly
HPMC	hydroxypropyl methyl cellulose	Sparingly	Sparingly
PEO	poly(ethylene oxide)	Sparingly	No
PSS	polystyrene sulfonate	Sparingly	No
EPDM-OH	hydroxylated ethylene-propylene-diene terpolymer	Sparingly	Yes

AMP	amylopectin	No	No
HEC	hydroxyethyl cellulose	No	No
PAM-PEO	polyacrylamide-*graft*-poly(ethylene oxide)	No	No

A.4.2 Chord length distribution monitored via FBRM

Figure A-4 presents the chord length distribution of kaolinite particles used for flocculation screening determined using FBRM. Kaolinite is the most common clay material found in bitumen [171], so screening for its flocculation was used as a starting point in this comparative investigation.

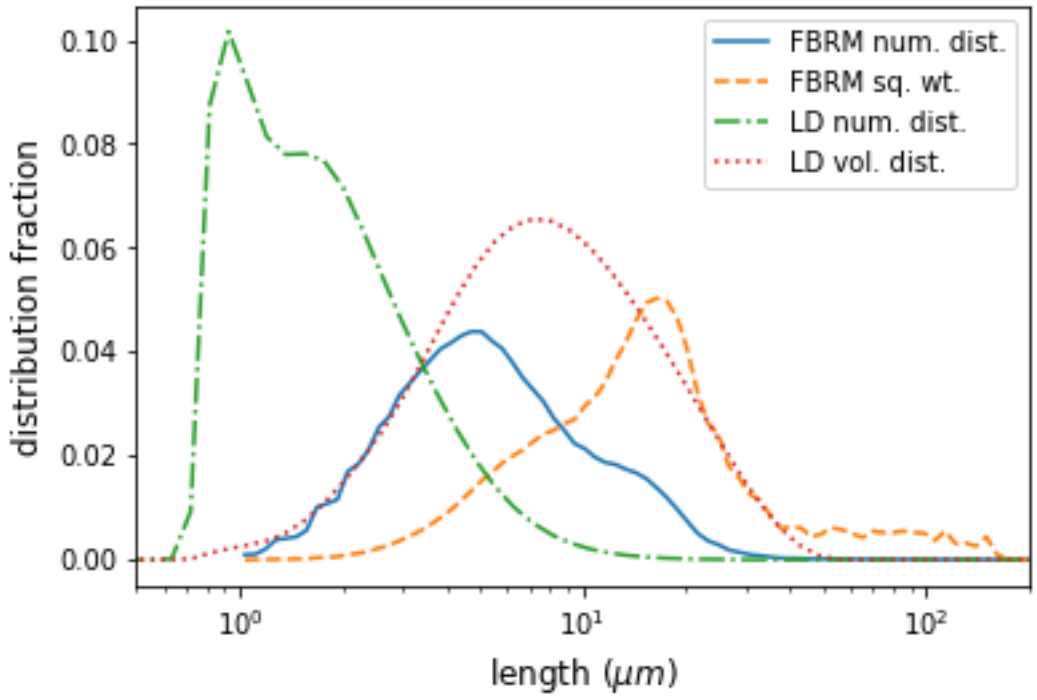

Figure A-4: Chord length distribution of kaolinite particles suspended in a 10 wt% bitumen solution in toluene: number-average chord length distribution (blue solid line), square weighted average chord length distribution (orange dashed line) measured using FBRM. Particle size distribution of kaolinite in water: number-average distribution (green dotted

dashed line) and volume-average distribution (red dotted line), measured using laser diffraction (LD).

Kaolinite particles have a bimodal chord length distribution, which is consistent with the laser diffraction data. The FBRM measurements done in toluene show that kaolinite exists in larger aggregates compared to the kaolinite samples measured in water (Figure A-4). This observation is consistent with the fact that kaolinite is more readily dispersible in water, where the clay can more readily participate in hydrogen bonding with water. In nonpolar solvents, the kaolinite particles would more likely be attracted to themselves than to the solvent in the system. This phenomenon has been demonstrated in simulations of kaolinite platelets in water, toluene, and cyclohexane. Stronger short-range attractive forces are present in cyclohexane and toluene than in water [172,173]. These FBRM results demonstrate that the chord length distribution can be measured under experimental conditions that consist of a dark 10 wt% bitumen solution. Although chord-lengths are not the same measure as particle sizes, as determined by conventional laser diffraction techniques [174], the trends in the data are the same and allow to demonstrate whether particle aggregation would occur.

A.4.3 FLOCCULATION

The polymers that were found to be soluble, or sparingly soluble, in toluene were tested for their flocculation performance at increasing dosages from 500 mg of polymer/kg of solids in suspension to 50000 mg/kg. If flocculation were to occur, then a shift in the chord length distribution to higher values would be expected. Figure A-5 summarizes a sampling of experiments using kaolinite in a 10 wt% bitumen solution in toluene.

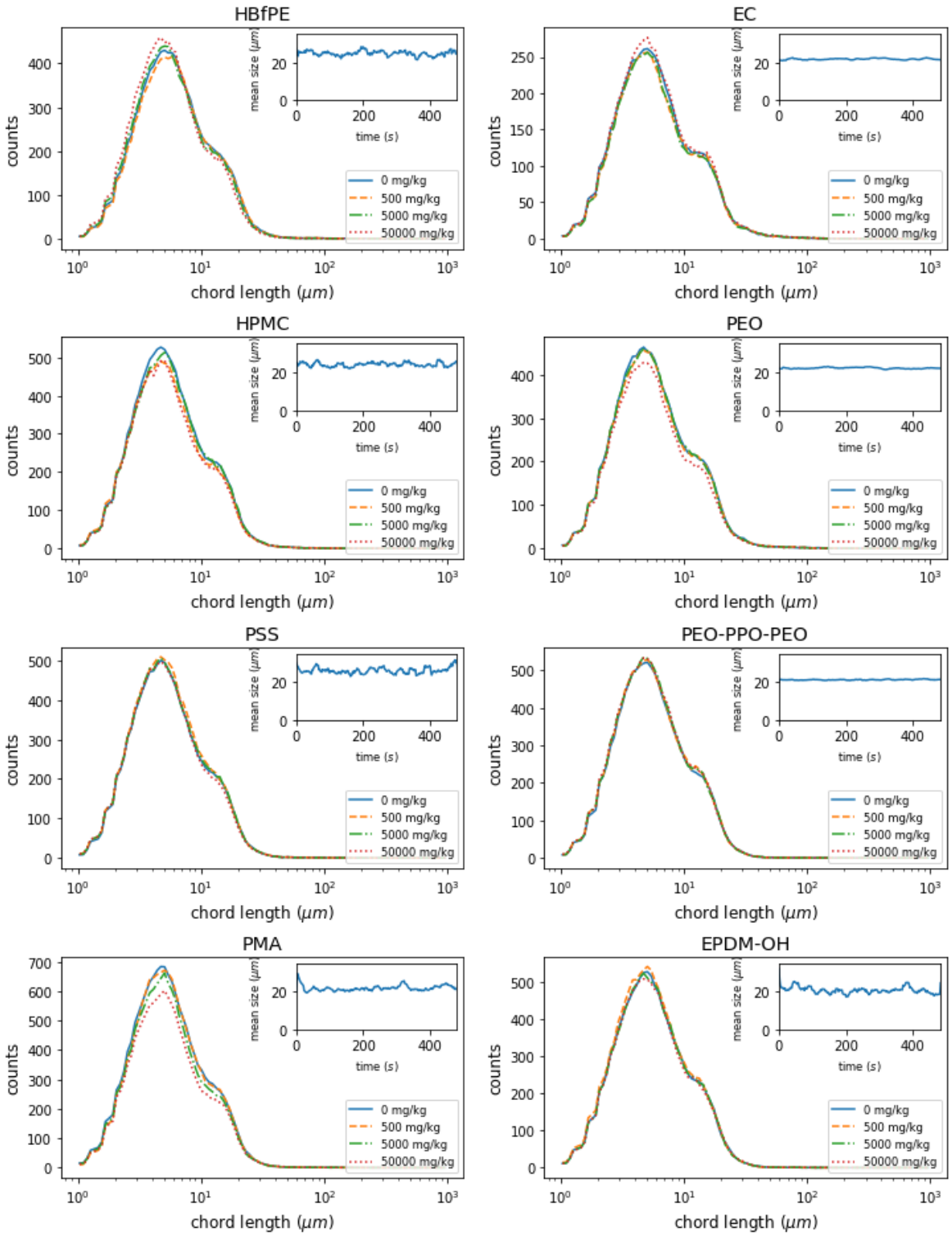

Figure A-5: Chord length distribution (CLD) in bitumen-treated kaolinite suspended in a 10 wt% bitumen in toluene solution, before (solid line) and after (dashed line) polymer

addition monitored using the FBRM technique. Insets: Mean square weighted chord length over the course of the experiment.

All tested polymers failed to flocculate kaolinite as measured by the FBRM probe. This suggests that either no flocculation occurred or, if it did occur, it happened at such low rates that it could not be observed by FBRM. Failure to flocculate could be a result of polymers failing to adsorb onto the clay surface or a failure of adsorbed polymers to act as bridges promoting flocculation. Some simple adsorption tests using FTIR to detect polymer adsorbed on the clay surface were performed to determine whether polymer adsorption was the limiting step (Supplementary Information Figure S1 and Figure S2). Of the screening tests done no polymer was detected on the clay samples after mixing and washing. Alternative techniques to monitor flocculation and polymer adsorption should be used to confirm these findings.

Of the polymers tested, PEO and PMA exhibited a slight decrease in the number of particle counts, as can be seen in Figure A-5. No change in aggregate size was detected and the mean square chord length remained stable throughout the experiment. We speculate that some particles did aggregate and settle out of solution without being detected by the FBRM, but did not occur in large enough quantities to have any measurable effect on the particle sizes. The use of PEO to aid in the sedimentation of kaolinite in cyclohexane was recently demonstrated [130]. Therefore, this hypothesis has some merit but, at this scale and size of particles, no firm conclusions can be drawn.

Finding a polymer that is both soluble in the desired solvent and that will interact with clays is a fine balance. It appears, from the present work, that the polymers used did not interact appreciably with the hydrophilic clays.

A.4.4 SEDIMENTATION

Monitoring the sedimentation of solids using a force tensiometer is an alternative method to measure the rate of solids settling out of suspension. This technique is particularly useful because more common optical techniques, such as changes in turbidity or optical density, are limited to mostly translucent solutions. To verify the findings from the FBRM experiments several flocculation experiments were monitored using the sedimentation probe.

Figure A-6 presents the results from mass accumulation measurements over time on the sedimentation probe, in the presence of PSS or HBfPE in doses of 5000 ppm. The slopes showing the initial and final sedimentation rates with and without polymer addition are very similar. The initial settling rates are 0.04 ± 0.01 mg/s for HBfPE and 0.06 ± 0.01 mg/s for kaolin and PSS. Steady rates measured after 2 min of 0.013 ± 0.003 mg/s for HBfPE, 0.014 ± 0.004 mg/s for PSS, and 0.016 ± 0.004 mg/s for kaolin. The results show that the rate of mass sedimentation is not altered to a statistically significant extent.

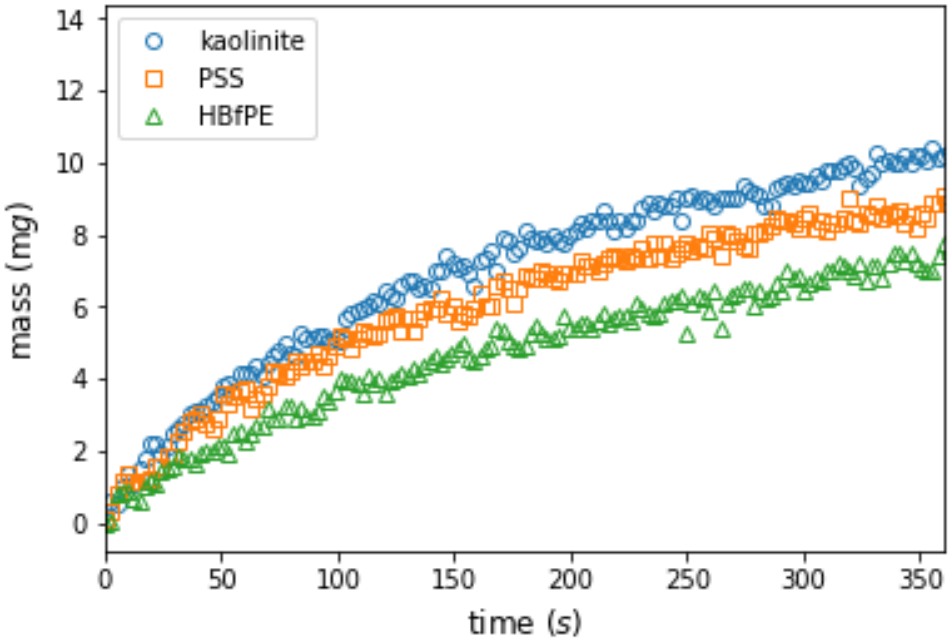

Figure A-6: Sedimentation of kaolinite in a 10 wt% bitumen solution in toluene. Circles: sedimentation with no polymer added. Squares: Sedimentation with 5000 mg/kg polystyrene sulfonate (PSS) added. Triangles: Sedimentation with 5000 mg/kg hyperbranched functionalized polyethylene (HBfPE) added.

None of the polymers screened conclusively indicate the occurrence of any aggregation or flocculation of particles in bitumen-rich organic media. The complexity of the bitumen medium makes it difficult to isolate and identify specific factors that may have affected the flocculation performance. Predicting structures that are soluble in petroleum and act as flocculants is challenging. Additional fundamental understanding of the clay and bitumen, and how these interact with polymers, would be needed. Some recent experiments have been conducted with polymer-modified organo-clays suspended in cyclohexane that indicate flocculation may be possible, but adapting this work to bitumen-rich media would require an extensive effort [130].

A.5 CONCLUSIONS

A way to improve the removal of solids from diluted bitumen produced using naphthenic froth treatment and non-aqueous bitumen extraction processes is still desired. Polymer flocculants could help improve the effectiveness of separation of solids from bitumen, reducing the energy required for mechanical separation. Effective polymer flocculants must be hydrophobic for enhanced solubility (or dispersibility in petroleum) and contain polar or charged groups for bonding to fine solid particles. Candidates with potential include hydrophobic polymers with hydrophilic branches, block copolymers containing a main hydrophobic chain with hydrophilic chain ends, and random copolymers containing hydrophilic and hydrophobic monomers. As part of the evaluation of polymer candidates from these types with respect to solubility in hydrocarbon media and flocculation effectiveness, experimental techniques for determination of flocculation and sedimentation in dark and opaque media are identified. Observations show that the polymers tested do not exhibit notable flocculation effects on kaolinite in toluene, highlighting the challenges arising from the polymer selection requirements and demonstrating that significant rethinking is needed on how to develop polymer flocculants for non-aqueous media.

Developing new polymers to address the removal of fine solids from diluted bitumen is a potentially significant opportunity. A new class of oil-soluble polymer flocculants would facilitate the flocculation and sedimentation of solids out of the bitumen phase. In addition to being bitumen-soluble, the polymer flocculants must be able to extend in the diluted bitumen in order to bind and bring together multiple fine particles to form dense flocs. Polymer compositions and structures containing an oleophilic backbone for enhanced solubility in bitumen and hydrophilic functional groups for binding to solids would be of interest. A fundamental understanding of how polymer flocculants would behave in complex mixtures of bitumen, solvent, and mineral solids is a non-trivial challenge that offers the opportunity to effectively guide the development of the polymer structure and composition. Such understanding could also benefit the optimization of existing bitumen extraction processes.

Appendix B IN-SITU NMR EXPERIMENTS FOR DETERMINING POLYMERIZATION RATES AND REACTIVITY RATIOS

B.1 INTRODUCTION

Nuclear magnetic resonance (NMR) spectroscopy is a powerful method for the characterization of chemical compounds. Proton NMR is especially useful for the identification of functional groups on organic compounds. With the use of initiators that can work within the operating temperatures of an NMR spectrometer radical polymerization can be monitored in real time by tracking the concentration of the monomers and polymer product. As a result, *in-situ* NMR experiments can be used to gather large amounts of data for the determination of polymerization rates and reactivity ratios. This technique has been used on a number of copolymer systems including acrylamide, acrylic acid, methyl methacrylate, and diallyldimethylammonium chloride, and 2-(acryloyloxyethyl)trimethylammonium chloride monomers [175–178]. In this section the lumped polymerization rate constant for vinylbenzyl trimethylammonium chloride (VBTMAC) and the reactivity ratio for the copolymerization of acrylamide (Am) and VBTMAC is determined from *in-situ* NMR experiments and verified with bench scale experiments.

B.2 POLYMERIZATION RATE OF VBTMAC

Free radical polymerization kinetics are well established, the generally accepted reaction mechanisms (with the exclusion of transfer reactions) is as follows [179]:

Initiation:

$$I \xrightarrow{k_d} 2I^* \qquad (B-1)$$

$$I^* + M \xrightarrow{k_i} P_1^* \qquad (B-2)$$

Propagation:

$$P_n^* + M \xrightarrow{k_p} P_{n+1}^* \qquad (B-3)$$

Termination:

$$P_n^* + P_m^* \xrightarrow{k_{tc}} P_{n+m} \qquad (B-4)$$

$$P_n^* + P_m^* \xrightarrow{k_{td}} P_n + P_m \qquad (B-5)$$

where I is the initiator, I^* are active initiator fragments, M is the monomer, P_n^* is a living polymer chain made of n monomeric units, and P_n is a dead chain with length n. $k_d, k_i, k_p, k_{tc}, k_{td}$ are rate constants for initiator dissociation, initiation, propagation, termination by combination, and termination by dissociation, respectively. Assuming the concentration of initiator radicals is approximately constant the rate of polymerization is:

$$R_p = -\frac{d[\mathrm{M}]}{\mathrm{dt}} = \frac{k_p}{k_t^{0.5}}[M] f k_d^{0.5} [I]^{0.5} \qquad (B-6)$$

where f is the initiator efficiency. The rate constants k_p and k_t are difficult to estimate separately so they can often be treated as a lumped constant, $k_p/k_t^{0.5}$.

There are no polymerization kinetic studies published for VBTMAC so to get an estimate of the polymerization rates *in-situ* NMR experiments were used to estimate $k_p/k_t^{0.5}$. The polymerization reaction of VBTMAC was performed in standard 5 mm NMR tubes in an Agilent 400 MHz spectrometer. 0.25 M of VBTMAC in D_2O was prepared with V-50 as the initiator, experiments were done at two initiator concentrations, 1 mM and 2.5 mM. The solution of monomer, initiator, and solvent was purged of air and backfilled with N_2 before being sealed in the NMR tube. NMR tubes were refrigerated until the NMR spectrometer was ready. The NMR sample chamber in the spectrometer was heated to 50 ˚C with hot air flowing through the chamber. Once the temperature had reached equilibrium the sample was added and the spectrometer was tuned and shimmed at the reaction temperature. ^{1}H NMR spectra were collected every two minutes for two hours (60 spectra). Sample NMR spectra from one reaction are depicted in Figure B-1.

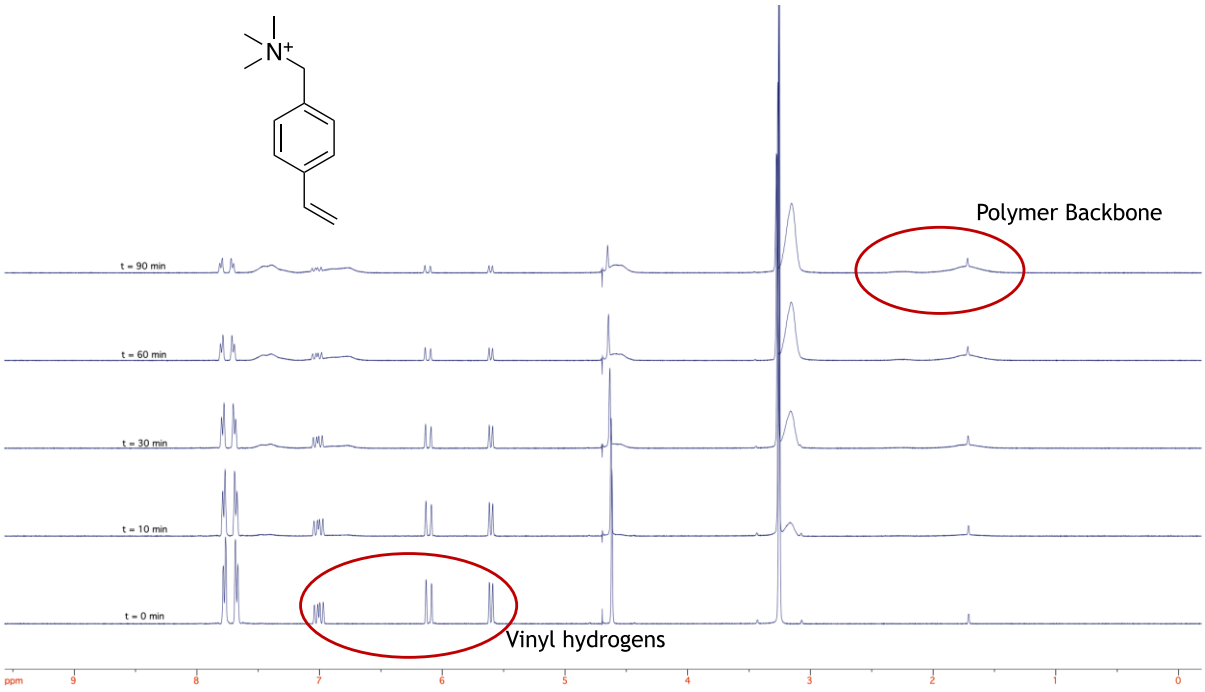

Figure B-1: ^{1}H NMR spectra of the polymerization VBTMAC over time. Vinyl hydrogen peaks between 5.5 ppm and 7.1 ppm decay over the course of the reaction. Broad polymer peaks begin to form over time.

The change in monomer concentration over time was calculated from the decay in the vinyl hydrogen peaks, conversion was calculated from the monomer concentration. Using the conversion data from the NMR experiments and Equation (B-6), a value of the lumped kinetic constant, $k_p/k_t^{0.5}$, was estimated through non-linear least-squares. A value of f = 0.8, and $k_d = 8.2 \times 10^{-6}$ s^{-1} were used. A value of $k_p/k_t^{0.5} = 2.31 \pm 0.02$ was found, where the reported error is a 95% confidence interval. Figure 2 is a plot of the conversion over time with the experimental data and fitted model. Bench scale experiments done in a 200 mL reactor were also done with 0.25 M VBTMAC and 2.5 mM of the initiator, the conversion agrees well with the NMR experiment done under the same conditions (Figure B-2).

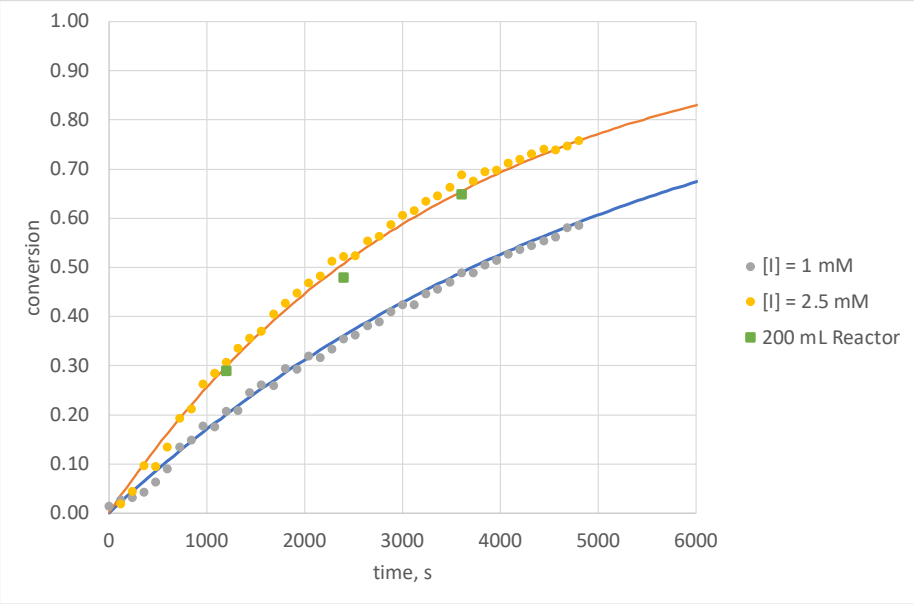

Figure B-2: VBTAMC conversion over time for different initiator concentrations. Points are experimental values and lines are model predictions.

B.3 Determining Reactivity Ratios of VBTMAC and AM

Polyacrylamides are commonly used as flocculants. To modify the properties of acrylamides creating copolymers is a common approach to try and improve performance. Monomers have different reactivity so the polymer product will usually not have the same copolymer composition as the composition of monomer solution before the reaction occurs. The Mayo-Lewis equation, Equation (B-7), described the relationship between the molar fraction of monomers 1 and 2 in solution and the average molar fraction of monomer 1 in the polymer, F_1.

$$F_1 = \frac{r_1 f_1^2 + f_1 f_2}{r_1 f_1^2 + 2 f_1 f_2 + r_2 f_2^2} \qquad (B-7)$$

$$f_1 = \frac{[M_1]}{[M_1] + [M_2]} \qquad (B-8)$$

where f_1 and f_2 are the molar fraction of monomer 1 and 2 in solution, and r_1 and r_2 are the reactivity ratios. Reactivity ratios are defined as the ratio of the reaction rate constant for the addition of a monomer on a living polymer chain where the chain end is the same species, k_{11} or k_{22}, over the rate constant for when a monomer of the other type is added, k_{12} or k_{21}.

$$r_1 = \frac{k_{11}}{k_{12}} \qquad (B-9)$$

$$r_2 = \frac{k_{22}}{k_{21}} \qquad (B-10)$$

To calculate reactivity ratios the instantaneous Mayo-Lewis equation can be solved simultaneously with the differential material balance, Equation (B-11).

$$\frac{df_1}{dx} = \frac{f_1 - F_1}{1 - x} \qquad (B-11)$$

In-situ NMR polymerization reactions were used to monitor the conversion of VBTMAC and acrylamide to polymer. Experimental details are similar to what was described in the previous section for the polymerization of VBTMAC. A total monomer concentration of 0.25 M with varying ratios of VBTMAC to Am were prepared with V-50 (2.5 mM) used as the initiator. All experiments were performed at 50 ˚C. ^{1}H NMR spectra were collected every two minutes for two hours (60 spectra). A set of sample spectra for the copolymerization of VBTMAC and Am may be seen in Figure 3.

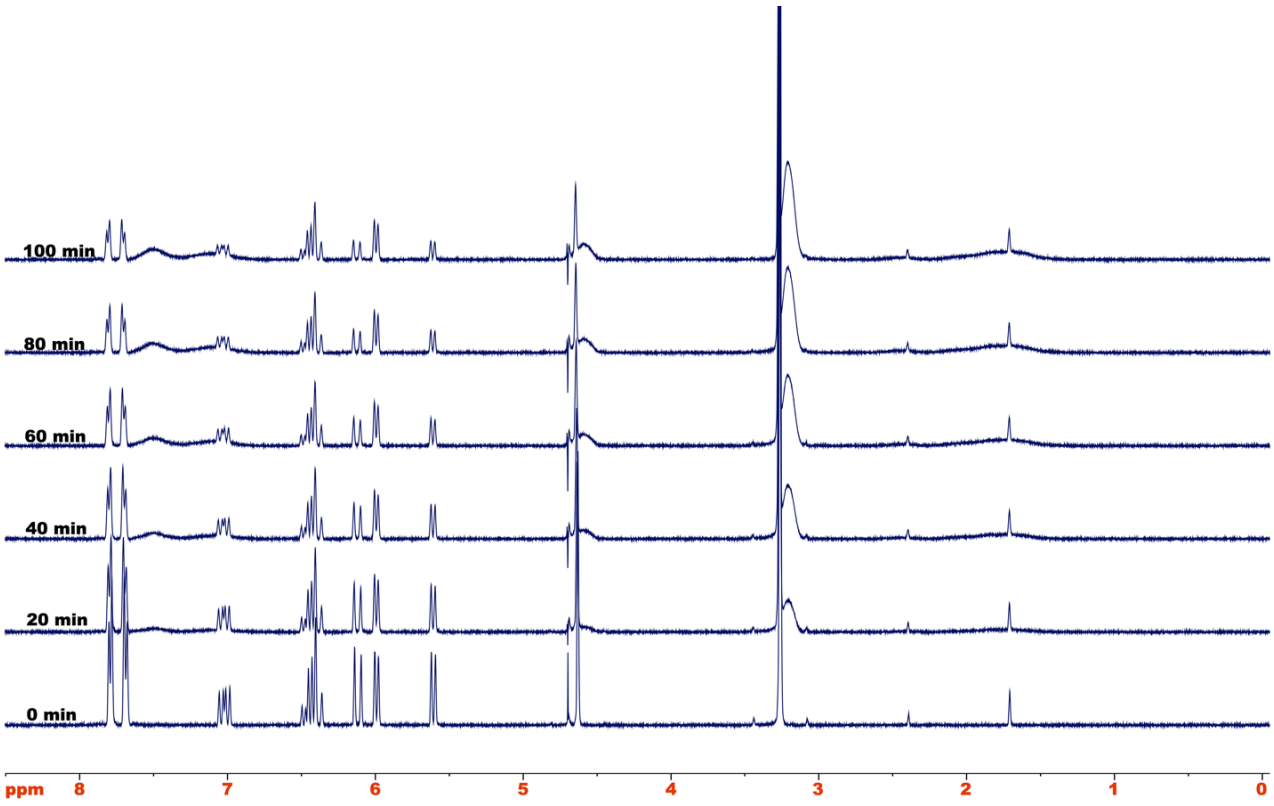

Figure B-3: ^{1}H NMR spectra of the polymerization of Am with VBTMAC over time. Vinyl hydrogen peaks between 5.5 ppm and 7.1 ppm decay over the course of the reaction. Broad polymer peaks begin to form over time.

Reactivity ratios for the copolymerization of Am with VBTMAC were estimated from the comonomer fraction data using a non-linear parameter estimation technique along with direct numerical integration. Figure B-4 depicts the change in fraction of acrylamide (f_{Am}) as a function of conversion. The data was fitted with a model by simultaneously solving the Mayo-Lewis Equation (B-7) with Equation (B-11). Reactivity ratios were estimated using orthogonal distance regression and converged when $r_{Am} = 0.46 \pm 0.03$ and $r_{VB} = 2.48 \pm 0.09$ where the errors reported are the 95% confidence intervals.

The reactivity ratios demonstrate that VBTMAC reacts faster than acrylamide with the copolymer chain ends. Similar results have been observed with water soluble ionic monomers when reacting with Am [177,178]. Further studies to see the effect of monomer concentration and ionic strength of these ratios would be of interest as these water soluble,

ionic monomers sometimes have a concentration dependence on reaction rate constants [177,178].

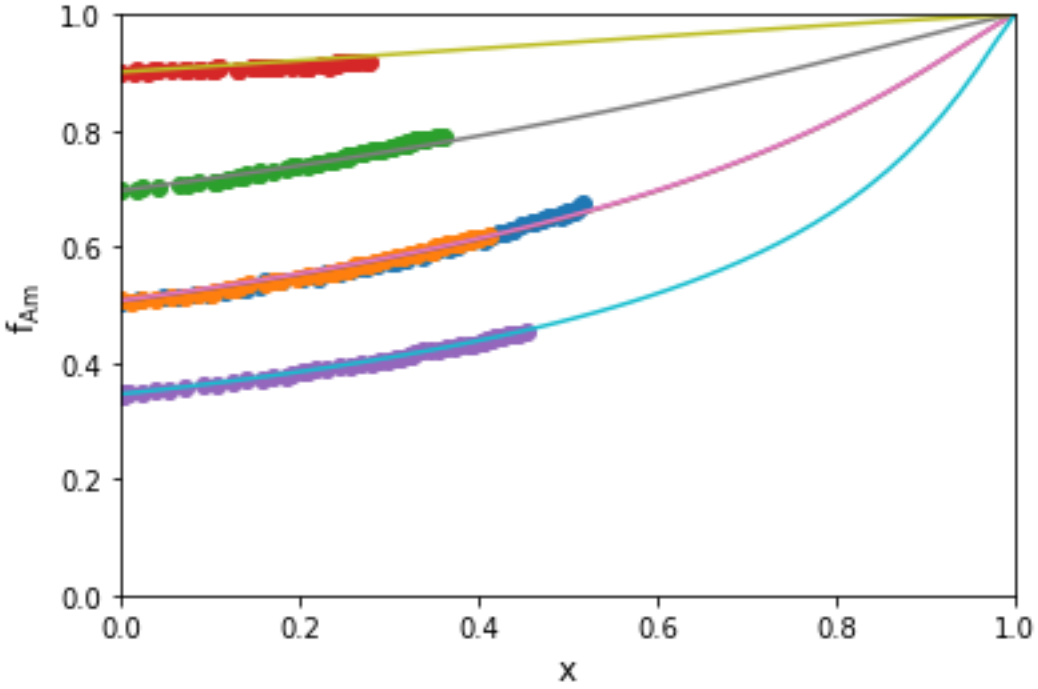

Figure B-4: Acrylamide fraction f_{Am} as a function of copolymerization reaction conversion. Each color represents an independent reaction monitored by NMR. Model fit (solid lines) with reactivity ratios $r_{Am} = 0.46$ and $r_{VB} = 2.48$.

The reactivity ratios were validated by experiments done at the bench scale. Samples from reactions were taken at low conversion (< 5%) to ensure no composition drift was occurring. Figure B-5 is the Mayo-Lewis plot illustrating how the instantaneous copolymer composition depends on the monomer mole fraction. The composition of the synthesized copolymers was measured by NMR, as described in the next section, and the results agree with the reactivity ratios calculated from the NMR kinetic experiments.

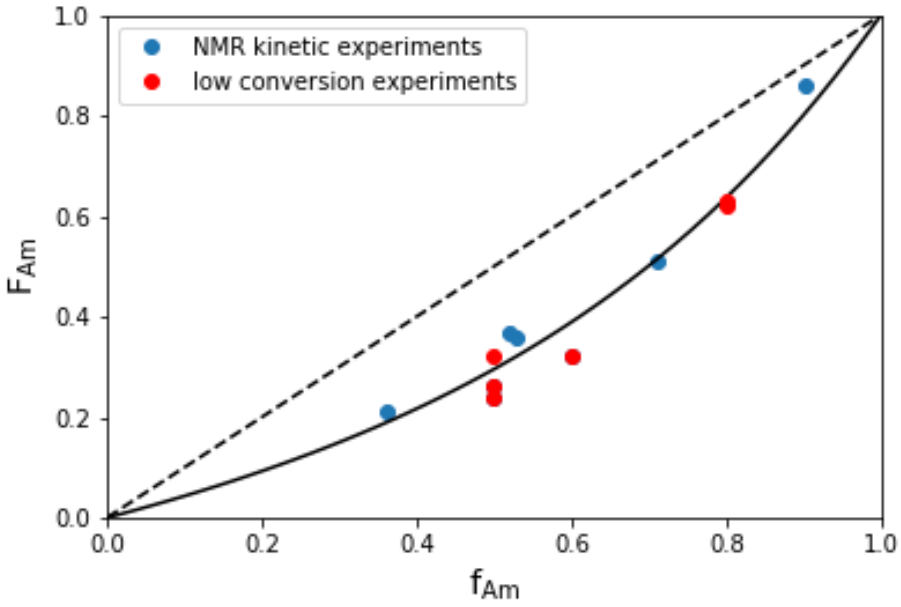

Figure B-5: Mayo-Lewis plot of the instantaneous copolymer composition. Blue circles are data collected from NMR kinetic experiments. Red circles are from samples collected at low conversion.

B.4 Characterization of PVBTMAC/PAM copolymers

Polymer samples synthesized at the bench scale were prepared in D_2O and analyzed using an Agilent 400 MHz spectrometer. Figure B-6 depicts sample spectra for copolymers of Am and VBTMAC. The copolymer composition was determined by the ratio the VBTMAC peaks to the polymer backbone peaks. VBTMAC repeat unit peaks appear at 6.6-7.5 ppm (aromatic H), 4.2-4.6 ppm (Ar-CH2-N), and 2.6-3.3 ppm ($-N^+(CH_3)_3$). The polymer backbone peaks appear at 1.0-2.0 ppm ($-CH_2-$) 2.0-2.5 ppm (-CHR-). Smaller peaks from 5.3-6.3 ppm, and at 7.5 ppm are signal from residual monomer.

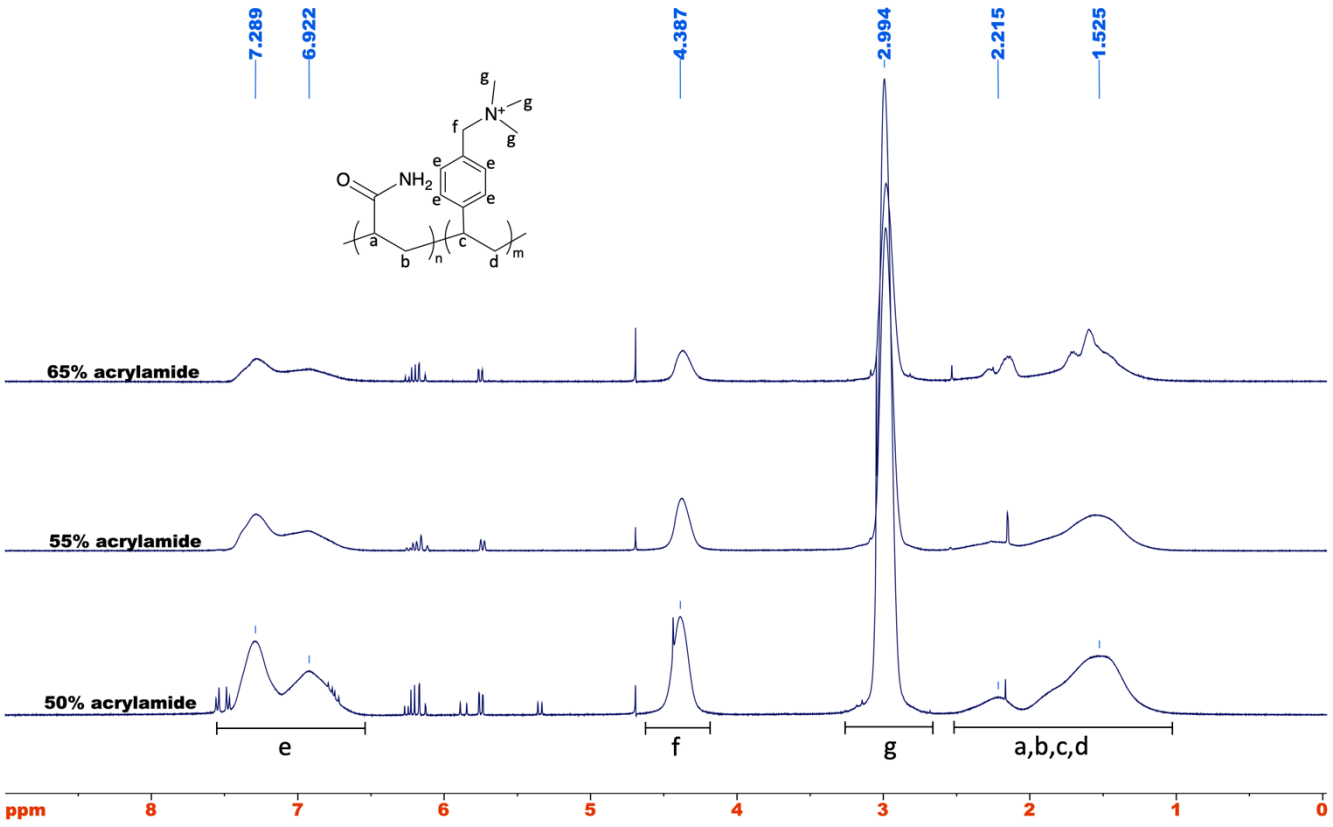

Figure B-6: Sample spectra of acrylamide/vinylbenzyl trimethylammonium chloride copolymers. Peaks are labelled with the assigned functional groups.

Referring to Figure B-6 the average copolymer composition of a polymer sample may be calculated from the area under the curve for the VBTMAC peaks over the area under the curve for the polymer backbone peaks. The area of each peak is normalized to the number of hydrogens in the functional group. The average of the three VBTMAC peaks were used to minimize integration error compared to using just one peak for the calculation. Equation (B-12) is the formula used to calculate the average copolymer composition. The sample spectra in Figure B-6 correspond to copolymers with 50%, 55%, and 65% acrylamide content. As the acrylamide content increases the relative area of the VBTMAC peaks decreases compared to the polymer backbone.

$$\bar{F}_{AM} = 1 - \frac{\frac{1}{3}\left(\frac{1}{4}A_e + \frac{1}{2}A_f + \frac{1}{9}A_g\right)}{\frac{1}{3}A_{abcd}} \qquad (B-12)$$

where A_e, A_f, A_g, and A_{abcd} are the areas under the curve for peak e, f, g, and abcd, respectively.

Appendix C SUPPORTING INFORMATION FOR CHAPTER 4

C.1 FLOCCULATION EXPERIMENTS

Table C-1: Experimental ISR, CST, and % solids results of dual HPAM, PVBTMAC flocculation of 10 wt% MFT.

HPAM Dose (kppm)	PVBTMAC Dose (kppm)	HPAM Charge (%)	ISR (m/h)	CST (s)	% Solids
3.5	1.5	20.6	15.6	78.4	31.4
2.5	4.182	37	24.0	8.3	30.9
2.5	2.5	49.3	6.9	8.6	30.4
2.5	0.818	37	18.1	35.1	32.9
3.5	3.5	20.6	27.2	8.8	32.5
2.5	2.5	37	20.1	6.5	30.5
1.5	3.5	20.6	20.1	8.9	31.6
4.182	2.5	37	21.4	31.6	32.2
1.5	3.5	45.4	10.2	8.6	29.5
2.5	2.5	37	18.8	8.0	30.1
3.5	1.5	45.4	15.6	24.9	32.1
3.5	3.5	45.4	8.6	9.9	29.2
0.818	2.5	37	0.6	17.4	25.1
1.5	1.5	45.4	9.7	7.4	29.6
2.5	2.5	37	19.4	6.0	30.8
2.5	2.5	8.6	0.01	104.9	21.2
1.5	1.5	20.6	16.2	7.1	30.4
2.5	2.5	37	18.1	7.65	28.2
3.5	3.5	45.4	20.7	7.35	26.9
1.5	1.5	45.4	11.0	7.25	27.2

Table C-2: Experimental turbidity and zeta potential results of dual HPAM, PVBTMAC flocculation of 10 wt% MFT.

HPAM Dose (kppm)	PVBTMAC Dose (kppm)	HPAM Charge (%)	Turbidity (NTU)	Zeta Potential (mV)
3.5	1.5	20.6	109	-33.1
2.5	4.182	37	82	48.2
2.5	2.5	49.3	2	-9.3
2.5	0.818	37	132	-41.3
3.5	3.5	20.6	67	45.0
2.5	2.5	37	40	32.2
1.5	3.5	20.6	63	48.8
4.182	2.5	37	121	-40.6
1.5	3.5	45.4	94	49.4
2.5	2.5	37	23	39.3
3.5	1.5	45.4	148	-40.5
3.5	3.5	45.4	8	-23.5
0.818	2.5	37	13	-15.3
1.5	1.5	45.4	28	28.7
2.5	2.5	37	31	27.7
2.5	2.5	8.6	22	-23.9
1.5	1.5	20.6	32	36.6

Table C-3: Experimental solids content results of dual HPAM, PVBTMAC flocculation of undiluted MFT.

HPAM Dose (kppm)	PVBTMAC Dose (kppm)	HPAM Charge (%)	% Solids - Undiluted
3.5	1.5	20.6	28.5
2.5	4.182	37	32.9
2.5	2.5	49.3	31.8
2.5	0.818	37	32.0
3.5	3.5	20.6	30.0
2.5	2.5	37	32.0
1.5	3.5	20.6	37.4
4.182	2.5	37	27.7
1.5	3.5	45.4	60.0
2.5	2.5	37	30.8
3.5	1.5	45.4	29.7
3.5	3.5	45.4	43.2
0.818	2.5	37	52.8
1.5	1.5	45.4	50.5
2.5	2.5	37	32.1
2.5	2.5	8.6	28.5
1.5	1.5	20.6	30.7
1.5	3.5	45.4	61.5
0.818	2.5	37	51.0
1.5	1.5	45.4	55.8
1.5	4.182	49.3	52.2
0.818	4.182	49.3	52.1

C.1.1 ISR

Table C-4: Parameter estimates of linear regression model for the prediction of ISR.

	β	Standard Error	t	P>|t|	95% Confidence Interval
Intercept	20.9336	2.442	8.573	0*	[15.493, 26.374]
PVBTMAC Dose	1.871	1.235	1.515	0.161	[-0.88, 4.622]
HPAM Dose	3.4521	1.235	2.796	0.019*	[0.701, 6.204]
HPAM Charge	-2.9978	1.303	-2.3	0.044*	[-5.902, -0.094]
PVBTMAC Dose × HPAM Dose	0.9067	1.503	0.603	0.56	[-2.442, 4.255]
PVBTMAC Dose × HPAM Charge	-2.3019	1.514	-1.52	0.159	[-5.676, 1.072]
HPAM Dose × HPAM Charge	0.6071	1.514	0.401	0.697	[-2.767, 3.981]
PVBTMAC Dose ^ 2	1.5167	1.293	1.173	0.268	[-1.365, 4.398]
HPAM Dose ^ 2	-2.0357	1.293	-1.574	0.147	[-4.917, 0.846]
HPAM Charge ^ 2	-5.9743	1.378	-4.336	0.001*	[-9.044, -2.904]

C.1.2 CST

Table C-5: Parameter estimates of linear regression model for the prediction of CST.

	β	Standard Error	t	P>|t|	95% Confidence Interval
Intercept	0.8389	0.114	7.366	0*	[0.585, 1.093]
PVBTMAC Dose	-0.1696	0.058	-2.946	0.015*	[-0.298, -0.041]
HPAM Dose	0.1622	0.058	2.817	0.018*	[0.034, 0.291]
HPAM Charge	-0.1123	0.061	-1.848	0.094	[-0.248, 0.023]
PVBTMAC Dose × HPAM Dose	-0.201	0.07	-2.867	0.017*	[-0.357, -0.045]
PVBTMAC Dose × HPAM Charge	0.0605	0.071	0.857	0.411	[-0.097, 0.218]
HPAM Dose × HPAM Charge	-0.0666	0.071	-0.943	0.368	[-0.224, 0.091]
PVBTMAC Dose ^ 2	0.0799	0.06	1.324	0.215	[-0.055, 0.214]
HPAM Dose ^ 2	0.1286	0.06	2.133	0.059	[-0.006, 0.263]
HPAM Charge ^ 2	0.1763	0.064	2.743	0.021*	[0.033, 0.319]

C.1.3 SOLIDS CONTENT

Table C-6: Parameter estimates of linear regression model for the prediction of solids content in sediment.

	β	Standard Error	t	P>|t|	95% Confidence Interval
Intercept	30.6436	1.28	23.948	0*	[27.792, 33.495]
PVBTMAC Dose	-0.2607	0.647	-0.403	0.695	[-1.703, 1.181]
HPAM Dose	1.1051	0.647	1.708	0.119	[-0.337, 2.547]
HPAM Charge	-0.162	0.683	-0.237	0.817	[-1.684, 1.36]
PVBTMAC Dose × HPAM Dose	-0.7551	0.788	-0.959	0.36	[-2.51, 1]
PVBTMAC Dose × HPAM Charge	-0.7769	0.793	-0.979	0.351	[-2.545, 0.991]
HPAM Dose × HPAM Charge	0.1664	0.793	0.21	0.838	[-1.602, 1.934]
PVBTMAC Dose ^ 2	0.9209	0.678	1.359	0.204	[-0.589, 2.431]
HPAM Dose ^ 2	-0.2226	0.678	-0.328	0.749	[-1.733, 1.288]
HPAM Charge ^ 2	-1.7732	0.722	-2.456	0.034*	[-3.382, -0.164]

C.1.4 TURBIDITY

Table C-7: Parameter estimates of linear regression model for the prediction of turbidity.

	β	Standard Error	t	P>|t|	95% Confidence Interval
Intercept	29.8897	14.497	2.062	0.078	[-4.391, 64.171]
PVBTMAC Dose	-11.3079	6.574	-1.72	0.129	[-26.853, 4.238]
HPAM Dose	22.1682	6.574	3.372	0.012*	[6.623, 37.714]
HPAM Charge	-2.8463	7.197	-0.395	0.704	[-19.865, 14.172]
PVBTMAC Dose × HPAM Dose	-34.875	8.469	-4.118	0.004*	[-54.901, -14.849]
PVBTMAC Dose × HPAM Charge	-8.0935	8.295	-0.976	0.362	[-27.708, 11.521]
HPAM Dose × HPAM Charge	-3.3812	8.295	-0.408	0.696	[-22.996, 16.233]
PVBTMAC Dose ^ 2	28.2771	7.131	3.965	0.005*	[11.415, 45.139]
HPAM Dose ^ 2	14.1385	7.131	1.983	0.088	[-2.724, 31.001]
HPAM Charge ^ 2	-4.7365	7.698	-0.615	0.558	[-22.94, 13.467]

C.1.5 Zeta Potential

Table C-8: Parameter estimates of linear regression model for the prediction of zeta potential.

	β	Standard Error	t	P>|t|	95% Confidence Interval
Intercept	38.1152	16.918	2.253	0.059	[-1.89, 78.121]
PVBTMAC Dose	21.0418	7.672	2.743	0.029*	[2.9, 39.183]
HPAM Dose	-18.1245	7.672	-2.362	0.05*	[-36.266, 0.017]
HPAM Charge	-9.5411	8.399	-1.136	0.293	[-29.401, 10.319]
PVBTMAC Dose × HPAM Dose	7.7781	9.883	0.787	0.457	[-15.592, 31.148]
PVBTMAC Dose × HPAM Charge	-4.9555	9.68	-0.512	0.624	[-27.845, 17.934]
HPAM Dose × HPAM Charge	-5.761	9.68	-0.595	0.57	[-28.651, 17.129]
PVBTMAC Dose ^ 2	-4.6264	8.322	-0.556	0.596	[-24.304, 15.052]
HPAM Dose ^ 2	-15.7296	8.322	-1.89	0.101	[-35.408, 3.948]
HPAM Charge ^ 2	-15.798	8.984	-1.759	0.122	[-37.041, 5.445]

C.1.6 Undiluted Solids Content

Table C-9: Parameter estimates of linear regression model for the prediction of solids content for treatment of undiluted MFT.

	β	Standard Error	t	P>|t|	95% Confidence Interval
Intercept	32.8708	3.694	8.899	0*	[24.823, 40.919]
PVBTMAC Dose	1.7926	1.866	0.961	0.356	[-2.272, 5.858]
HPAM Dose	-5.9938	1.79	-3.349	0.006*	[-9.893, -2.095]
HPAM Charge	5.189	1.922	2.7	0.019*	[1.001, 9.377]
PVBTMAC Dose × HPAM Dose	2.2142	2.107	1.051	0.314	[-2.376, 6.804]
PVBTMAC Dose × HPAM Charge	-0.2073	2.174	-0.095	0.926	[-4.943, 4.528]
HPAM Dose × HPAM Charge	-2.9957	2.242	-1.336	0.206	[-7.88, 1.889]
PVBTMAC Dose ^ 2	-0.2333	1.812	-0.129	0.9	[-4.182, 3.715]
HPAM Dose ^ 2	2.2546	1.784	1.264	0.23	[-1.633, 6.142]
HPAM Charge ^ 2	1.46	2.016	0.724	0.483	[-2.932, 5.852]